INFORMATION TO USERS

This manuscript has been reproduced from the microfilm master. UMI films the text directly from the original or copy submitted. Thus, some thesis and dissertation copies are in typewriter face, while others may be from any type of computer printer.

The quality of this reproduction is dependent upon the quality of the copy submitted. Broken or indistinct print, colored or poor quality illustrations and photographs, print bleedthrough, substandard margins, and improper alignment can adversely affect reproduction.

In the unlikely event that the author did not send UMI a complete manuscript and there are missing pages, these will be noted. Also, if unauthorized copyright material had to be removed, a note will indicate the deletion.

Oversize materials (e.g., maps, drawings, charts) are reproduced by sectioning the original, beginning at the upper left-hand corner and continuing from left to right in equal sections with small overlaps. Each original is also photographed in one exposure and is included in reduced form at the back of the book.

Photographs included in the original manuscript have been reproduced xerographically in this copy. Higher quality 6" x 9" black and white photographic prints are available for any photographs or illustrations appearing in this copy for an additional charge. Contact UMI directly to order.

UMI®

Bell & Howell Information and Learning
300 North Zeeb Road, Ann Arbor, MI 48106-1346 USA
800-521-0600

Electrochemical and Photoelectrochemical Oxidation of Selected Organic Compounds on TiO_2 Electrodes and the Effect of Adsorption on the Oxidation Potentials

Aref Taghizadeh

A Thesis

In

The Department

Of

Chemistry and Biochemistry

Presented in Partial Fulfillment of the requirements
For the Degree of Master of Science at
Concordia University
Montreal, Quebec, Canada

August, 1998

ABSTRACT

Electrochemical and Photoelectrochemical Oxidation of Selected Organic Compounds on TiO_2 Electrodes and the Effect of adsorption on the Oxidation Potentials

Aref Taghizadeh

A commercially available TiO_2 powder (Degussa P-25) has been used to prepare thin particulate films on optically transparent SnO_2 conducting glass electrodes. The oxidation potentials of Resorcinol (RSRCL), 4-Chlororesorcinol (4-CR), 4,6-Dichlororesorcinol (4,6-DCR), Catechol (CC), 3,4-Dihydroxybenzoic acid (3,4-DHBA), and 1,2,4-benzenetriol (1,2,4-THB) in 0.5M KCl were measured. The effect of adsorption on the oxidation potentials of the above-mentioned compounds on TiO_2 electrodes, were examined by cyclic voltammetry under various conditions.

The results show different oxidation potentials vs. SCE for adsorbed versus non-adsorbed species. The scan rate dependencies of the peak currents indicate, that the lower oxidation potential may be assigned to adsorbed reactants while the one at higher potential corresponds to diffusion-controlled oxidation of material from solution. This was also confirmed by the dependence of peak current on the concentration for selected compounds. Illumination causes no significant change in the measured oxidation potentials. However, photocurrent was observed under illumination, indicating the photoactivity of TiO_2. These

studies tend to indicate that associating the oxidation of such compounds to a single oxidation potential does not adequately describe the situation. Depending on the type of working electrode used, an important distinction is to be made between adsorbed and dissolved species.

ACKNOWLEDGMENT

It is a pleasure to acknowledge the support and technical guidance given to me by Dr. M. F. Lawrence and most importantly his confidence in me, which enabled me to carry this research to completion. I would also like to acknowledge Dr. N. Serpone for his useful suggestions and helpful discussions.

Thanks are also due to Dr. P. Banks and Dr. D. Jack for serving on my research committee.

Finally, I dedicate this thesis to my family for their unconditional support and encouragement throughout this work.

TABLE OF CONTENTS

LIST OF FIGURES

LIST OF TABLES

LIST OF SYMBOLS

E_{CB}	Conduction band potential
E_{VB}	Valence band potential
E_g	Band gap potential
I_p	Peak current
E	Peak potential
ν	Scan rate
D	Diffusion coefficient
n	Number of electrons being transferred
C_o	Bulk concentration
$TiO_2(h)$	Photo-generated hole
Ar	Aromatic compounds

CHAPTER 1

INTRODUCTION

1.1 Overview

Water contamination from extended agricultural and industrial processes in the last few decades has resulted in a growing concern regarding the quality of water[1]. Consequently, decontamination of natural and drinking water has become an increasingly important task in environmental protection.[2]

Detoxification of water has long relied on conventional methods such as chlorination and ozonation that use strong oxidants of a seriously hazardous and therefore undesirable nature[3]. The non-destructive technologies in use, *i.e.*, air-stripping and carbon adsorption, also have their own problems. Thus, air-stripping, for removing volatile contaminants, converts a liquid contamination problem into an air pollution problem and carbon adsorption produces a hazardous solid which in turn must be disposed of [3].

Limitations associated with the above-mentioned methods have resulted in a search for a new technique whose end-products are non-toxic. An interesting process that has gained popularity in recent years is the photomineralization of organic pollutants sensitized by semiconductor photocatalysts[4-25]. This method relies on photoelectrochemical processes, which may be defined as redox reactions initiated by absorption of a photon within the electrode forming an interface with an electrolyte[26]. The popularity of this method is due to the fact

that the mineral 'effluent' it produces is harmless to the environment. The semiconductor that has attracted most attention for sensitizing the photomineralization of organic contaminants is TiO_2[4-20]. The prevalence of TiO_2 arises from its low cost, insolubility under most conditions, photo-stability and non-toxicity[27].

Photochemical reactions on semiconductors can be separated into two groups: i) semiconductor-mediated photocatalysis in which hydroxyl radicals generated from decomposition of water by holes at the surface of TiO_2 react with the organic compound in solution (equation 1.1 and 1.2)[28, 29].

$$TiO_2(h) + OH^- \rightarrow TiO_2 + OH^\bullet \quad (1.1)$$

$$OH^\bullet + Ar \rightarrow \text{Products} \quad (1.2)$$

ii) Direct transformation of substrates adsorbed on semiconductor particles (equation 1.3)[28, 29].

$$TiO_2(h) + Ar \rightarrow \text{Products} \quad (1.3)$$

As is evident by the numerous publications cited in the literature, many aspects of water remediation initiated by irradiation of the TiO_2 photocatalyst have been investigated[1-27]. In many cases, adsorption of species under investigation plays an important role in the degradation process, whose behavior is normally expressed in terms of a Langmuir isotherm[27]. In most photochemical and photoelectrochemical processes, if not all, a single redox potential which reflects

the oxidation potential of dissolved species was used to describe the redox behavior of the organic compound regardless of the state in which the substrate was present[5, 7, 8, 26] (free or adsorbed on TiO_2 surface).

It is the aim of this thesis to determine the redox potentials of selected aromatic compounds on TiO_2 electrodes and to show that the potentials of non-adsorbed organic compounds differ from those adsorbed on TiO_2, as illustrated in figure 1.1. Therefore, a single redox potential is inadequate to describe the redox behavior of many organic compounds on these semiconductor materials. For this reason, the remainder of this chapter is devoted to the theory required to understand the processes involved.

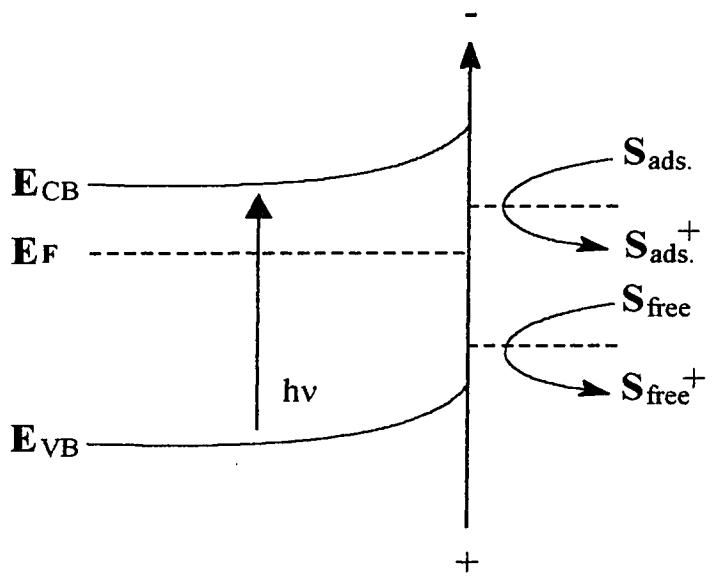

Figure 1.1: Oxidation of free and adsorbed substrates on an n-type semiconductor On the electrochemical scale.

1.2 Semiconductors and Their Electronic Properties

By definition, a semiconductor unlike a metal does not have a continuum of states but rather has band structure[26]. The filled level referred to as the valence band (E_{VB}) consists of an energetically closely spaced array of bonding orbitals derived from the valence electrons of the material[26]. An energy gap exists between the top edge of this band and the lower edge of a similar closely spaced array of orbitals that are unoccupied in the ground state. Since population of these latter orbitals makes the material conductive, this band is referred to as the conduction band[26] (E_{CB}). The gap separating the valence band from the conduction band is known as the band gap E_g (figure 1.2).

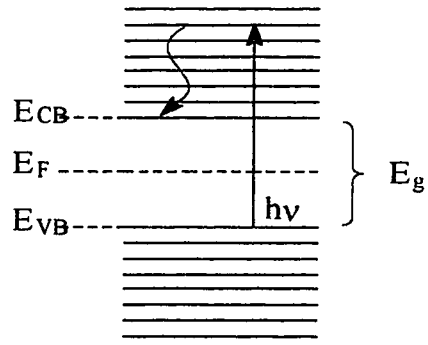

Figure 1.2: Excitation of a semiconductor.

A photon that is spectrally matched with the accessible band levels of the semiconductor possesses sufficient energy to promote an electron from the valence band to the conduction band (figure 1.2). Therefore every semiconductor has a characteristic onset wavelength for absorption[26]. If a photon of sufficient

energy is used to promote an electron from the valence band to the conduction band, an electron-hole pair is generated. That is, a vacancy is created in the valence band from its normal occupancy, and an electron is placed in the conduction band. Recombination of the electron-hole pair is energetically highly favorable, since the semiconductor lacks the state continuity found in metals. However, quantum restrictions slow the rate of recombination so that the hole can, in principle, behave as a photo-anode and the electron can, in principle, act as a photo-cathode if the site-specific localization of these respective redox reagents can be attained[26].

Semiconductors can be classified into three types; 1) the intrinsic, in which the Fermi-level (the energy at which the probability of an energy level being occupied by an electron is exactly ½) is in the middle of the band gap; 2) n-type, in which the Fermi level is shifted near the conduction band edge; and 3) p-type, in which the Fermi energy is moved to a position just above the valence band edge. Figure 1.3 represents the three types of semiconductors[26].

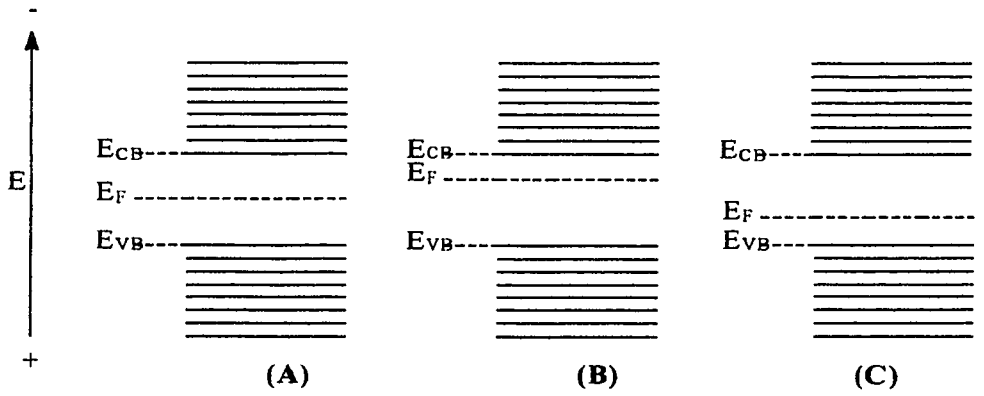

Figure 1.3: Different types of semiconductors. (A) Intrinsic, (B) n-type, (C) p-type[4]

When a semiconductor is brought into contact with an electrolyte solution, a potential difference is established at the interface. The conductivity of an even doped semiconductor is usually well below that of an electrolyte solution; so practically the entire potential drop occurs in the boundary layer of the semiconductor, and very little on the solution side of the interface[30 (a)]. The situation is opposite to that of a metal electrode in contact with an electrolyte, but very similar to that at the interface between a semiconductor and a metal. The transfer of mobile charge carriers between the semiconductor and the contact phase, or the trapping of charge carriers at surface states at the interface, produces a space charge layer.[5] The electrochemistry of the semiconductor is dominated by the band-bending. Band bending determines whether majority carriers or minority carriers move towards the electrode surface (figure 1.4)[30 (a)].

In the case of an n-type semiconductor, at potentials more negative than the flat-band potential (external applied voltage needed to cancel band bending, V_{fb}) the majority carriers (electrons in the conduction band), flow towards the semiconductor surface resulting in an increase in electron concentration near the surface within the space charge layer. The resulting space charge layer is termed an accumulation layer[30 (a)] (fig. 1.4A). The bands of the semiconductor are bent downward as one moves toward the surface causing an accumulation of negative charges at the interface within the semiconductor. Redox couples with formal potentials negative of V_{fb} readily exchange electrons in both directions. When the applied potential moves positive of V_{fb}, the charge carrier flow

reverses, and now minority carriers (holes) accumulate at the surface. Since the majority carriers are moved from the surface, the space charge layer is called a depletion layer and the bands bend upward toward the surface[30 (a)] (fig. 1.4B). When the depletion of the majority charge carriers extends far into the semiconductor, the Fermi-level can decrease below the intrinsic level, which is half way between the bottom of the conduction band and the top of the valence band. The surface of the semiconductor appears to be p-type while the bulk still exhibits n-type behavior. This space charge layer is called an inversion layer [30 (a)] (fig. 1.4C).

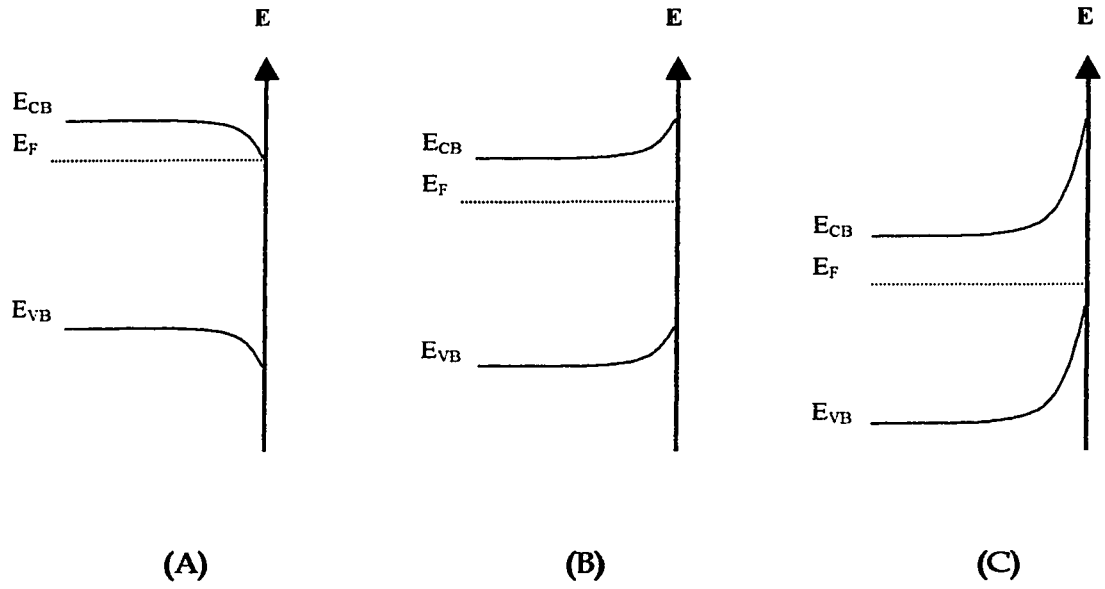

Figure 1.4: Space charge layer formation and band bending for an n-type Semiconductor; A) Accumulation layer, B) Depletion layer, C) Inversion layer.

1.3 Electrode - Solution Interface

According to the widely accepted model of the electrode-solution interface which evolved from a simpler model proposed by Helmholtz[30 (b)] , the electrode is covered by a sheath of oriented solvent molecules. Adsorbed species (ions or molecules) contact the electrode directly and are not fully solvated. The plane that passes through the center of these molecules is called the inner Helmholtz plane (IHP). Such molecules or ions are said to be chemisorbed[31 (a)]. The molecules in the next layer carry their hydration shell and are separated from the electrode by a monolayer of oriented solvent molecules in contact with the IHP. The plane passing through the center of these solvated species is referred to as the outer Helmholtz plane (OHP). Beyond the layer defined by the OHP is a Boltzmann distribution of ions determined by electrostatic interaction of the ions, the potential at the OHP and the random collision of ions and solvent molecules. This region is referred to as the diffuse layer. In the diffuse layer, random thermal motion tends to distribute the ions evenly throughout the solution, whereas electrostatic forces tend to attract or deploy ions from the surface depending on their charge. These two tendencies counterbalance each other, resulting in a non-uniform distribution of ions near the surface. Beyond the diffuse layer, ions in the homogeneous bulk solution phase can not feel the presence of the electrode, since the potential diminishes exponentially with distance from the surface of the electrode. Figure 1.5 illustrates the electrode-solution interface[31 (a)]. As a result of the availability of charge carriers, all the

potential differences between two electrodes occur across the two solid/electrolyte interfaces and not across the bulk solution. When a current passes through the solution, there is a possibility that a potential difference will develop due to the finite conductivity of the solution. In most electroanalytical experiments this is very small compared to the interfacial potential difference and always results in a comparatively weak electric field (small potential drop across a large distance).

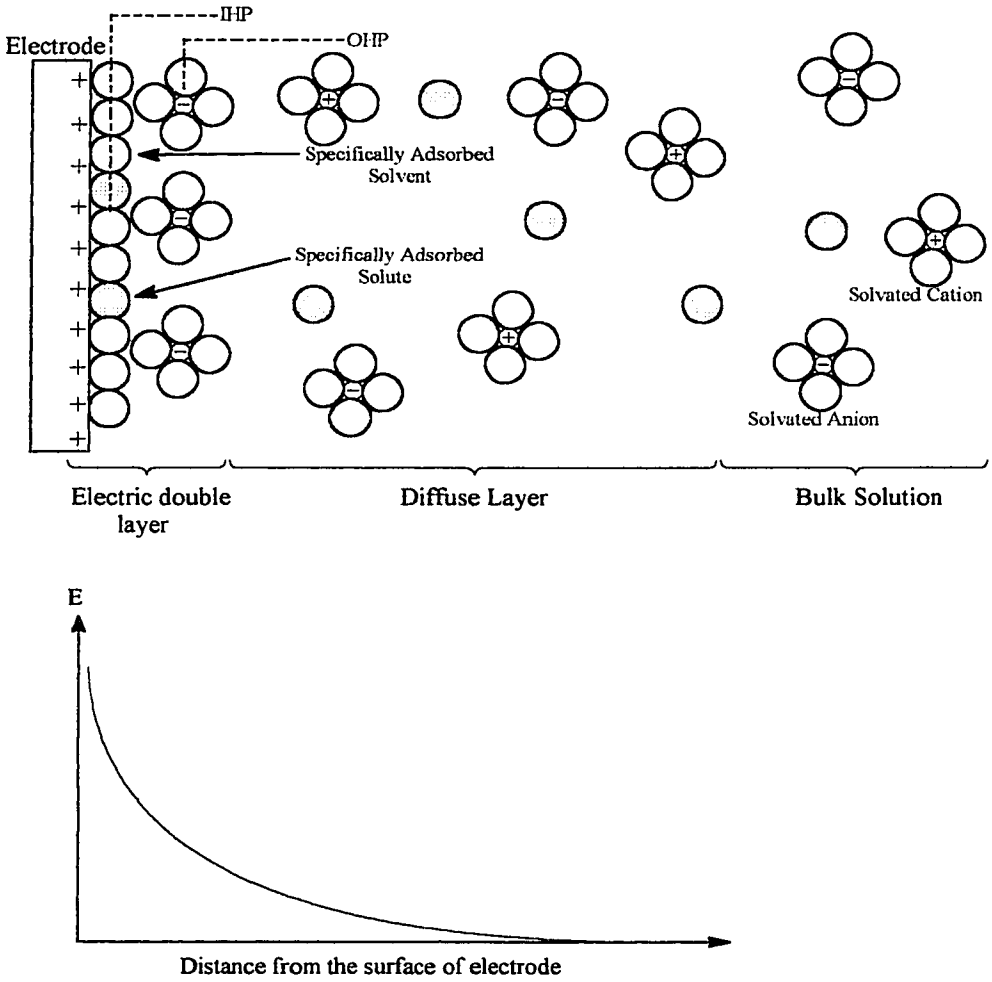

Figure 1.5: The electrode- solution interface (top); Distribution of charge and potential at the electrode-electrolyte interface (bottom).

1.4 Adsorption Phenomena

Many species dissolved in solution exhibit a tendency to adsorb on the electrode surface that can markedly alter the course of an electrode reaction by either enhancing the rate of the electron exchange or inhibiting such a process. Whenever the concentration of a species at the interface is greater than can be accounted for by electrostatic interactions, we speak of specific adsorption[31 (a)]. It is usually caused by chemical interaction between the adsorbate and the electrode, and is then denoted as chemisorption. In some cases adsorption is caused by weaker interactions such as Van Der Waals forces; this is referred to as physisorption. Of course, the solvent is always present at the interface so that the interaction of a substrate with the electrode must be greater than that of the solvent if it is to be adsorbed on the surface of the electrode. Adsorption is responsible for many "unusual" electrochemical behaviors and is frequently blamed for unexplained results. Thus, it is important for the chemist to recognize phenomena that are attributable to adsorption and to realize which techniques are useful for studying the effect of adsorbed species.

1.5 Cyclic Voltammetry

The method of choice to investigate the effect of adsorption in this study was cyclic voltammetry. This technique was employed as a diagnostic tool due to its powerful ability to provide qualitative and quantitative information about electrochemical processes under various conditions[31 (b)]. Furthermore, it can

provide useful information about redox reactions in a form that is easily obtained and interpreted. In cyclic voltammetry, the potential of a stationary working electrode is changed linearly with time, starting from a potential where no electrode reaction occurs and moving to potentials where reduction or oxidation of a solute occurs. After traversing the potential region in which one or more electrode reactions take place, the direction of the linear sweep is reversed and the electrode reactions of intermediates and/or products formed during the forward scan, often can be detected. The time scale of the experiment, controlled by the scan rate and the total potential traversed, can be varied over a range of the order of 10^{2}–10^{-5} s.

CHAPTER 2

EXPERIMENTAL METHODS

2.1 Chemicals

The source and purity of all chemicals used in this research are given in table.2.1 and 2.2. All chemicals were used as received without further purification. Water used in preparing solutions was distilled and deionized. Figure 2.1 illustrates the structures of the model compounds used in this study.

Table 2.1: List of Chemicals, Their Source and Purity.

Chemical	Source	Purity
TiO_2 (P-25)	Degussa	Not Specified
SnO_2 Electrodes	Pittsburgh Plated Glass	50Ω/cm
H_2O_2 (30%)	Caledon	Not Specified
Acetonitrile	Sigma-Aldrich	HPLC grade
Methanol	Fisher Scientific	HPLC grade
Sulfuric Acid	Mallinckrodt	99.99%
Chromic Acid	Fischer Scientific	Reagent grade
Potassium Chloride	Fischer Scientific	Reagent grade
Tetrabutylammonium Hexaflurophosphate	Aldrich	Not Specified

Table 2.2: List of Model Compounds, Their Source and Purity.

Chemical	Source	Purity
4-Chlororesorcinol	Aldrich	98%
4,6-Dichlororesorcinol	Aldrich	97%
Resorcinol	Fisher Scientific	99%
Catechol	Anachemia	99+%
3,4-Dihydroxy benzoic acid	Acros Organics	97%
1,2,4-Benzenetriol	Aldrich	99%

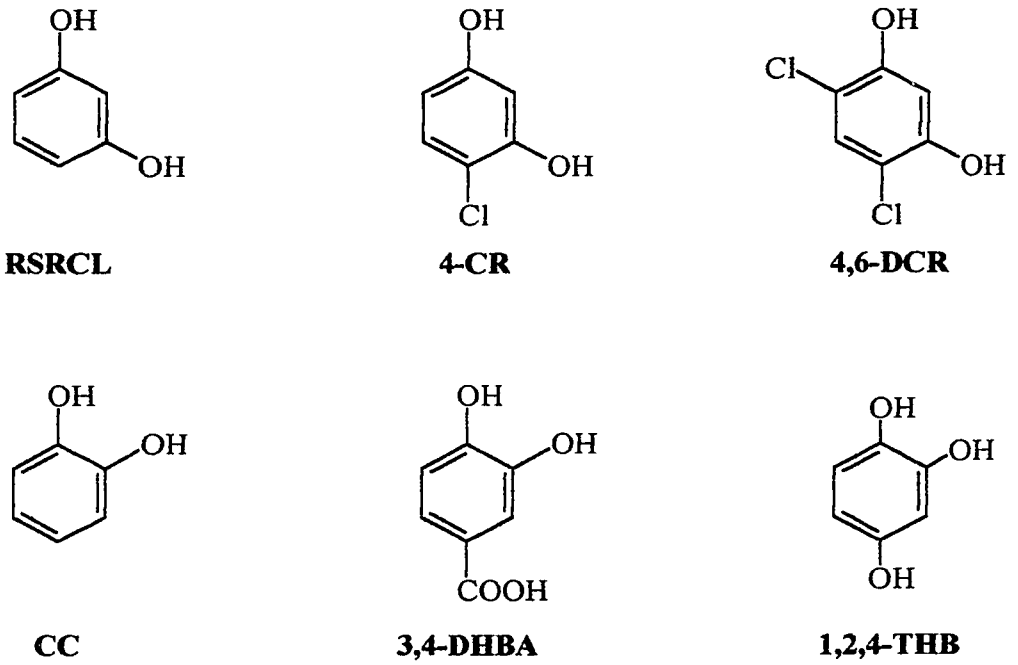

Figure 2.1: Molecular structure of model compounds.

2.2 Preparation of Concentrated Sulfochromic Acid

The concentrated sulfochromic acid was prepared by adding 12 ml of saturated aqueous solution of chromium trioxide acid to 2.7 liter of sulfuric acid. This solution was used to clean the conducting plates (SnO_2 electrodes) and the electrochemical cell.

2.3 Cleaning of SnO_2 Optically Transparent Electrodes (OTE)

SnO_2 glass plates were cut in pieces whose dimensions were 2×3 cm^2. They were placed in sulfochromic acid for 5 minutes and then rinsed with tap water for several minutes. After primary rinsing with tap water, these electrodes were rinsed three times with distilled-deionized water and dried under a stream of nitrogen gas prior to utilization.

2.4 Preparation of TiO_2 Electrodes

Three different types of TiO_2 electrodes were prepared for this work.

2.4.1 Particulate TiO_2 Electrodes

A suspension of TiO_2 powder was prepared by suspending a known amount of Degussa P-25 in water (10g/L) to which 0.5 ml of concentrated HCl was added. The mixture was stirred for about 4 hours prior to use. 0.4 ml of the TiO_2 slurry (cooled to 0 °C in an ice bath) was applied over 2×2 cm^2 area of the conducting electrode's surface and was dried overnight. The TiO_2 coated

electrodes were then sintered at 450°C under ambient atmosphere for one hour. The thickness of TiO_2 layers obtained in this manner were determined to be 22 ±5 μm by scanning electron microscopy. Figure 2.2 illustrates the top and side views of particulate TiO_2 electrodes obtained by scanning electron microscopy.

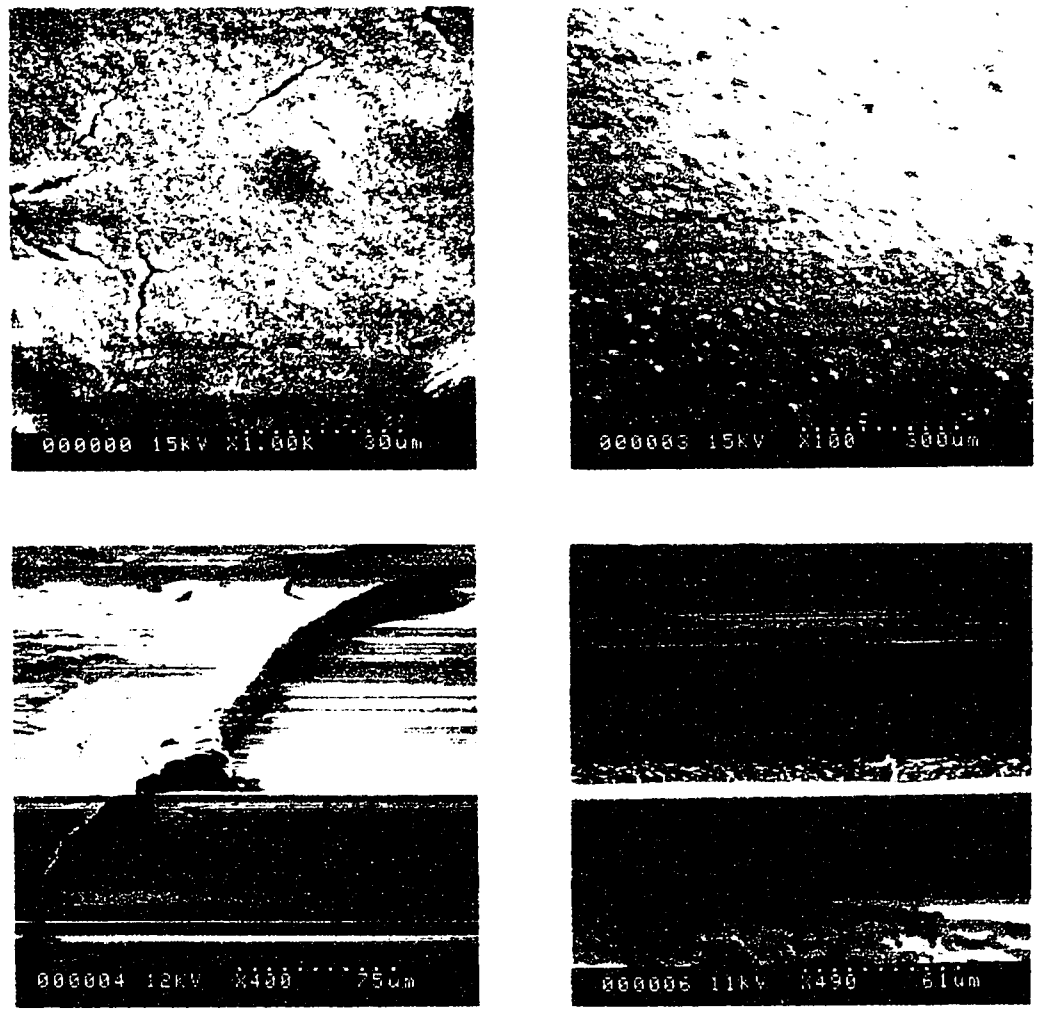

Figure 2.2: scanning electron micrograph of particulate TiO_2 electrode, top view (top micrographs) and side view (bottom micrographs).

2.4.2 Preparation of Glassy TiO_2 Electrodes

An aqueous sol of TiO_2 was prepared by combining water, TiIV(I-Pr)$_4$, and 70% HNO_3 at a ratio of 800ml/66 ml/5.7 ml respectively. The mixture was stirred 3 days until clear suspension was obtained. This suspension was then dialyzed in 3500 M.W-cutoff dialysis tubing for 3 days. Dialyzing water was changed every day. Final sol pH was 3.5. The OTE samples were dipped into the sol until all but ~ 5mm were submerged. The samples were then withdrawn at 2.6 cm/min. and allowed to dry. The coated samples were then fired at 300 °C for one hour.

Profilometry tests on quartz plates coated under identical conditions have characterized coatings of 110 ± 10 nm in thickness. These electrodes were fabricated at the University of Wisconsin, USA. by Mr. L. Miller.

2.4.3 Tandem TiO_2 Electrodes

The glassy TiO_2 electrodes described in the previous section were also coated with TiO_2 (P-25) in the same manner used to prepare particulate TiO_2 electrodes.

2.5 Solutions

The optimal concentration with respect to the variable water solubility of the compounds under study was found to be 0.005M in 0.5M KCl electrolyte. This concentration was used to prepare the solutions employed to determine the

oxidation potential of free substrates. For these experiments, the solutions were prepared on the same day the experiments were performed.

For determination of the oxidation potentials of adsorbed substrates on TiO_2 electrodes, a 0.1M solution of the compound in methanol was used.

2.6 Electrochemical Cell

The electrochemical cell used in this study was a three-electrode cell specifically designed to facilitate the photoelectrochemical experiments. The design of the electrochemical cell is shown in figure 2.3. The cell was made of pyrex glass but the front side which was exposed to light was made of quartz glass. The area of the working electrode in contact with the solution was 0.4 cm^2. The counter electrode was a 0.5 cm^2 platinum foil; a saturated calomel electrode (SCE) was used as reference. The light source used for photoelectrochemical measurements was a 150W Xenon lamp (Bausch and Lomb).

2.7 Instrumentation

A BAS-100A Electrochemical Analyzer (Bioanalytical system) was used to perform Cyclic Voltammetry experiments. The current-voltage response was recorded on a DMP-40 series digital plotter (AMETEK/ HOUSTON Instrument Inc.).

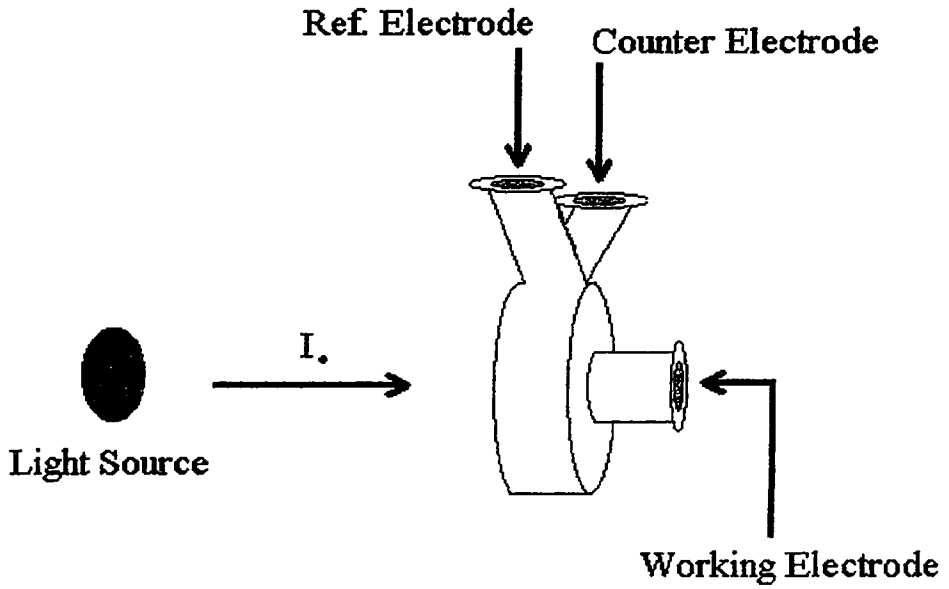

Figure 2.3: Electrochemical Cell used for cyclic voltammetry measurements.

2.8 Method

For determination of the oxidation potential of each substrate in solution, 15±0.5 ml of a 0.005M substrate solution was introduced into the cell. The solution was purged with nitrogen gas for 15 minutes prior to each run. The experiments were carried out in the dark and under illumination.

To determine the effect of adsorption, two consecutive 10 µl portions of a 0.1M substrate solution in methanol was applied on the TiO_2 electrode. The TiO_2 electrode was air-dried for several minutes. The dry electrode was then attached to the cell and a 15 ml aqueous solution containing only 0.5M KCl supporting

electrolyte (pre-purged with N_2 gas) was added prior to the execution of each run. In all cases, a single run was performed at scan rates of 25, 50, 100, 150 and 200 mV/S. Each scan was recorded using a fresh electrode All the oxidation potentials reported in this study are vs. SCE reference electrode.

CHAPTER 3

RESULTS AND DISCUSSION: PART I

3.1 General Concepts

Figure 3.1 shows a typical voltammogram. In this voltammogram, the oxidation or reduction potential is taken at the maximum current for the oxidation or reduction peak.

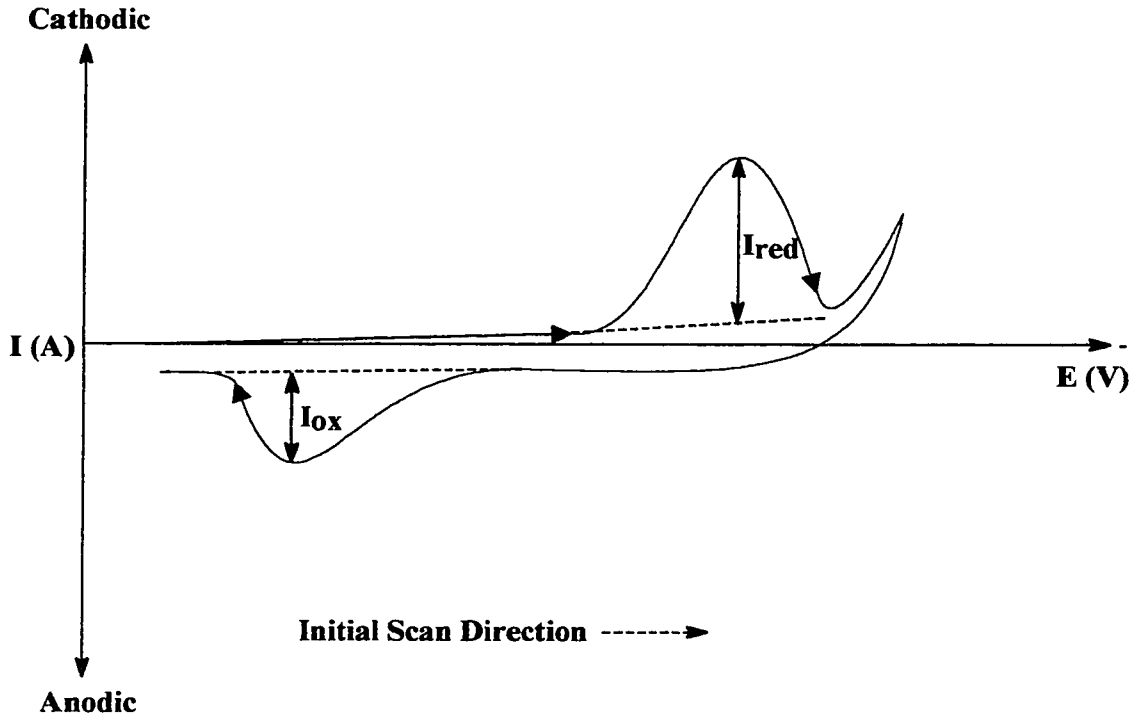

Figure 3.1: A typical cyclic voltammogram.

The working potential ranges were determined by running voltammograms using supporting electrolyte only. These working ranges were found to be –0.30V to 1.70V for particulate and tandem TiO_2

electrodes, 0.30V to 1.70V for glassy TiO_2 electrode, and –0.30V to 1.20V for Pt electrode. No oxidations were observed in these potential ranges for the supporting electrolyte itself, regardless of whether the voltammogram was taken in the dark or under illumination. Figures 3.2 and 3.3 illustrate the voltammograms of 0.5M KCl electrolyte on TiO_2 and Pt electrodes respectively.

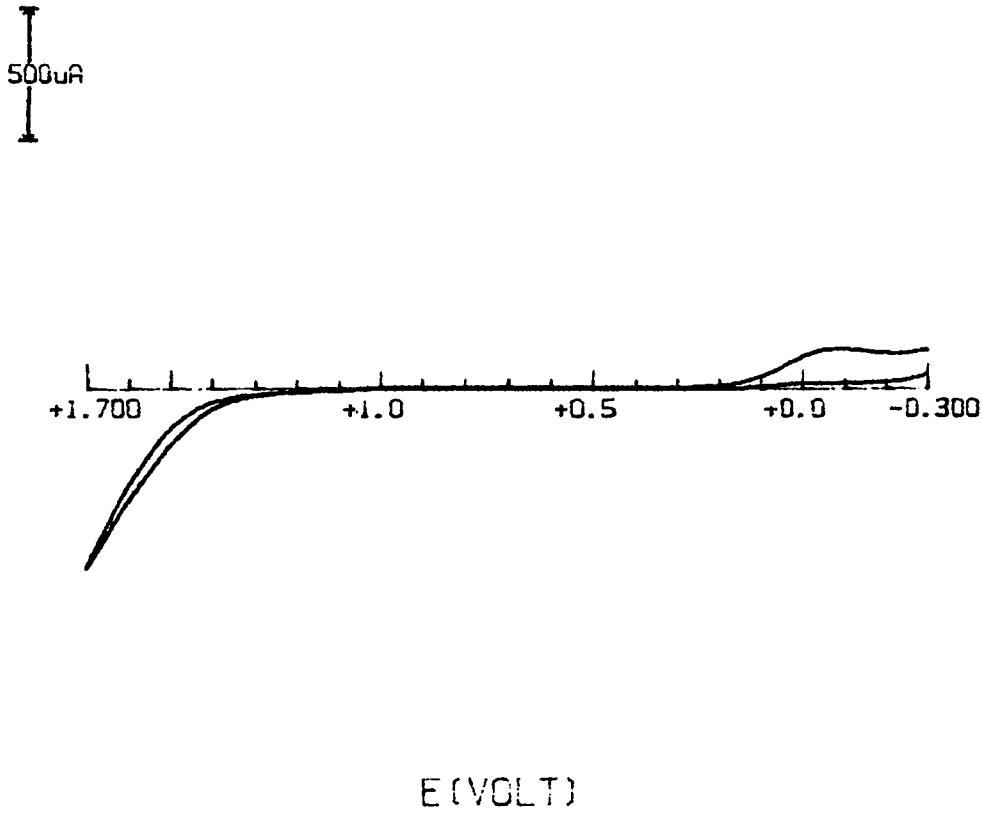

Figure 3.2: Voltammogram of 0.5M KCl electrolyte on a TiO_2 electrode. Scan rate = 100 mV/S.

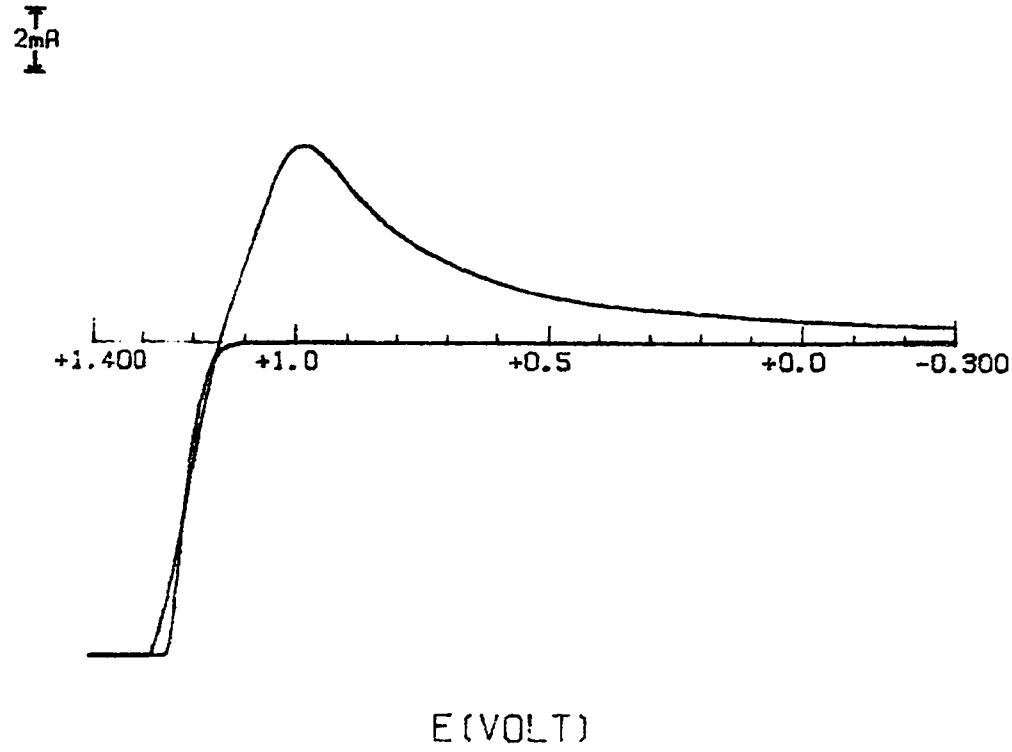

Figure 3.3: Voltammogram of 0.5M KCl electrolyte on a Pt electrode. Scan rate = 100 mV/S.

The working potential window was also determined for the particulate TiO_2 electrodes in acetonitrile solution. The working range was found to be from –0.30V to 2.80V. Figure 3.4 depicts the Voltammogran of 0.5M Tetrabutylammonium Hexaflurophosphate (TBAHFP) electrolyte in acetonitrile on a particulate TiO_2 electrode.

The reduction peak seen in figure 3.2 at about –0.08V may be due to the reduction of hydrogen in an aqueous solution[32 (a)]. Furthermore,

the reduction peak seen in figure 3.3 on a Pt electrode is a consequence of oxygen evolution on this electrode in an aqueous solution[32 (a)].

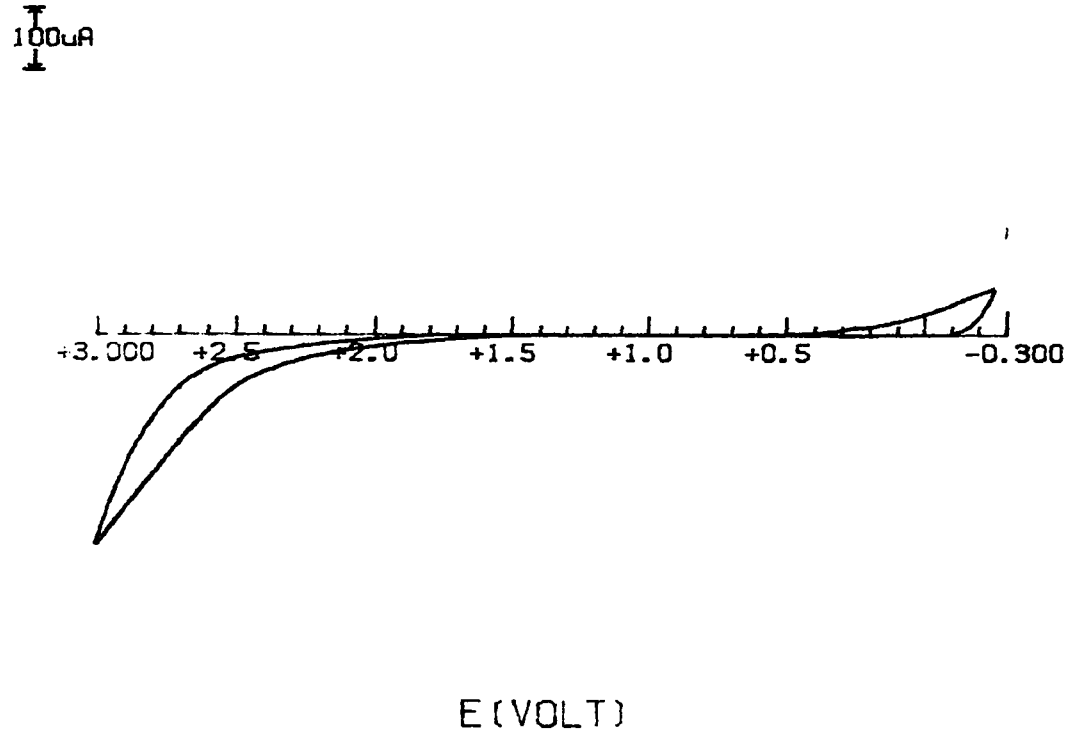

Figure 3.4: Voltammogram of 0.5M TBAHFP in acetonitrile on a TiO_2 electrode.

Three different types of TiO_2 electrodes (particulate TiO_2, glassy TiO_2, and tandemTiO_2 electrodes) were employed to ascertain the origin of oxidation peaks on the working electrode. Our studies indicate that the oxidation potentials observed are solely due to oxidation of model compounds at the top TiO_2 layer and not to oxidation of material that penetrated through this layer onto the SnO_2 OTE. The voltammogram of 4-CR on glassy TiO_2, tandem TiO_2 and particulate TiO_2 electrodes are

shown in figure 3.5a, 3.5b and 3.5c respectively. If one compares voltammograms 3.5a and 3.5b, one sees that the working potential window for the glassy TiO_2 electrode is reduced by approximately 0.6V towards the negative potential, compared to that of the particulate (3.5b) and tandem TiO_2 electrodes (3.5c). The voltammogram of a particulate TiO_2 electrode is similar to that of a tandem TiO_2 electrode, indicating that the observed potentials and currents are originating from the same source, which in this case would be the top particulate TiO_2 layer (P-25).

To determine the effect of pH, adsorption, and illumination on the oxidation potentials of the organic compounds at TiO_2, two sets of compounds have been chosen. The first set consisted of Resorcinol (RSRCL), 4-Chlororesorcinol (4-CR) and 4,6-Dichlororesorcinol (4,6-DCR) for which the hydroxyl groups present on the benzene ring are in meta position with respect to one another. The second set consisted of Catechol (CC), 3,4-Dihydroxybenzoic acid (3,4-DHBA) and 1,2,4-Benzenetriol (Trihydroxybenzene, 1,2,4-THB) for which the hydroxyl groups are in ortho position (with the exception of 1,2,4-THB). The stereochemical configuration of the latter three compounds favors chemisorption on the TiO_2 surface[33]. Correlation of the peak currents (I_p) to the square root of scan rates ($\nu^{1/2}$), in accordance with the Randles-Sevcik equation (3.1), was used to analyze the obtained data[34] ;

$$I_p = 2.69 \times 10^5 \, n^{3/2} \, A \, C_o \, D^{1/2} \, \nu^{1/2} \qquad (3.1)$$

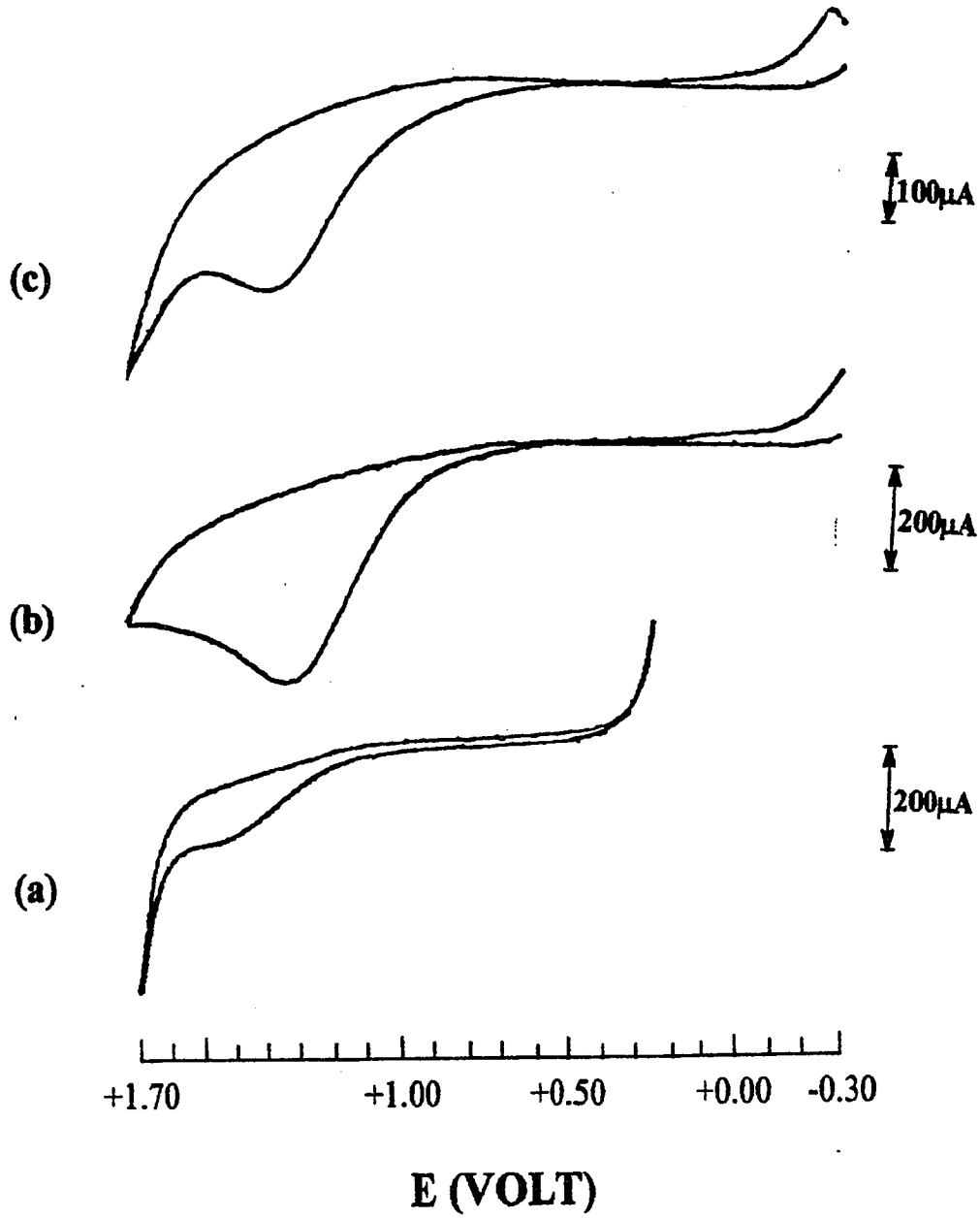

Figure 3.5: Voltammogram of 4-CR on, a) glassy TiO_2, b) tandem TiO_2, c) particulate TiO_2

where I_p is the peak current, n is the number of electrons being transferred, A is the surface area of the electrode in contact with the solution, C_o is the bulk concentration of the analyte, D is the diffusion coefficient, and ν is the scan rate. A plot of I_p vs. $\nu^{1/2}$ should be linear for diffusion-controlled processes with zero-intercept; a deviation from this behavior is expected for adsorbed species.

CHAPTER 4

RESULTS AND DISCUSSION: PART II

WEAKLY ADSORBED MODEL COMPOUNDS

The electrochemical and photoelectrochemical behaviors of weakly adsorbed organic compounds have been investigated under various conditions. The compounds chosen for these analyses consist of RSRCL, 4-CR and 4,6-DCR. Their behaviors under different conditions are discussed in the subsequent sections. Section 4.6 gives the scan rate dependencies of the observed oxidation waves obtained by cyclic voltammetry for the above-mentioned compounds.

4.1 Electrochemical Behaviors of Model Compounds on Pt and TiO_2 Electrodes

The electrochemical behaviors of model compounds on Pt electrodes were examined in an unbuffered solution for comparison to those obtained on TiO_2 electrodes. The initial pH of these solutions ranged form 5.8 to 6. All compounds exhibit a single oxidation peak on Pt electrodes with no reduction peak; a sample voltammogram is shown in figure 4.1. In all cases a linear relationship between I_p and $\nu^{1/2}$ was observed in accordance with the Randles-Sevcik equation, with correlation coefficients ranging from 0.98 to 0.99. The absence of a reduction peak is suggestive of a chemical reaction following the electrode reaction.

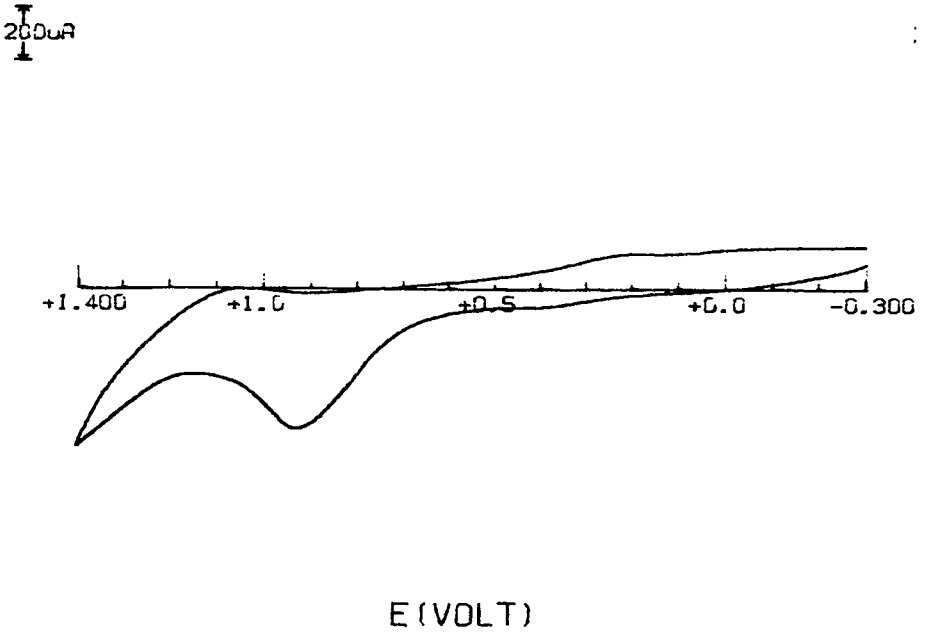

Figure 4.1: Voltammogram of RSRCL on a Pt electrode at pH 6. Scan rate = 100 mV/S.

Similar behaviors were encountered on TiO_2 electrodes in the dark for selected compounds. Single oxidation peaks were also observed for these compounds on TiO_2 electrodes. A sample voltammogram is given in figure 4.2. The peak potentials located for these substrates on TiO_2 electrodes were positioned at higher potentials as compared to those on Pt electrodes. The differences could be attributed to the difference in conductivity of the two electrodes, where Pt has a higher conductivity as compared to TiO_2, therefore less energy is required to remove an electron from the organic compounds present in the diffusion layer. Correlation between I_p and $\nu^{1/2}$ for these compounds on Pt and TiO_2 electrodes as

well as I_p versus ν on TiO_2 electrodes are given in figures 4.3, 4.4 and 4.5 respectively.

Although, the plots of I_p versus ν (figure 4.5) show some linearity, the non-zero y-intercepts clearly indicate that these oxidation peaks are due to diffusion-controlled phenomena rather than to adsorption

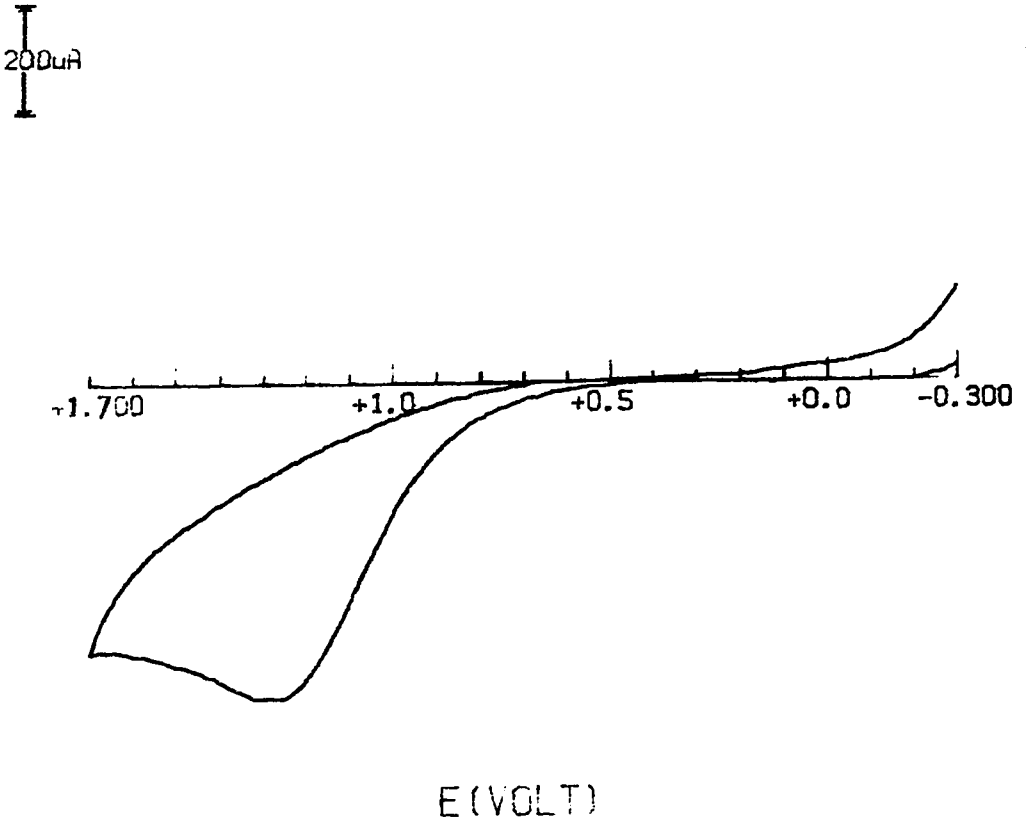

Figure 4.2: Voltammogram of 4-CR on a TiO_2 electrode at pH 6. Scan rate = 100 mV/S.

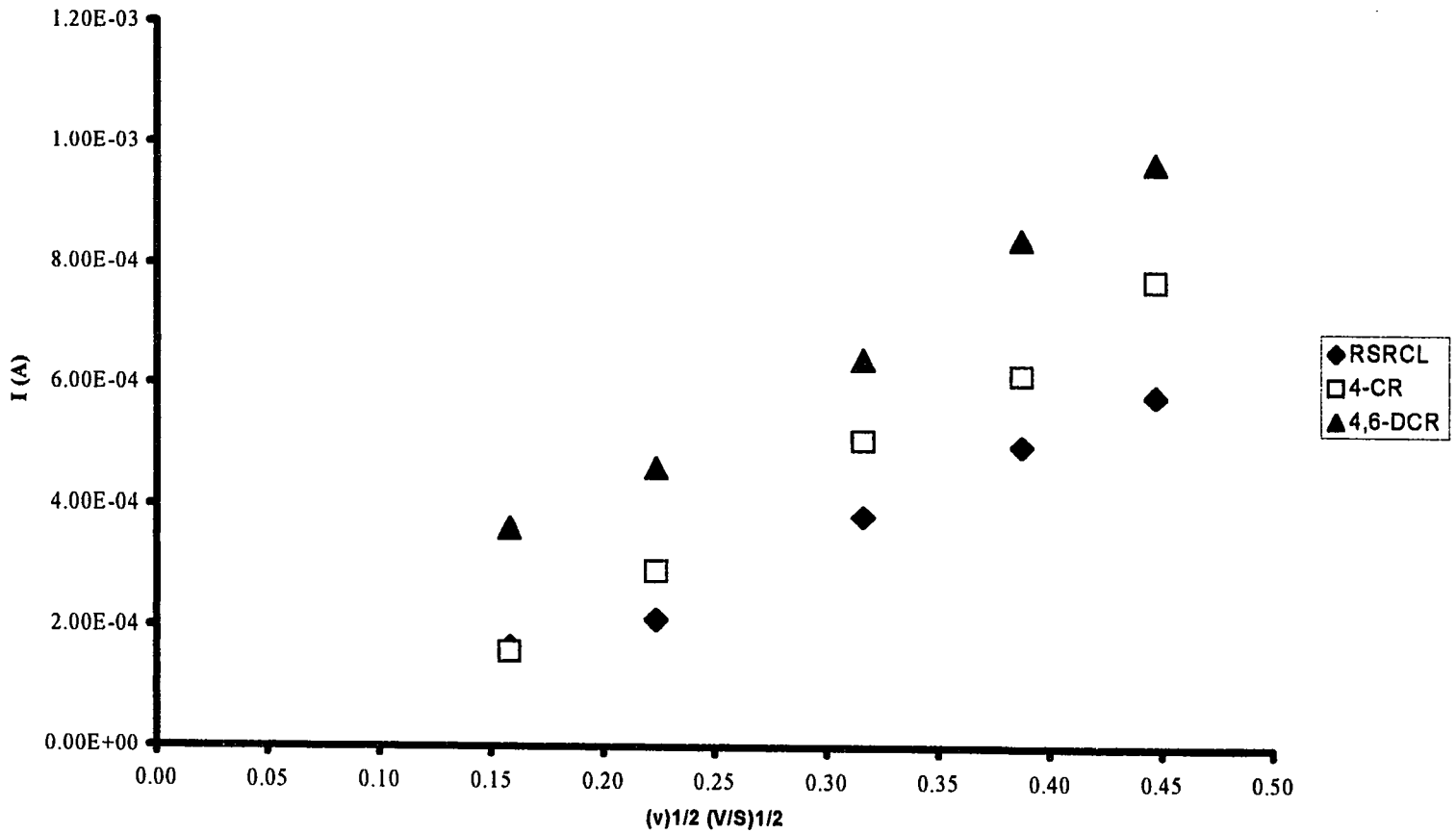

Figure 4.3: I_p vs. $v^{1/2}$ for model compounds on Pt electrodes.

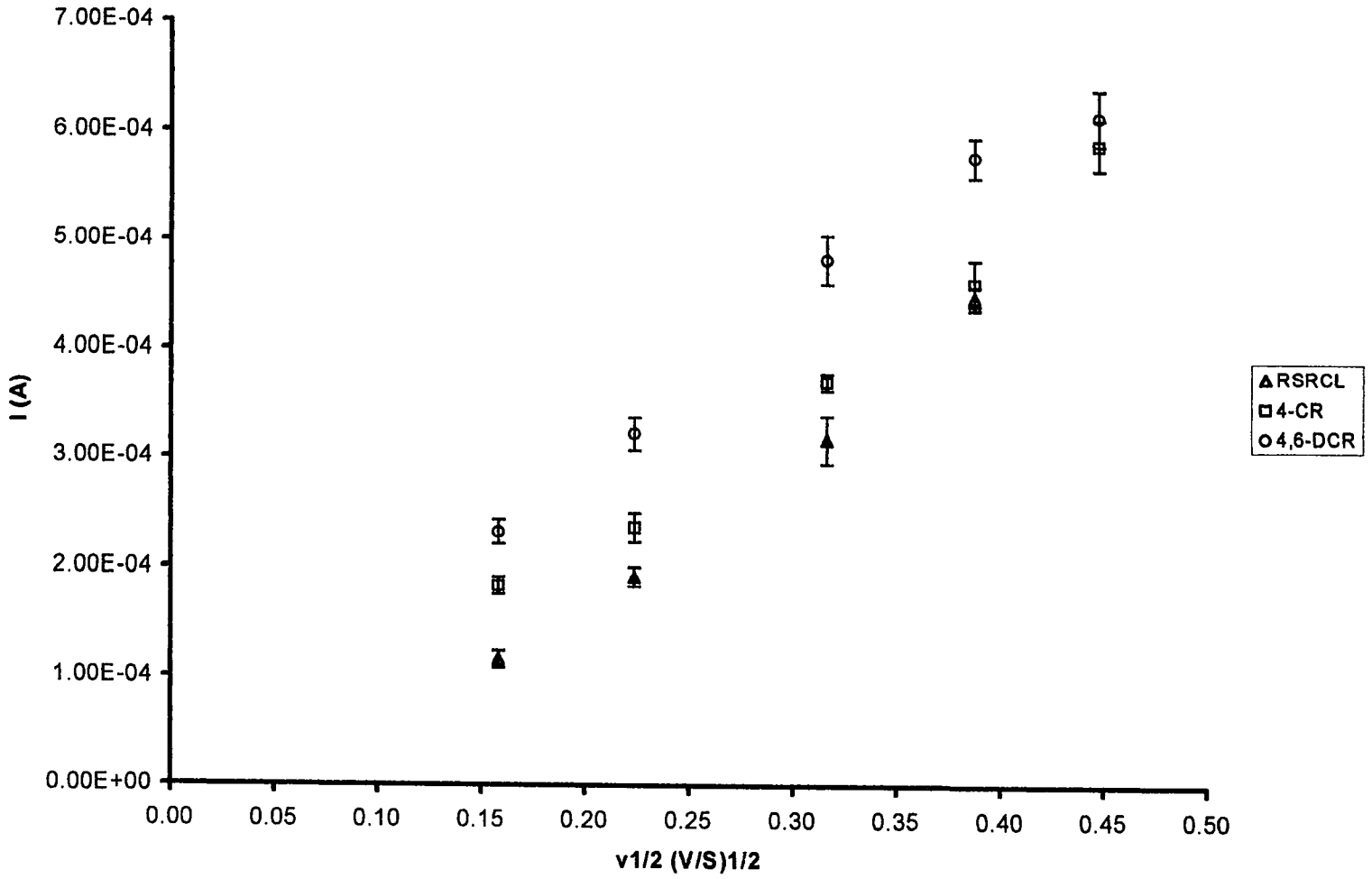

Figure 4.4: I_p vs. $v^{1/2}$ for model compounds on TiO_2 electrodes

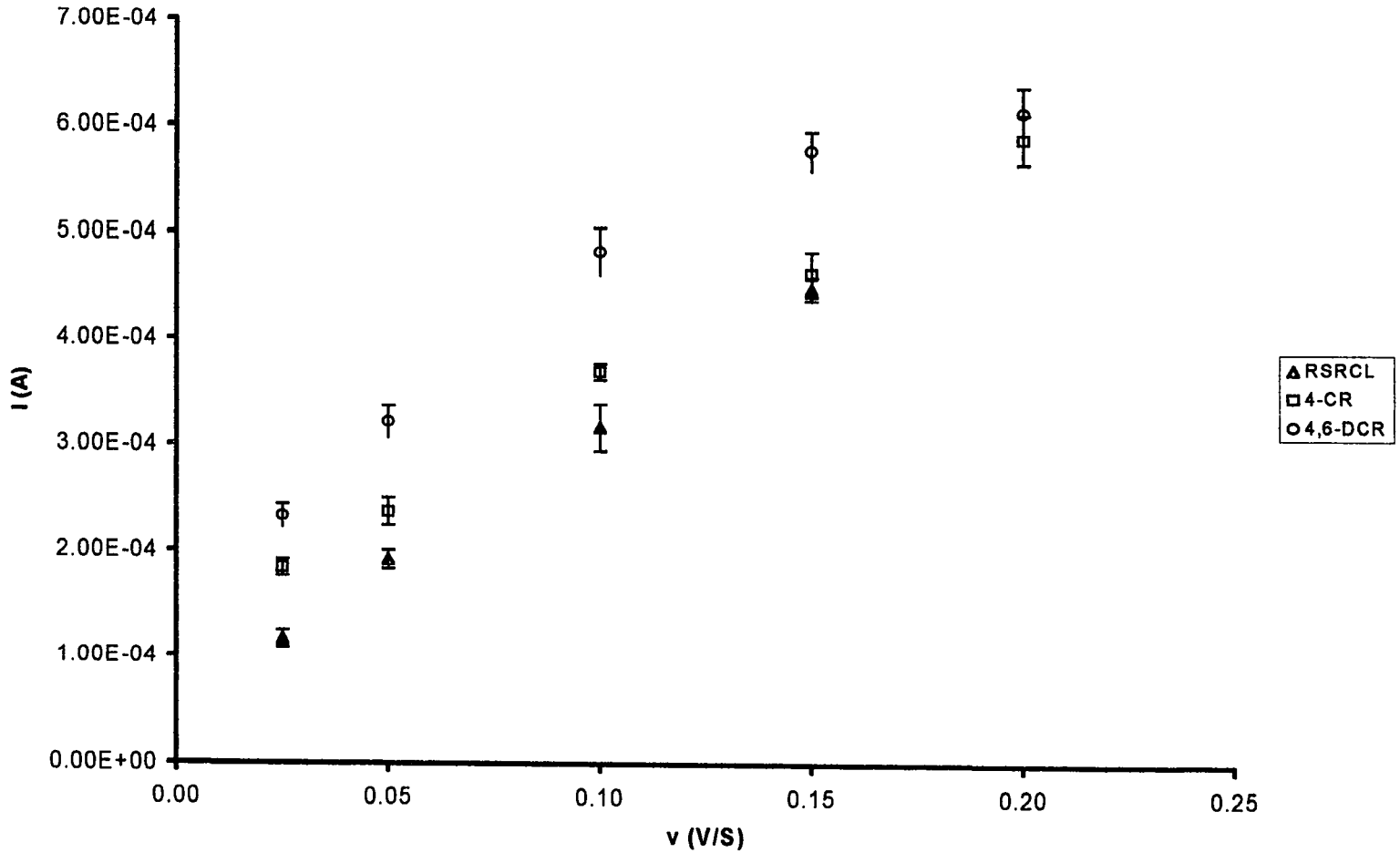

Figure 4.5: I_p vs. v for model compounds on TiO_2 electrodes.

4.2 Effect of Adsorption

The effect of adsorption on the oxidation potentials of model compounds on TiO_2 electrodes have been examined in the dark. For these experiments, the electrodes were prepared as described in the experimental section. Additional peaks were detected for 4-CR and 4,6-DCR under these conditions. However, the voltammograms of RSRCL remained unchanged. Figure 4.6 illustrates a voltammogram for adsorbed 4-CR.

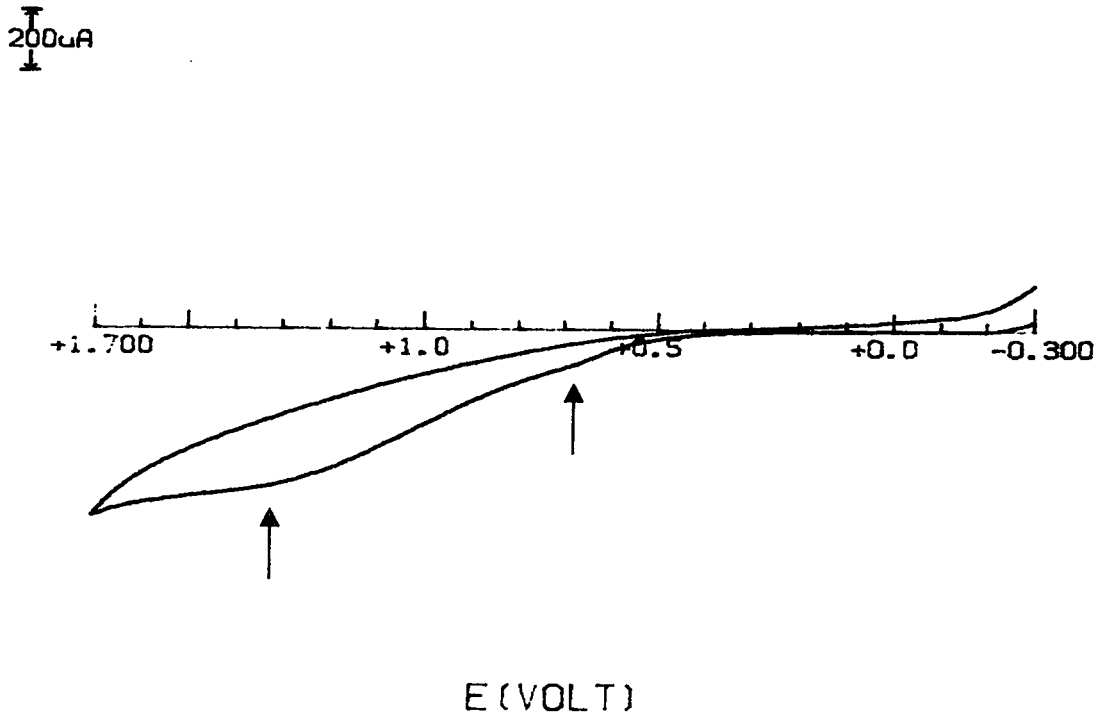

Figure 4.6: Voltammogram of adsorbed 4-CR on a TiO_2 electrode at pH 6. Scan rate = 100 mV/S.

Since two oxidation peaks have been observed (as indicated by the arrows in figure 4.6) for both adsorbed 4-CR and adsorbed 4,6-DCR, their oxidation potentials were compared to those obtained for free organics. Close agreement between the oxidation potentials of free organics with those at most positive potentials under adsorption conditions indicates that they are both due to diffusion-controlled processes.

It has been stated by Shain and coworkers[35] that the adsorption of a reactant produces an oxidation peak at lower potential compared to the oxidation peak for free organics. Such behavior has been observed for 4-CR and 4,6-DCR. The oxidation peaks detected at 0.65 V-0.70 V (depending on the scan rate) were only found for adsorption experiments. These observations strongly suggest that these oxidation peaks are originating from adsorbed initial reactants. Furthermore, the magnitude of the peak currents compared to peak currents obtained for free compounds, as well as the unusual behavior of these peaks with respect to the Randles-Sevcik equation (peak current dependency on the square root of scan rate) provides additional support for this conclusion.

The stereochemical configuration of these compounds do not allow for chemisorption (as discussed in chapter 3), therefore the adsorption is attributed to weak Van Der Waals interactions of these organic molecules with the surface of the TiO_2 electrodes[36,37]. The presence of electronegative elements (chlorine and oxygen) on the benzene ring

results in a dipole moment which may be responsible for the weak adsorption of these compounds on the surface of the TiO_2 electrodes[38]. The polarity created by the electronegativity of the oxygens on RSRCL is likely offset by the electropositivity of the attached hydrogens, in conjunction with the resonance effect of the benzene ring[37]. Therefore, no net dipole moment would be present, which may explain the absence of adsorption peaks for RSRCL. On the other hand, 4-CR and 4,6-DCR contain chlorine in addition to oxygen. The presence of chlorines on the ring strongly affects the charge density distribution, creating a net dipole moment on these compounds[38,39]. The interaction between these polar molecules with the surface of the TiO_2 electrode could be responsible for the observed adsorption peaks.

The peak current dependency on the square root of the scan rate was used to further analyze the electrochemical behavior of these compounds on the TiO_2 electrodes. Figure 4.7 illustrates these analyses. It has been described by Shain and coworkers[35], that the surface area of the electrode exposed to the solution limits the amount of adsorbate[20]. In these experiments, a large concentration of organic compound is initially deposited on the surface of the electrode and as soon as the electrolyte is added to the system, the excess material diffuses into the solution and manifests itself as a diffusion-controlled oxidation peak. Therefore two peaks are observed. It should be noted that in these adsorption experiments the presence of adsorbed species on the electrode surface is

an imposed condition. Therefore, the amount of adsorbed species on the electrode surface varies with time due to diffusion of these materials into the solution from the point at which contact is made with the electrolyte. Thus, the oxidation peak due to adsorption shows little or no increase in peak current upon an increase in the scan rate, as should normally be observed for a constant concentration of redox species, while the one due to diffusion shows a linear increase with $v^{1/2}$ (peaks at most positive potentials for 4-CR and 4,6-DCR).

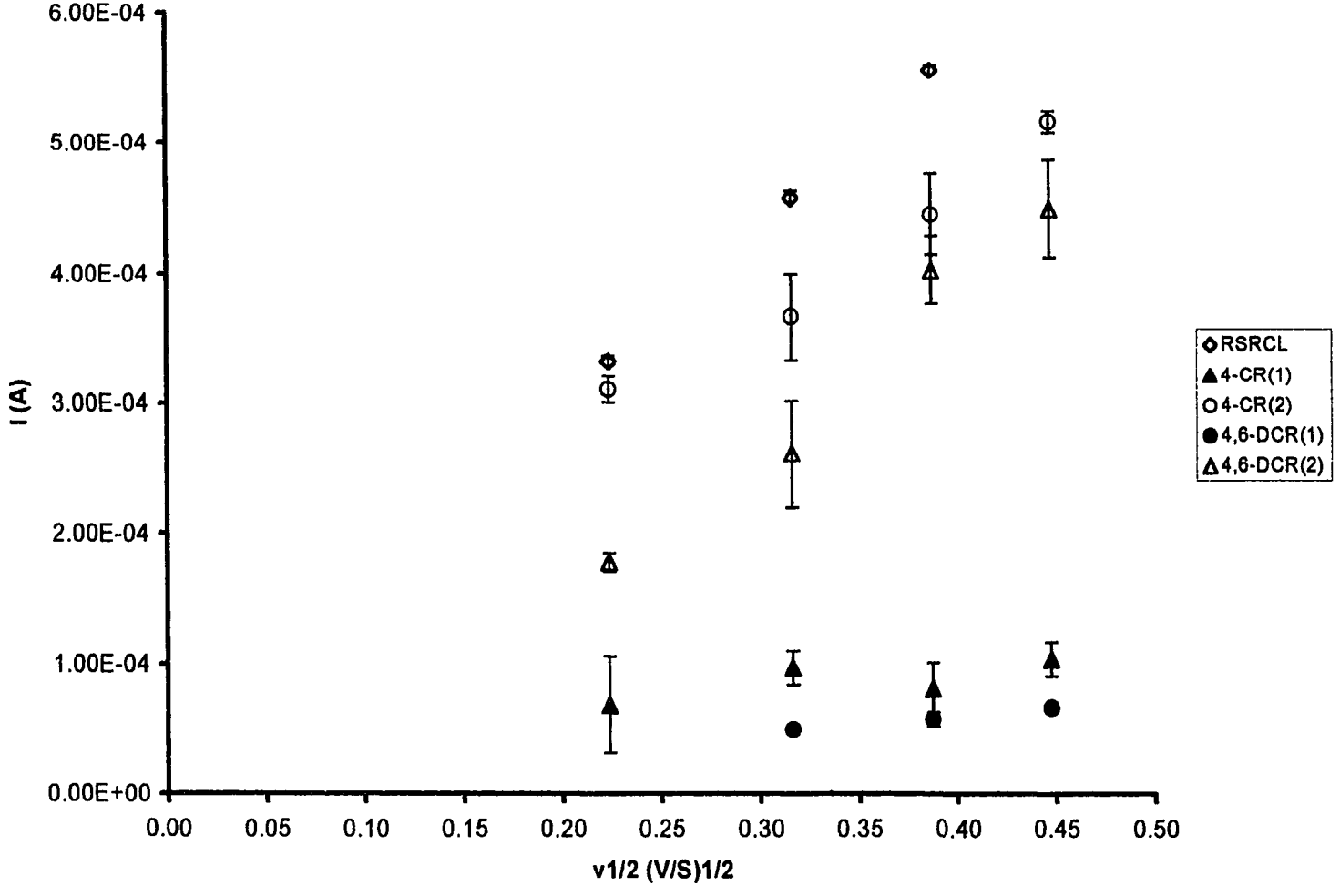

Figure 4.7: I_p vs. $v^{1/2}$ for adsorbed model compounds on the TiO_2 electrodes

4.3 Effect of Illumination

The oxidation of model compounds on TiO_2 electrodes also has been studied under illumination and was compared to those obtained in the dark. The correlation between I_p and $v^{1/2}$ was found to be in agreement with the behavior expected for diffusion-controlled oxidation. A shift in the baseline was detected for the oxidation of these compounds upon illumination of TiO_2, illustrating the photoactivity of the semiconductor electrode[30 (b)]. Figure 4.8 shows a sample voltammogram of 4-CR under illumination (see figure 4.2 for comparison)

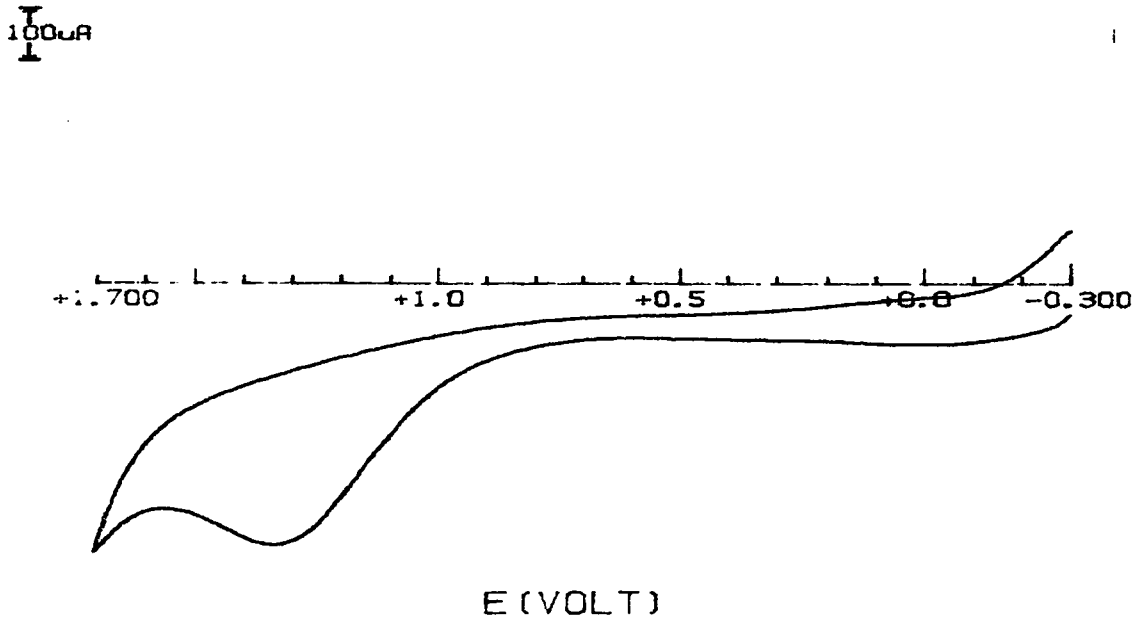

Figure 4.8: Voltammogram of 4-CR on an illuminated TiO_2 electrode at pH 6. Scan rate = 100 mV/S.

The magnitude of the generated photocurrent seems to be influenced by the nature of the organic compounds present in solution. A maximum baseline shift of about 100μA was observed for 4-CR compared to RSRCL and 4,6-DCR, which may be attributed to its greater ability to adsorb, as indicated by the dark response.

The oxidation potentials of these organic compounds on illuminated TiO_2 remains the same compared to those obtained in the dark. A shift in flat band potential was expected for TiO_2 under illumination, which would consequently result in a shift in the observed oxidation potentials[40]. The absence of such a shift in potential may be due to the relatively low light intensity used in these experiments or the inability of the organic species present in solution to accept photo-generated minority carriers at the electrode surface[40-42].

Shifts in the oxidation peak currents were detected under illumination compared to those measured in the dark. The difference between the magnitude of peak currents observed under illumination and in the dark ($I_i - I_d$) tends to decrease in parallel with the increasing number of chlorine atoms present on the benzene ring. This effect is shown in figure 4.9 where the difference in peak currents between photoelectrochemical (I_i) and the dark electrochemical (I_d) experiments were plotted against the scan rate. According to these observations, the oxidation efficiency of the TiO_2 electrodes under illumination decreases with the increasing number of chlorine on the benzene ring.

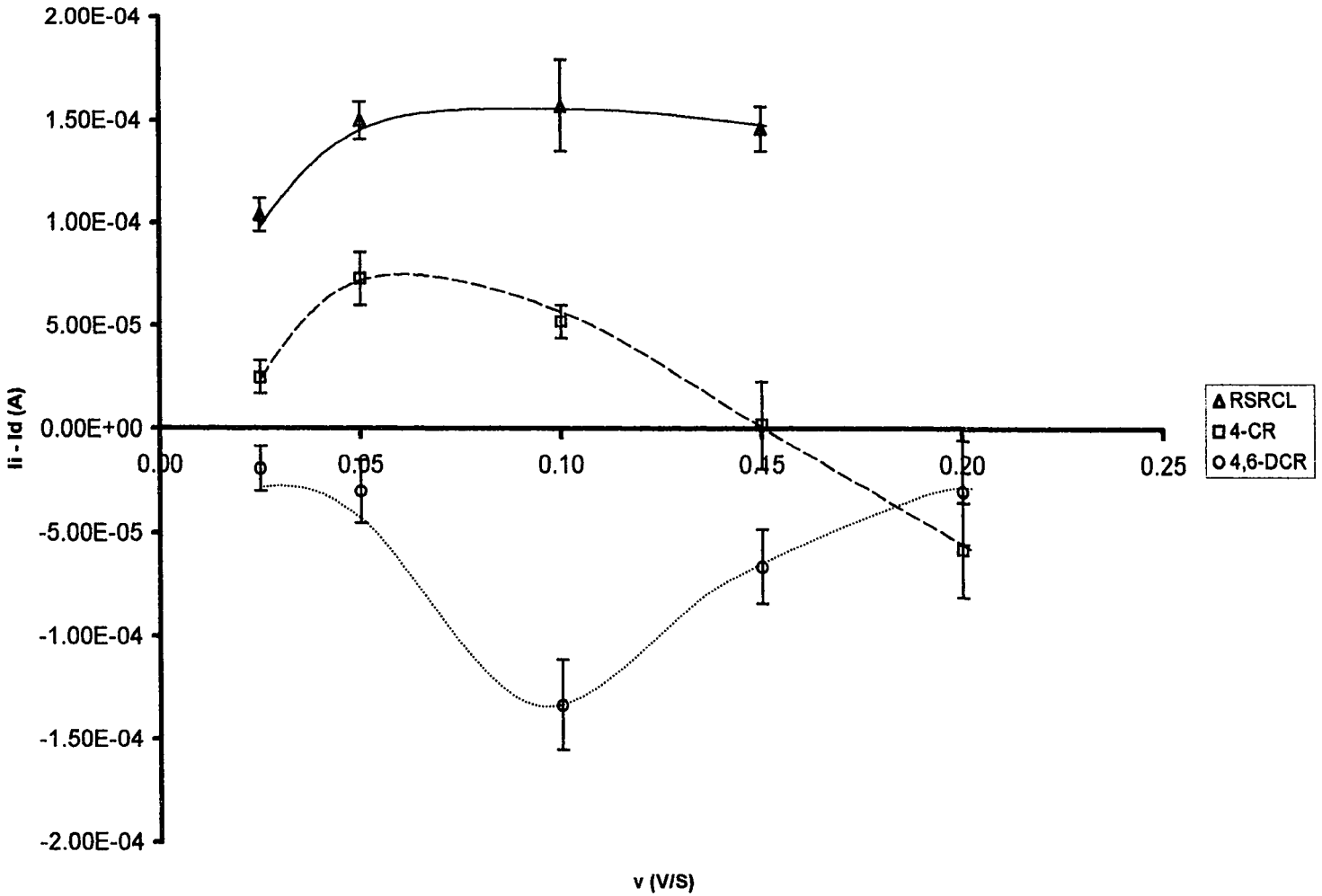

Figure 4.9: (I_i-I_d) vs. scan rate for model compounds on the illuminated TiO_2 electrodes.

4.4 Effect of pH

A single compound was chosen to investigate the effect of pH on the oxidation potentials of the weakly adsorbed compounds on the TiO_2 electrodes. 4-CR was chosen for these experiments, since its oxidation peaks were well resolved under various pH's, allowing more accurate measurement of the peak currents and potentials. The oxidation currents and potentials of 4-CR were first measured on a Pt electrode at pH 3 and pH 6, which were compared to those obtained on the TiO_2 electrodes under similar conditions. Increases in the peak currents were observed at lower pH due to the pH sensitive nature of phenols and quinones redox reactions[43]. However, no changes in the oxidation potentials were detected. Similar behaviors with respect to peak currents were also seen for the oxidation of this compound on the TiO_2 electrodes in the dark, under illumination, and in the adsorbed state. Unlike its behavior on the Pt electrodes, however, the oxidation potentials seemed to increase with decreasing pH. For a metal oxide semiconductor electrode in contact with an aqueous solution the band positions (E_{CB} and E_{VB}) are known to be pH dependent[44, 45]. The position of these bands shift by an amount equal to -0.06× pH in accordance to the equation 4.1[44].

$$\mathbf{E_{CB} = -0.50 - 0.06\ (pH)} \qquad \mathbf{4.1}$$

A shift in band positions would also shift the oxidation potentials of the species being oxidized on the TiO_2 electrodes. Based on this

equation, a shift of -0.18 V in the oxidation potential is expected as one moves from pH 3 to pH 6. The observed shift in peak potentials varies from 0.06 V to 0.18 V depending on the scan rate at which they are measured. The deviation from calculated shifts in the oxidation potentials may be attributed to the process of surface states (surface defects) on the TiO_2 electrodes, which may affect the redox reaction of the organic compounds on these electrodes[46]. The increase in the peak currents at lower pH may be accounted for by the effect of pH on the surface characteristic of TiO_2. Since TiO_2 possesses both acidic and basic properties, the surface is positively charged at pHs below the point of zero charge (pH 6)[47]. At pH 6 it is neutral and above pH 6 the surface is negatively charged. Because at pH 3 the surface is positively charged, a larger interaction is expected between this surface and the polar 4-CR as compared to that at pH6, where the surface is neutral.

4.5 Summary

RSRCL, 4-CR and 4,6-DCR were chosen to investigate the oxidation of weakly adsorbed organic compounds on the TiO_2 electrodes under various conditions. Similar redox behaviors were seen for these compounds on Pt and TiO_2 electrodes. The oxidation potentials of these compounds occur at higher potentials on TiO_2 compared to Pt electrodes due to higher conductivity of Pt electrodes. Adsorption oxidation peaks were observed for 4-CR and 4,6-DCR under imposed adsorption conditions at about 0.60 V to 0.75 V, depending on the scan rate and the compound under investigation. No adsorption was detected for RSRCL under these conditions. The magnitude of the adsorption peak currents seemed to be affected by the polarity of the compound. Photoactivity of TiO_2 was confirmed by the baseline shift observed under illumination. An increase in the oxidation peak currents were detected for these compounds on the illuminated TiO_2, but the magnitude of the photo-generated peak currents were found to be dependent on the polarity of the organic compound in solution. 4-CR was used to study the effect of pH on the oxidation potentials. Higher oxidation currents were observed at pH 3 due to the positively charged surface of TiO_2 particles at this pH compared to pH 6. A shift of about -0.08 v to -0.18 V in oxidation potentials were noticed as the pH of solution was changed from pH 3 to pH 6.

4.6 Tables

Table 4.1: Oxidation potentials and peak currents for RSRCL at pH 6. Working electrode = Pt.

Scan Rate (V/S)	E (V)	$I \times 10^{-4}$(A)
0.025	0.87	1.67
0.050	0.87	2.12
0.100	0.93	3.83
0.150	0.96	5.00
0.200	0.97	5.83

Table 4.2: Oxidation potentials and peak currents for RSRCL at pH 6. Working electrode = TiO_2.

Scan Rate (V/S)	E (V)	$I \times 10^{-4}$(A)
0.025	1.14±0.01	1.17±0.08
0.050	1.23±0.01	1.92±0.09
0.100	1.33±0.01	3.17±0.22
0.150	1.44±0.01	4.48±0.11
0.200	----------	----------

Table 4.3: Oxidation potentials and peak currents for RSRCL under illumination at pH 6. Working electrode = TiO_2.

Scan Rate (V/S)	E (V)	$I \times 10^{-4}$(A)
0.025	1.14±0.01	2.21±0.04
0.050	1.26±0.02	3.42±0.09
0.100	1.33±0.02	4.74±0.16
0.150	1.45±0.00	5.94±0.11
0.200	----------	----------

Table 4.4: Oxidation potentials and peak currents for adsorbed RSRCL at pH 6. Working electrode = TiO_2.

Scan Rate (V/S)	E (V)	I $\times 10^{-4}$ (A)
0.050	1.15±0.01	3.33±0.04
0.100	1.30±0.02	4.58±0.05
0.150	1.37±0.02	5.57±0.04
0.200	----------	----------

Table 4.5: Oxidation potentials and peak currents for 4-CR at pH 6. Working electrode = Pt.

Scan Rate (V/S)	E (V)	I $\times 10^{-4}$(A)
0.025	0.78	1.58
0.050	0.83	2.92
0.100	0.88	5.08
0.150	0.90	6.17
0.200	0.95	7.75

Table 4.6: Oxidation potentials and peak currents for 4-CR at pH 6. Working electrode =. TiO_2.

Scan Rate (V/S)	E (V)	I $\times 10^{-4}$(A)
0.025	1.22±0.02	1.84±0.08
0.050	1.23±0.04	2.37±0.13
0.100	1.36±0.04	3.70±0.08
0.150	1.41±0.03	4.62±0.21
0.200	1.50±0.01	5.89±0.23

Table 4.7: Oxidation potentials and peak currents for 4-CR under illumination at pH 6. Working electrode =. TiO_2.

Scan Rate (V/S)	E (V)	I $\times 10^{-4}$(A)
0.025	1.27±0.00	2.09±0.00
0.050	1.31±0.06	3.10±0.19
0.100	1.35±0.03	4.22±0.14
0.150	1.41±0.03	4.64±0.37
0.200	1.42±0.00	5.31±0.12

Table 4.8: Oxidation potentials and peak currents for adsorbed 4-CR at pH 6. Working electrode =. TiO_2.

Scan Rate (V/S)	E_1 (V)	$I_1 \times 10^{-4}$ (A)	E_2 (V)	$I_2 \times 10^{-4}$ (A)
0.050	0.63±0.02	0.69±0.37	1.28±0.01	3.11±0.10
0.100	0.66±0.01	0.97±0.13	1.27±0.02	3.67±0.33
0.150	0.65±0.00	0.81±0.20	1.29±0.04	4.46±0.31
0.200	0.66±0.01	1.04±0.13	1.41±0.01	5.17±0.08

Table 4.9: Oxidation potentials and peak currents for 4-CR at pH 3. Working electrode = Pt.

Scan Rate (V/S)	E (V)	$I \times 10^{-4}$(A)
0.025	0.82	2.13
0.050	0.84	2.92
0.100	0.90	5.83
0.150	0.93	7.17
0.200	0.96	8.50

Table 4.10: Oxidation potentials and peak currents for 4-CR at pH 3. Working electrode =. TiO_2.

Scan Rate (V/S)	E (V)	$I \times 10^{-4}$(A)
0.025	1.36±0.00	1.50±0.09
0.050	1.41±0.01	2.68±0.05
0.100	1.40±0.01	4.14±0.14
0.150	1.46±0.03	5.25±0.23
0.200	1.49±0.04	6.21±0.24

Table 4.11: Oxidation potentials and peak currents for 4-CR under illumination at pH 3. Working electrode =. TiO_2.

Scan Rate (V/S)	E (V)	$I \times 10^{-4}$(A)
0.025	1.31±0.05	2.09±0.14
0.050	1.36±0.01	2.88±0.01
0.100	1.43±0.04	3.35±0.06
0.150	1.50±0.04	5.11±0.44
0.200	1.52±0.00	6.19±0.41

Table 4.12: Oxidation potentials and peak currents for adsorbed 4-CR at pH 3. Working electrode =. TiO_2.

Scan Rate (V/S)	E_1 (V)	$I_1 \times 10^{-4}$ (A)	E_2 (V)	$I_2 \times 10^{-4}$ (A)
0.050	0.75±0.00	1.33±0.17	1.30±0.00	3.06±0.57
0.100	0.79±0.01	1.58±0.00	1.38±0.00	4.00±0.08
0.150	0.80±0.00	1.58±0.08	1.38±0.02	5.25±0.08
0.200	0.82±0.00	1.67±0.17	1.42±0.01	4.43±0.23

Table 4.13: Oxidation potentials and peak currents for 4,6-DCR at pH 6. Working electrode = Pt.

Scan Rate (V/S)	E (V)	$I \times 10^{-4}$(A)
0.025	0.82	3.62
0.050	0.89	4.62
0.100	0.93	6.42
0.150	1.00	8.44
0.200	1.03	9.69

Table 4.14: Oxidation potentials and peak currents for 4,6-DCR at pH 6. Working electrode = TiO_2.

Scan Rate (V/S)	E (V)	$I \times 10^{-4}$(A)
0.025	1.36±0.01	2.33±0.11
0.050	1.38±0.00	3.22±0.15
0.100	1.43±0.01	4.83±0.22
0.150	1.46±0.00	5.77±0.18
0.200	1.50±0.00	6.14±0.25

Table 4.15: Oxidation potentials and peak currents for 4,6-DCR under illumination at pH 6. Working electrode = TiO_2.

Scan Rate (V/S)	E (V)	$I \times 10^{-4}$(A)
0.025	1.36±0.00	2.14±0.04
0.050	1.39±0.00	2.92±0.09
0.100	1.42±0.00	3.50±0.17
0.150	1.45±0.20	5.07±0.46
0.200	1.50±0.20	5.84±0.30

Table 4.16: Oxidation potentials and peak currents for adsorbed 4,6-DCR at pH 6. Working electrode = TiO_2.

Scan Rate (V/S)	E_1 (V)	$I_1 \times 10^{-4}$ (A)	E_2 (V)	$I_2 \times 10^{-4}$ (A)
0.050	----------	----------	1.33±0.02	1.78±0.07
0.100	0.60±0.01	0.50±0.00	1.39±0.01	2.61±0.41
0.150	0.64±0.02	0.58±0.06	1.46±0.01	4.03±0.26
0.200	0.65±0.01	0.67±0.00	1.45±0.01	4.50±0.37

CHAPTER 5

RESULTS AND DISCUSSION: PART III

STRONGLY ADSORBED MODEL COMPOUNDS

The electrochemical and photoelectrochemical behaviors of model compounds exhibiting strong adsorption have been explored under different conditions. The organic compounds included in these analyses consist of CC, 3,4-DHBA and 1,2,4-THB. Completed results are given in section 5.6 and their behaviors in different environments are discussed in the following sections.

5.1 Electrochemistry of Solubilized Compounds

The electrochemical behaviors of the model compounds were initially studied on Pt electrodes and were compared to their behaviors on the TiO_2 electrodes. All these aromatic compounds contain hydroxyl groups in ortho position to one another and, therefore similar electrochemical behaviors were expected for these compounds. The resulting voltammograms, however, indicate marked differences in their behaviors on the Pt electrodes, which may be attributed to the presence of the additional functional groups on two of these compounds. CC displays a redox voltammogram typical of a quasi-reversible system. The I_{ox}/I_{red} ratio was found to be close to unity corresponding to a simple redox reaction on the working electrode. Figure 5.1 illustrates the voltammogram of CC on a Pt electrode. 3,4-DHBA displays similar

behavior, but the I_{ox}/I_{red} ratio for this compound deviates from unity with the reduction peak current being approximately half that of the oxidation peak, and is dependent on the scan rate. From these observations it can be concluded that the electrode reaction (oxidation process) is followed by a chemical reaction[48].

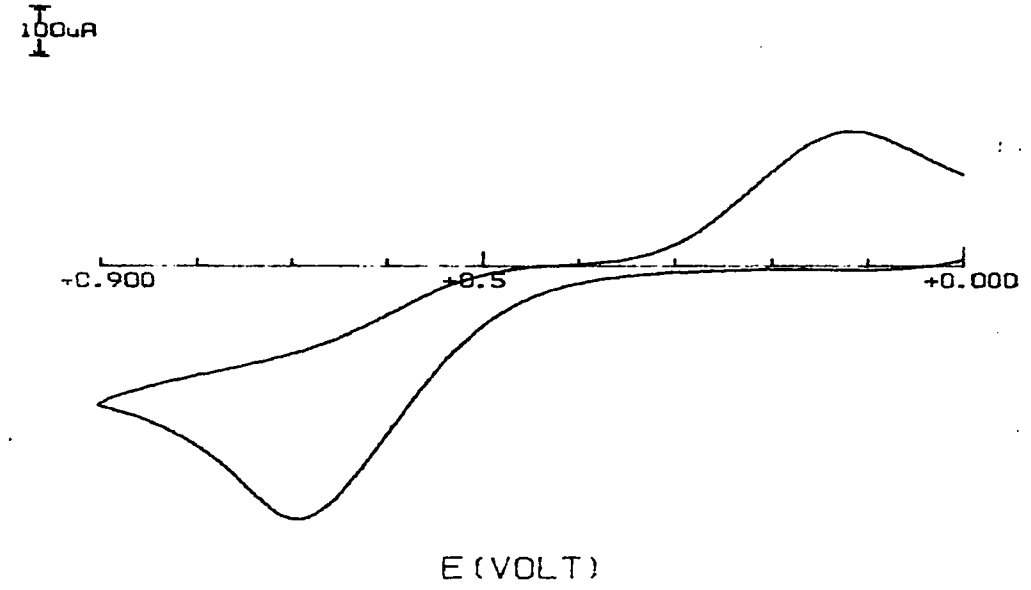

Figure 5.1: Voltammogram of CC on a Pt electrode. Scan rate = 100 mV/S.

1,2,4-THB showed a reversible redox reaction at low oxidation potential (0.40V-0.50V) and an irreversible oxidation at higher potentials similar to that observed for quinones[43] (1.0V-1.20V). The peak current ratios are similar to that found for 3,4-DHBA, indicating that the electrode reaction is accompanied by a chemical reaction[48]. Figure 5.2 and 5.3 illustrate the voltammograms of 3,4-DHBA and 1,2,4-THB on Pt electrodes. The oxidation peak currents relationship to $v^{1/2}$ as well as the

reduction peak currents versus $v^{1/2}$ are presented separately in figure 5.4 and 5.5 respectively.

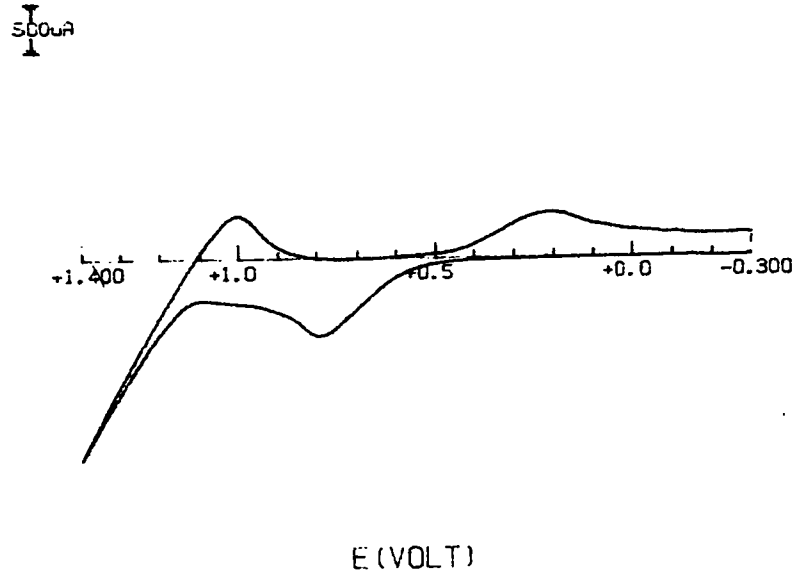

Figure 5.2: Voltammogram of 3,4-DHBA on a Pt electrode. Scan rate = 100 mV/S.

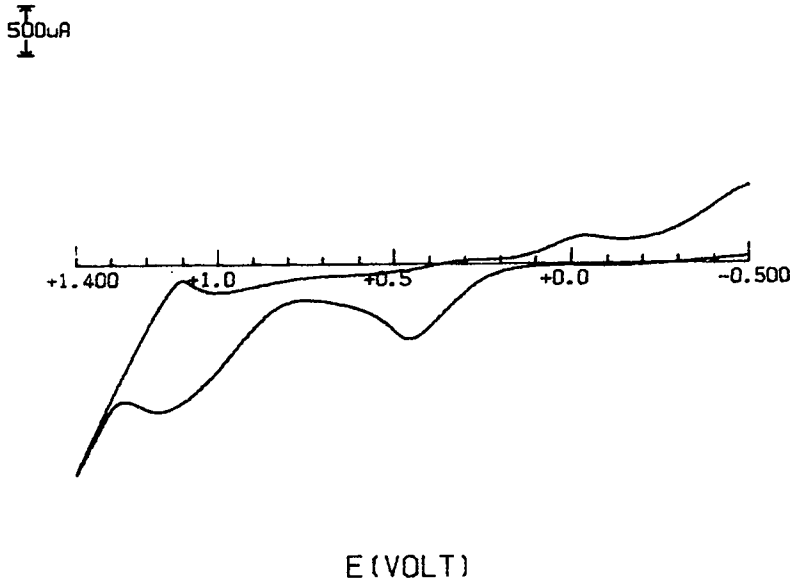

Figure 5.3: Voltammogram of 1,2,4-THB on Pt electrode. Scan rate = 100 mV/S.

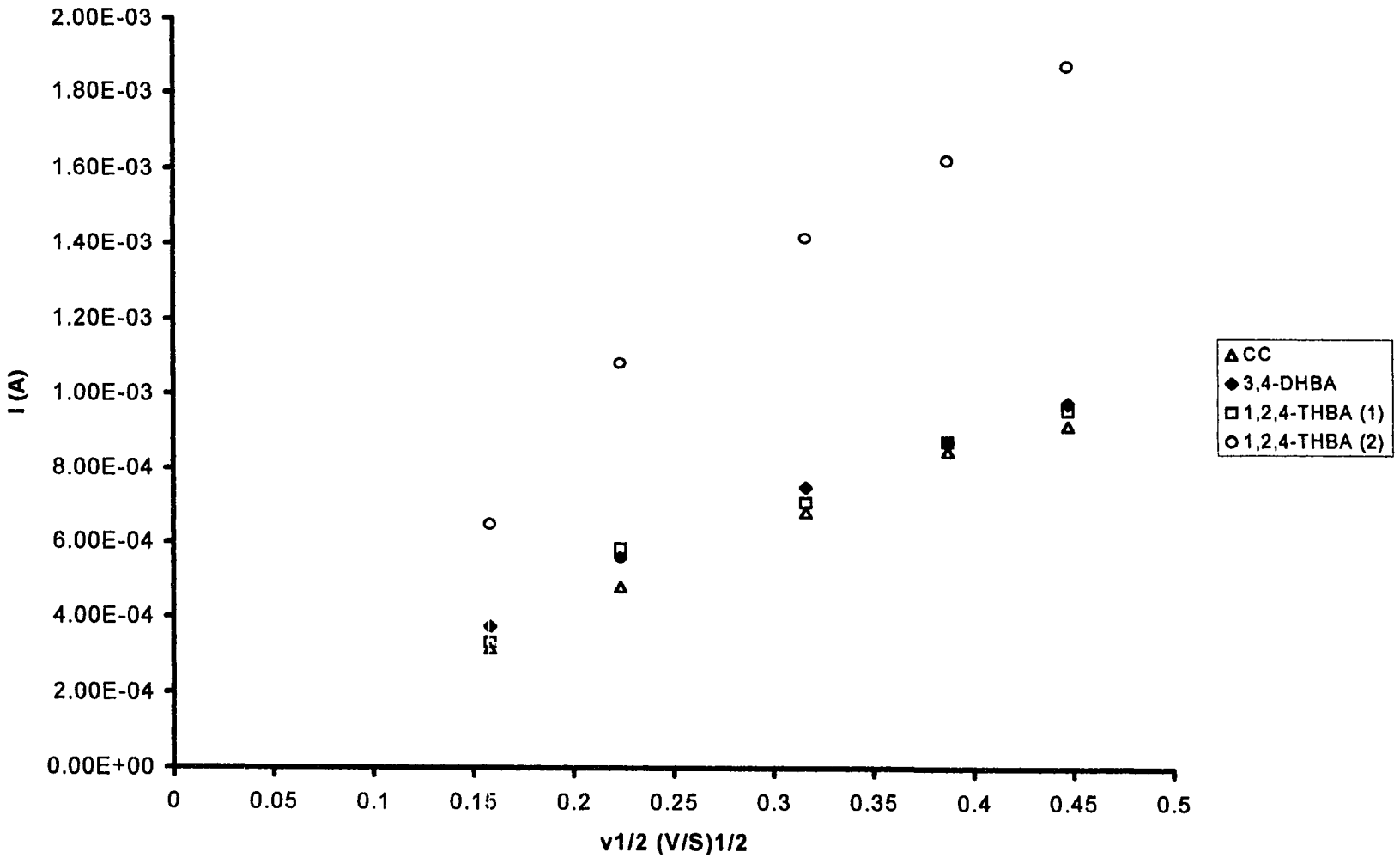

Figure 5.4: Oxidation peak currents vs. $v^{1/2}$ for model compounds on Pt electrodes.

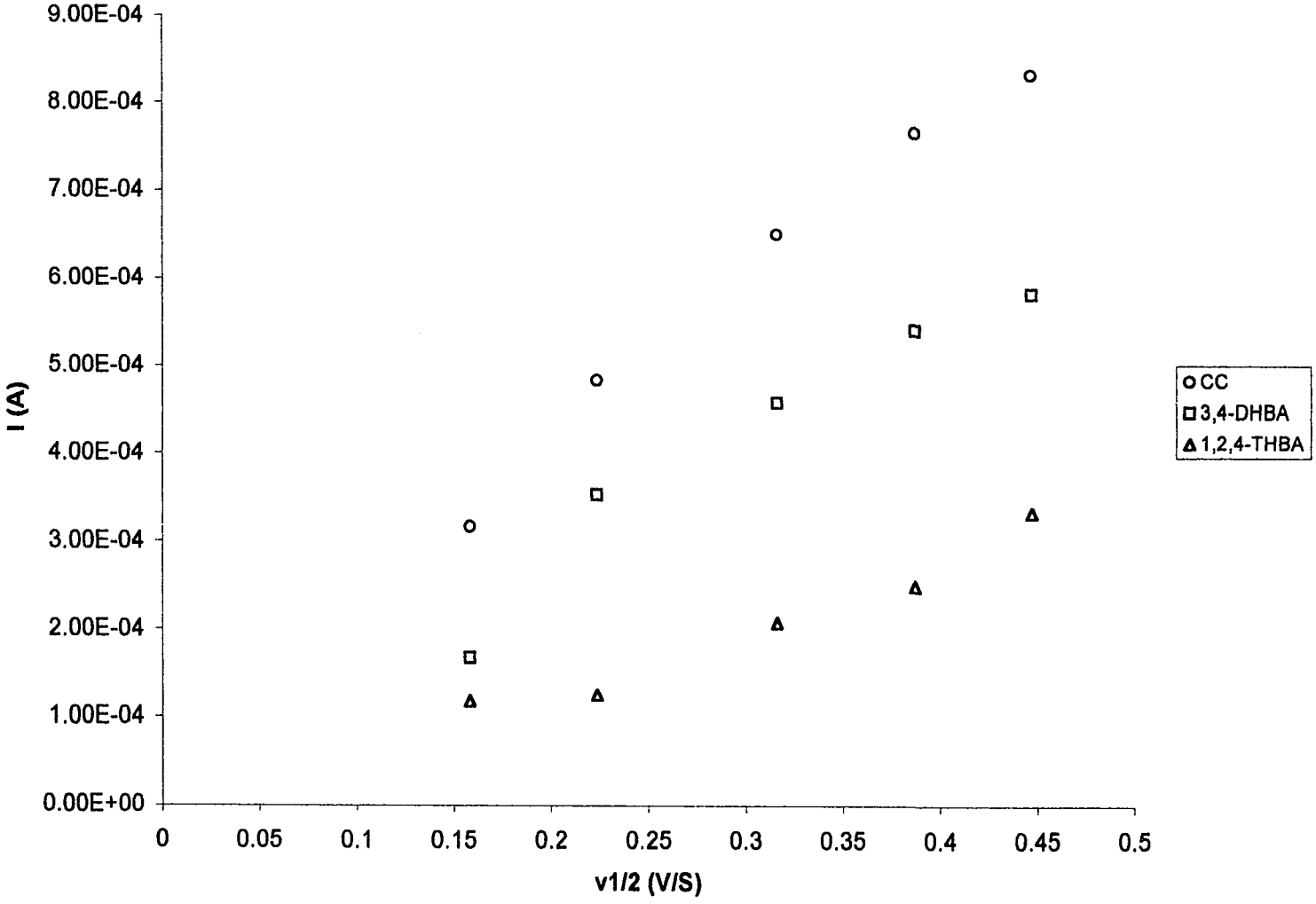

Figure 5.5: Reduction peak currents vs. $v^{1/2}$ for model compounds on a Pt electrode.

A linear correlation was observed for all compounds on Pt electrodes indicating that these peaks are due to diffusion-controlled processes. Furthermore, the log I-log ν plot provided additional support for this conclusion. Figure 5.6 displays the log I-log ν plot for these compounds on Pt electrodes, with linear correlation and slopes equal to 0.5. A plot of log I versus log ν is linear with a slope of 0.5 for a diffusion-controlled oxidation peak and a slope of 1 for an adsorption peak[48].

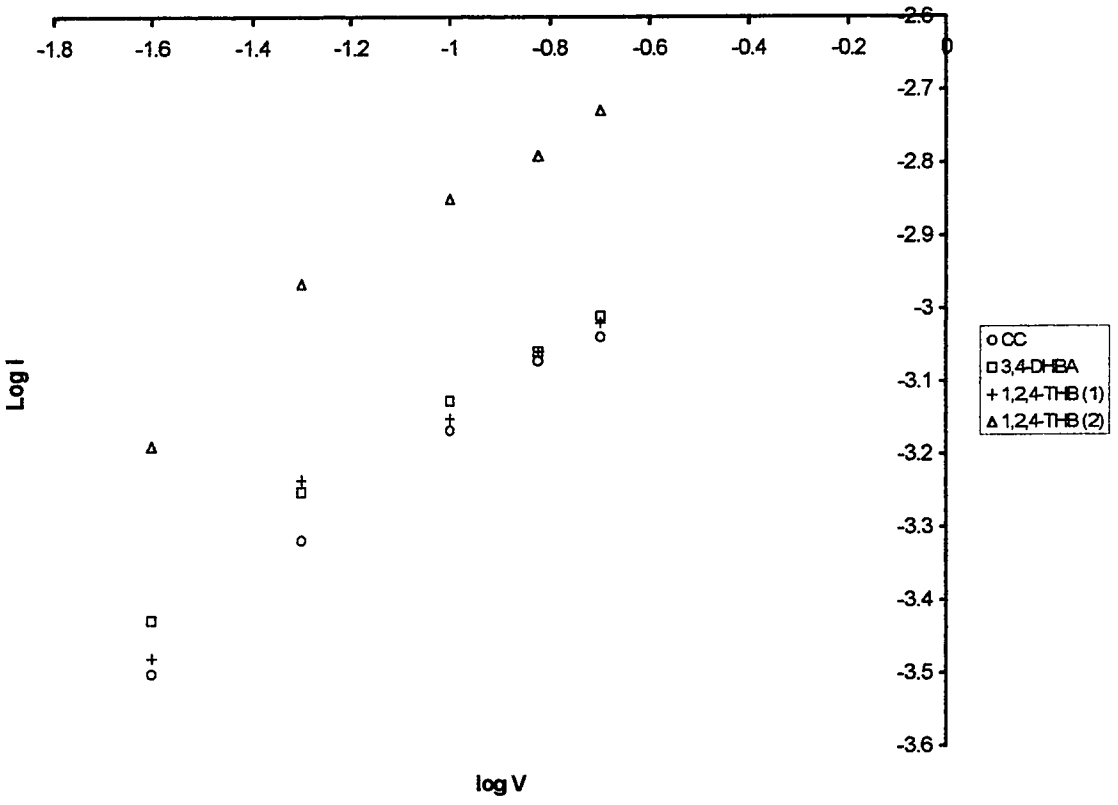

Figure 5.6: Log I vs. Log ν plot for oxidized compounds on Pt electrode.

Similar experiments were performed on TiO_2 electrodes under identical conditions. Unlike the oxidations on Pt electrodes, three oxidation peaks were detected. The oxidation peak at the most positive potential (~1.35 V) was not well resolved for all three compounds. Therefore its potential and current could only be determined for 3,4-DHBA due to adequate resolution. The peak currents could not be properly measured for CC and 3,4-DHBA owing to the extensive overlap of the oxidation peaks. Consequently, a plot of peak current versus $v^{1/2}$ could provide no useful information. For this reason, other methods were used to identify the origin of these oxidation peaks.

Reversal of the initial and final potentials for 3,4-DHBA resulted in a similar voltammogram but with lower current for the oxidation peaks. Figure 5.7 and 5.8 illustrate the voltammogram of 3,4-DHBA in an aqueous solution when the scan is initiated at negative potential (normal conditions), and when the scan was initiated from a positive potential, respectively. For 3,4-DHBA, on conducting multiple scans, the peak currents of the two-oxidation peaks at lower potentials tend to decrease by a larger amount compared to the one at the most positive potential. This observation may indicate that these oxidation peaks are due to adsorption. One should bear in mind that the structural configuration (hydroxyl groups in ortho position) of this compound favors strong adsorption. On the other hand the presence of the carbonyl group makes this compound slightly soluble in water which may result in a more

weakly adsorbed state. Figure 5.9 depicts the voltammogram of 3,4-DHBA on the TiO_2 electrode, where multiple scans were performed consecutively.

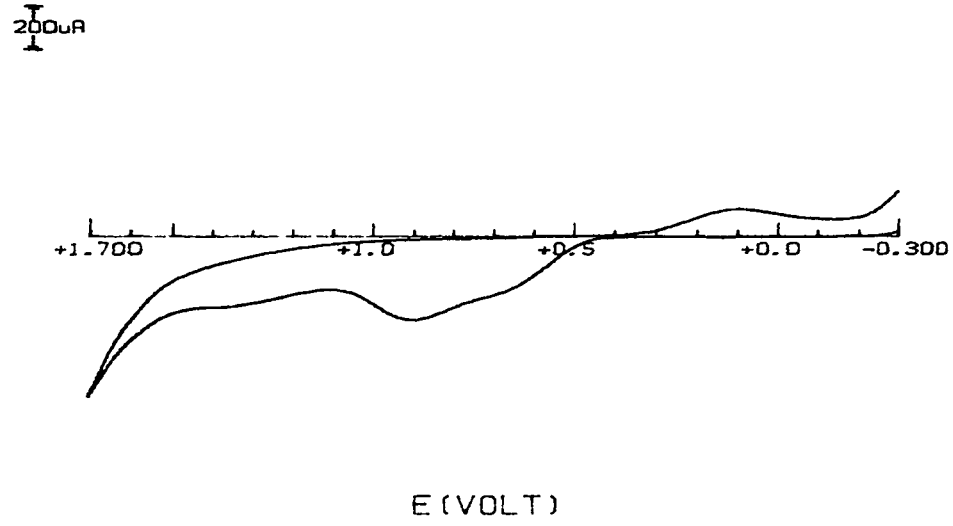

Figure 5.7: Voltammogram of 3,4-DHBA on a TiO_2 electrode. Scan was initiated from negative potential.

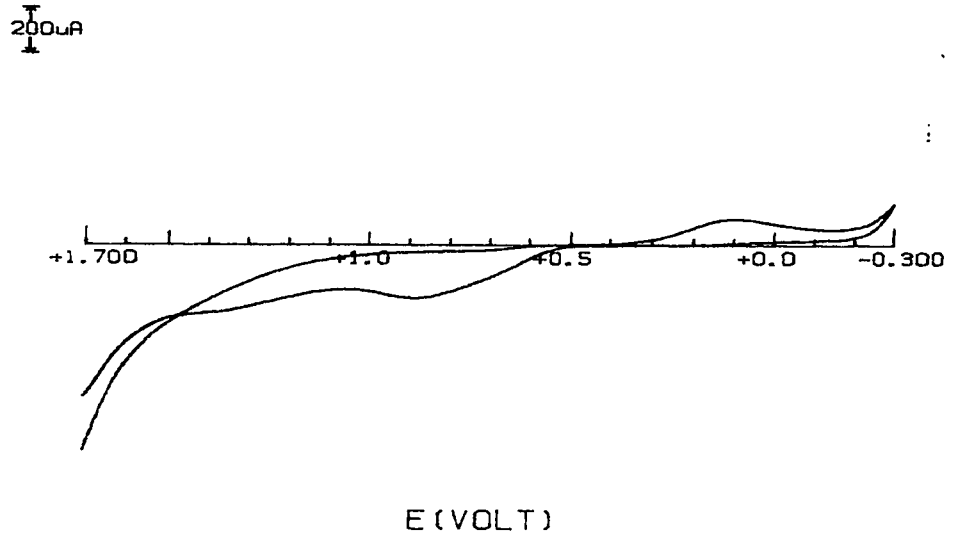

Figure 5.8: Voltammogram of 3,4-DHBA on a TiO_2 electrode. Scan was initiated from positive potential.

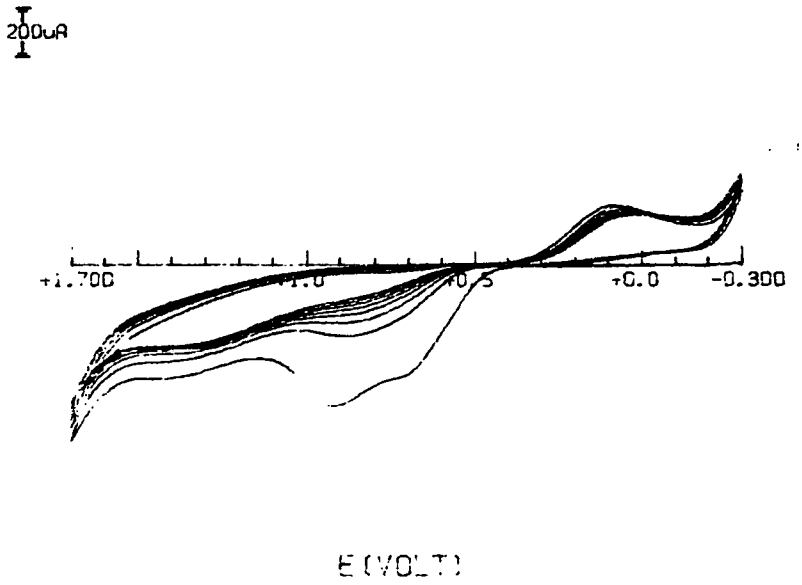

Figure 5.9: Voltammogram of 3,4-DHBA on a TiO_2 electrode. Scan rate = 100 mV/S.

Further evidence supporting the attribution of the oxidation peaks at 0.60 V to 1.10 V to adsorbed species is provided by experiments conducted in acetonitrile as the solvent medium. It is known that acetonitrile reduces or eliminates adsorption[32b, 48b]. CC and 3,4-DHBA were dissolved in acetonitrile and their electrochemical behaviors were examined. These compounds show a single oxidation potential in acetonitrile. The shift in the reduction peak potentials in acetonitrile compared to that in aqueous solution was used to correlate the single oxidation peak observed in acetonitrile to those seen in aqueous solution. For instance, for CC the entire voltammogram seems to be shifted toward positive potential in acetonitrile. The reduction peak has shifted to a

more positive potential by about 0.50 V in acetonitrile compared to aqueous solution. Therefore, one would expect the oxidation peak to be shifted also to a more positive potential by approximately 0.50 V, going from aqueous solution to an acetonitrile solution. Based on these considerations, the single oxidation peak in acetonitrile corresponds to the most positive oxidation potential for CC and 3,4-DHBA in aqueous solution. These results suggest that the additional peaks observed in aqueous solution may be caused by adsorption of the aromatic compounds examined. Figures, 5.10 illustrates the voltammogram of CC on the TiO_2 electrodes in aqueous solution. In addition, figures 5.11 and 5.12 display the behavior of CC and 3,4-DHBA in acetonitrile.

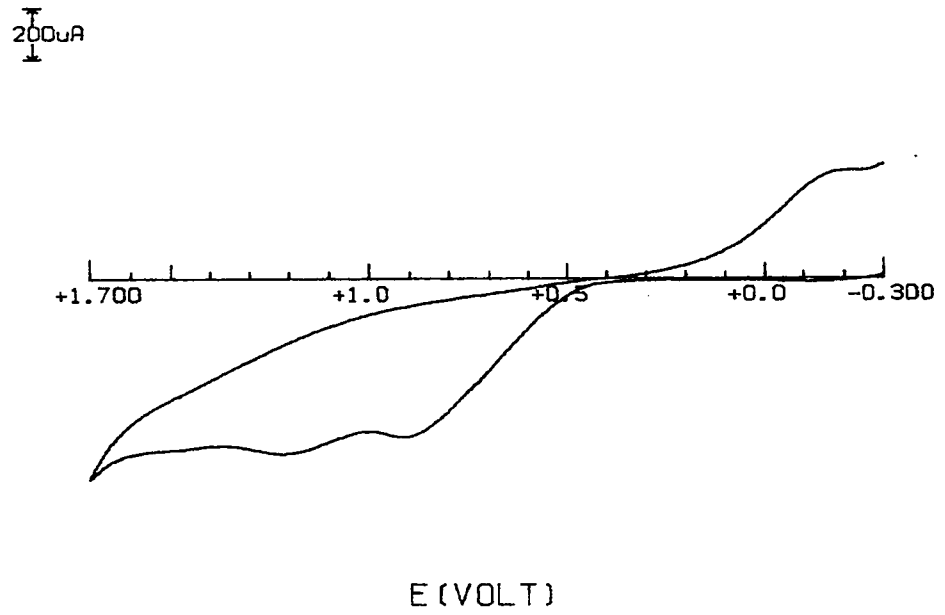

Figure 5.10: Voltammogram of CC in an aqueous solution on a TiO_2 electrode. Scan rate = 100 mV/S.

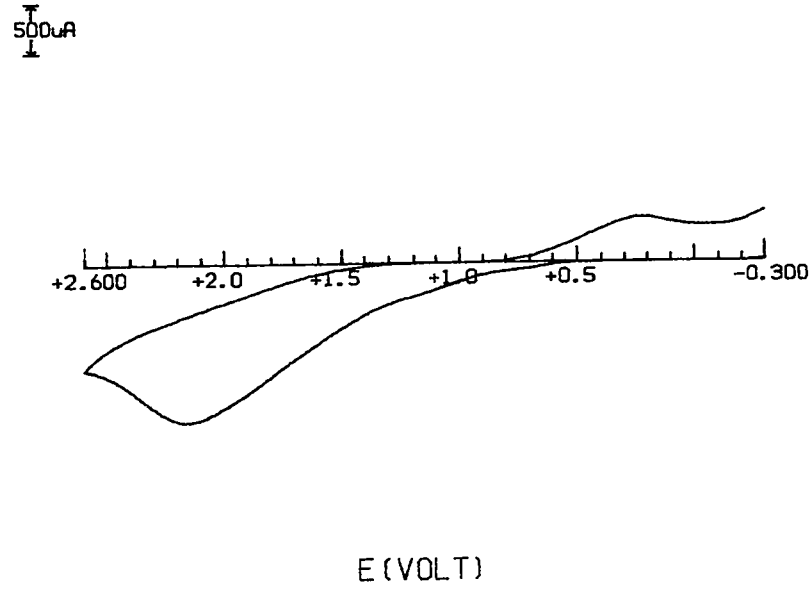

Figure 5.11: Voltammogram of CC in acetonitrile on a TiO_2 electrode. Scan rate = 100 mV/S.

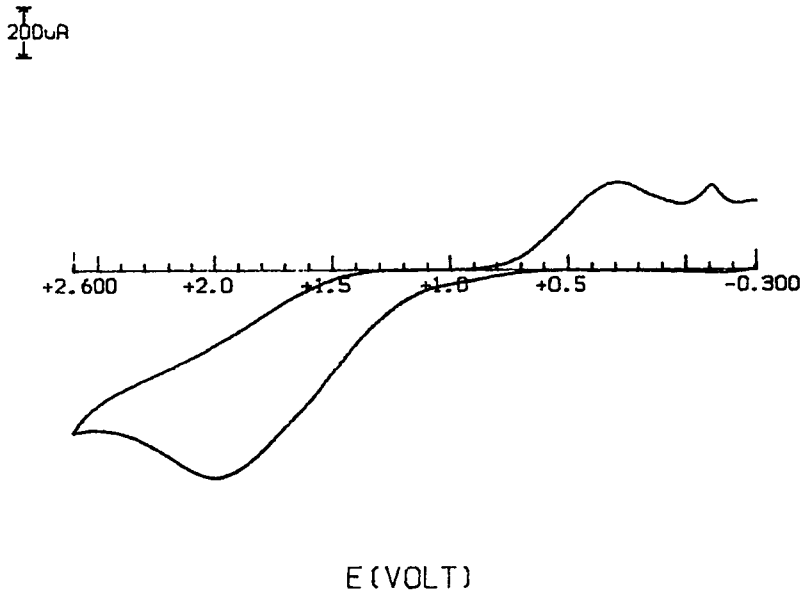

Figure 5.12: Voltammogram of 3,4-DHBA in acetonitrile on a TiO_2 electrode. Scan rate = 100 mV/S.

1,2,4-THB did not require the same treatment. The two oxidation peaks were well resolved and separated from one another, therefore a peak current dependency on the $v^{1/2}$ provided sufficient information to determine the origin of each oxidation peak. Figure 5.13 displays the voltammogram of 1,2,4-THB on a TiO_2 electrode. The plot of I_p versus $v^{1/2}$ is given in figure 5.14. According to this plot the peak at lower oxidation potential is an adsorption peak while the one at higher potential is due to diffusion.

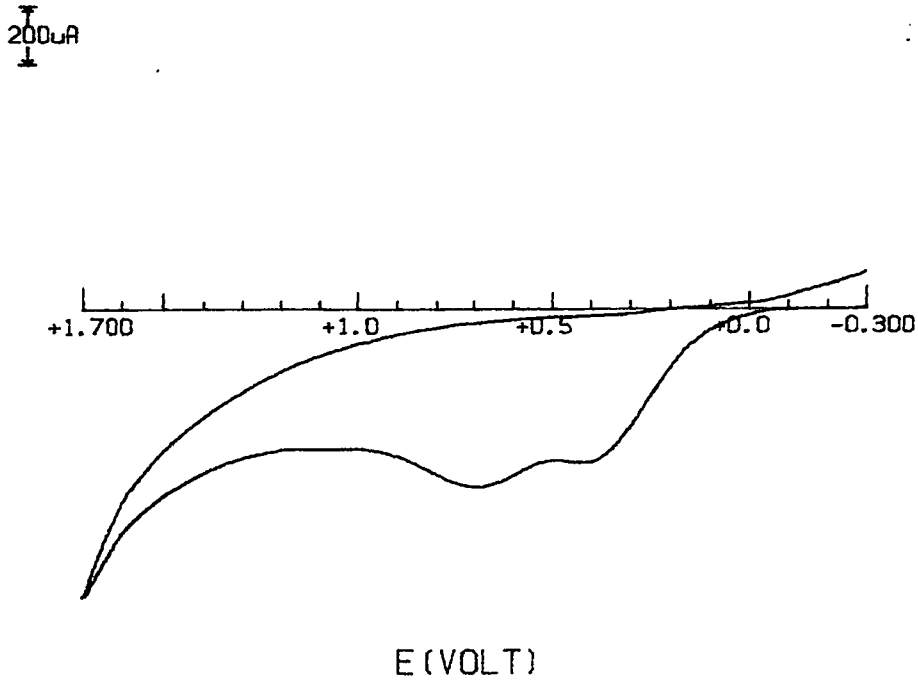

Figure 5.13: Voltammogram of 1,2,4-THB on a TiO_2 electrode. Scan rate = 50 mV/S.

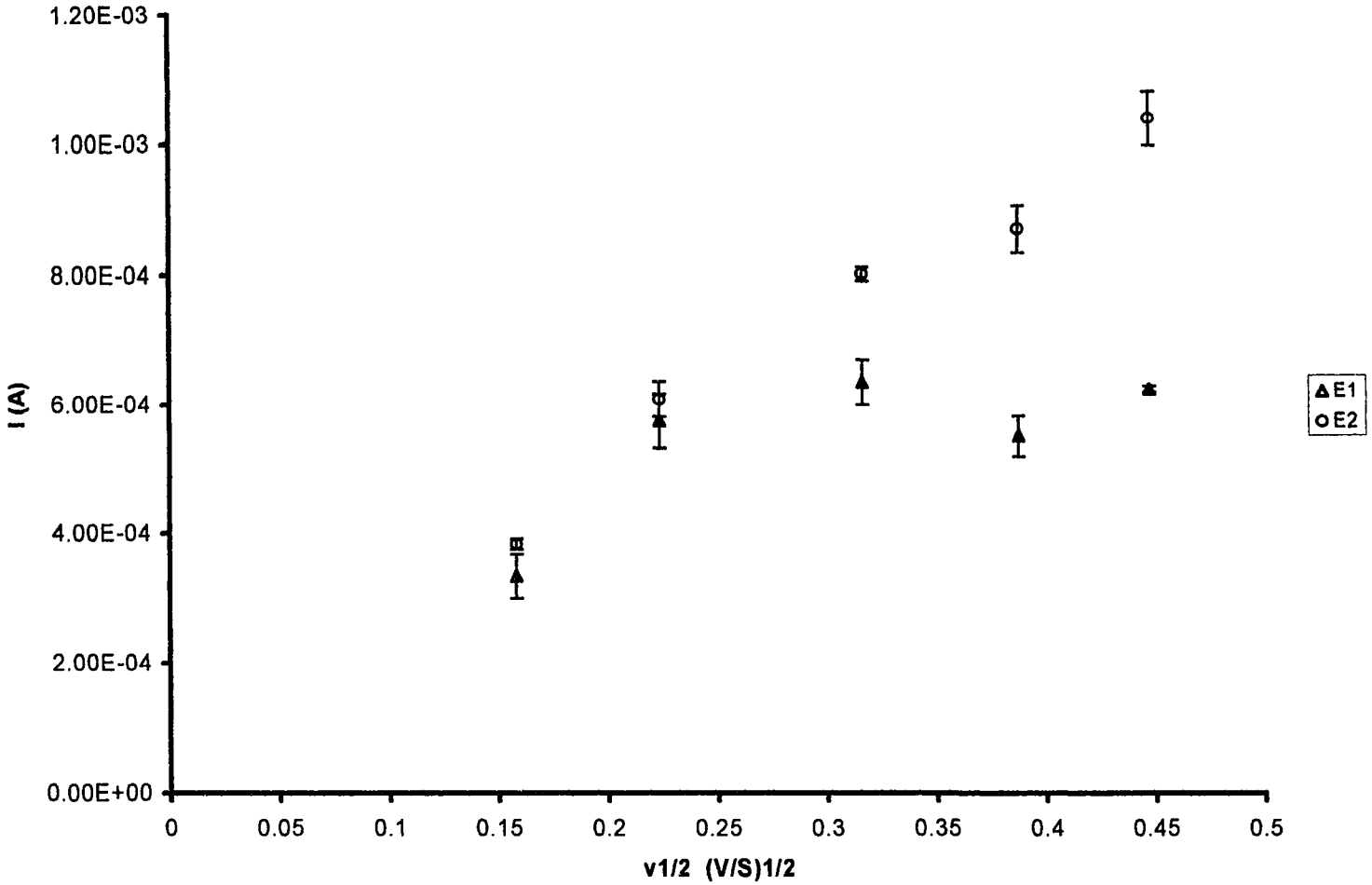

Figure 5.14: I_p vs. $v^{1/2}$ for 1,2,4-THB.

5.2 Imposed Adsorption Experiments

The effects of adsorption on the oxidation potentials of selected organic compounds were also examined on the TiO_2 electrodes. The preparation method is described in the experimental section (section 2.8). A single oxidation peak was detected for CC. The comparison of adsorption experiments with those of free CC indicate that oxidation peaks at lower potentials (0.84 V-1.00 V) are more likely due to chemical adsorption of the reactants on the surface of TiO_2 electrodes. Figures 5.15 and 5.16 depict the voltammogram of adsorbed CC on a TiO_2 electrode and I_p dependency on $\nu^{1/2}$, respectively.

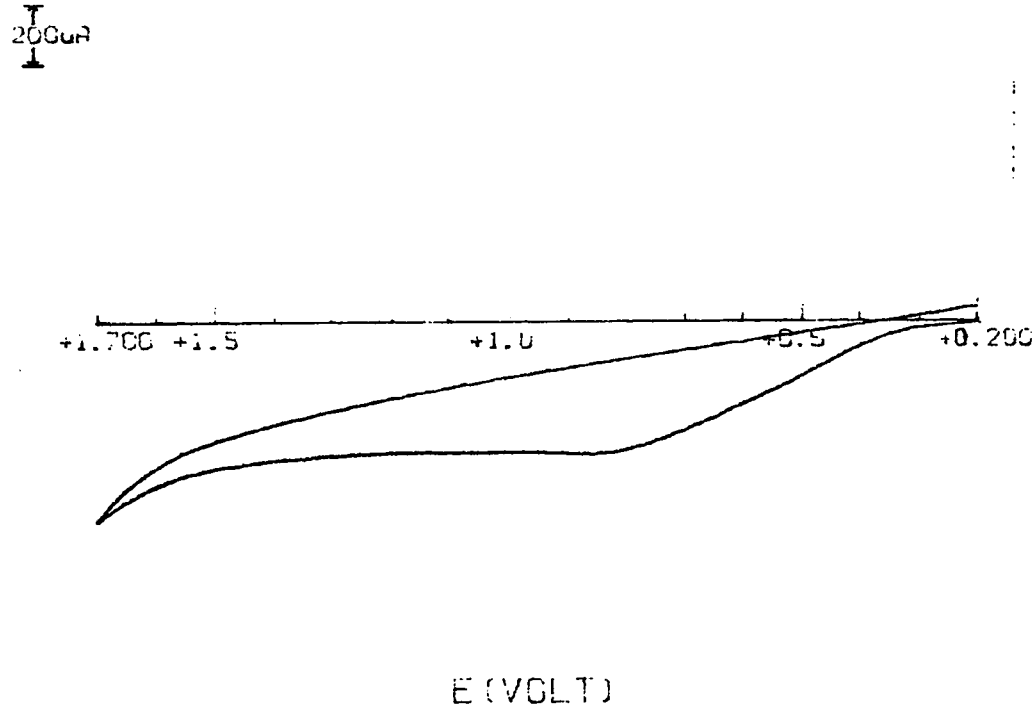

Figure 5.15: Voltammogram of adsorbed CC on a TiO_2 electrode. Scan rate = 100 mV/S.

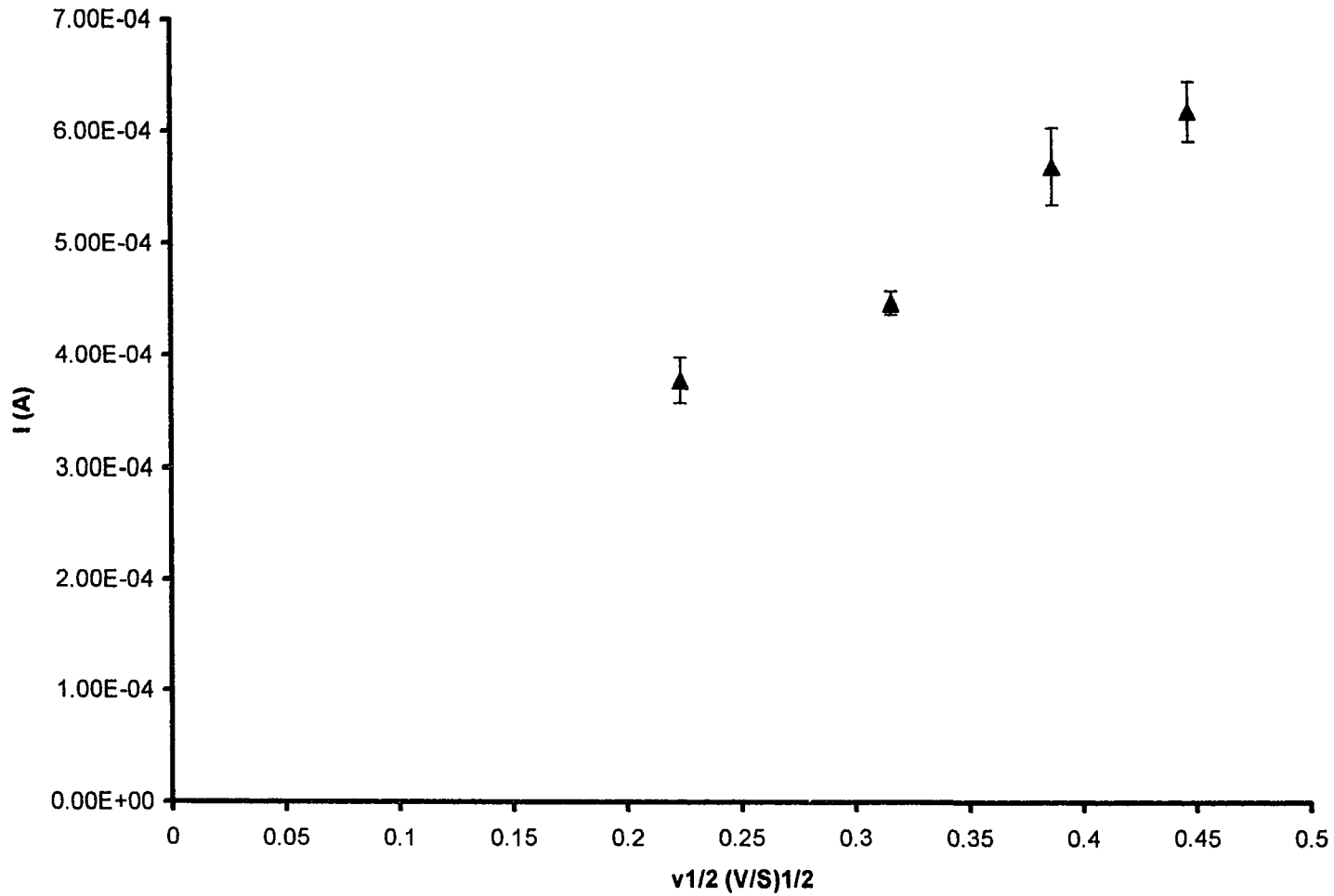

Figure 5.16: I_p vs. $v^{1/2}$ for adsorbed CC on the TiO_2 electrodes.

As noted in figure 5.16, the observed relationship significantly differs from that expected for a diffusion-controlled process (non-zero intercept). This has also been confirmed by the peak potential dependency on the concentration. Figure 5.17 displays the peak potential dependency on the concentration for CC. The oxidation peaks at lower potentials closely coincide with those attributed to adsorbed materials. The peak current dependence on the concentration indicates that the two peaks gradually merge into a single peak as the concentration is increased. Such behavior is typical of strong adsorption of reactants[35]. "Increasing the concentration of reactants results in saturation of the surface of the electrode and the total charge flowing during oxidation due to adsorbed substrate becomes constant, while the total charge due to diffusing materials continues to increase with concentration. This causes the fraction of the peak current due to adsorbed material to decrease with increasing concentration and the current function approaches that of the uncomplicated reversible case"[35].

Two oxidation peaks were seen for both 3,4-DHBA and 1,2,4-THB for adsorption experiments as compared to CC, where only one adsorption peak was observed. One would expect the same behavior for all these compounds with respect to adsorption. The presence of two adsorption peaks for 3,4-DHBA and 1,2,4-THB may be explained in terms of polarity.

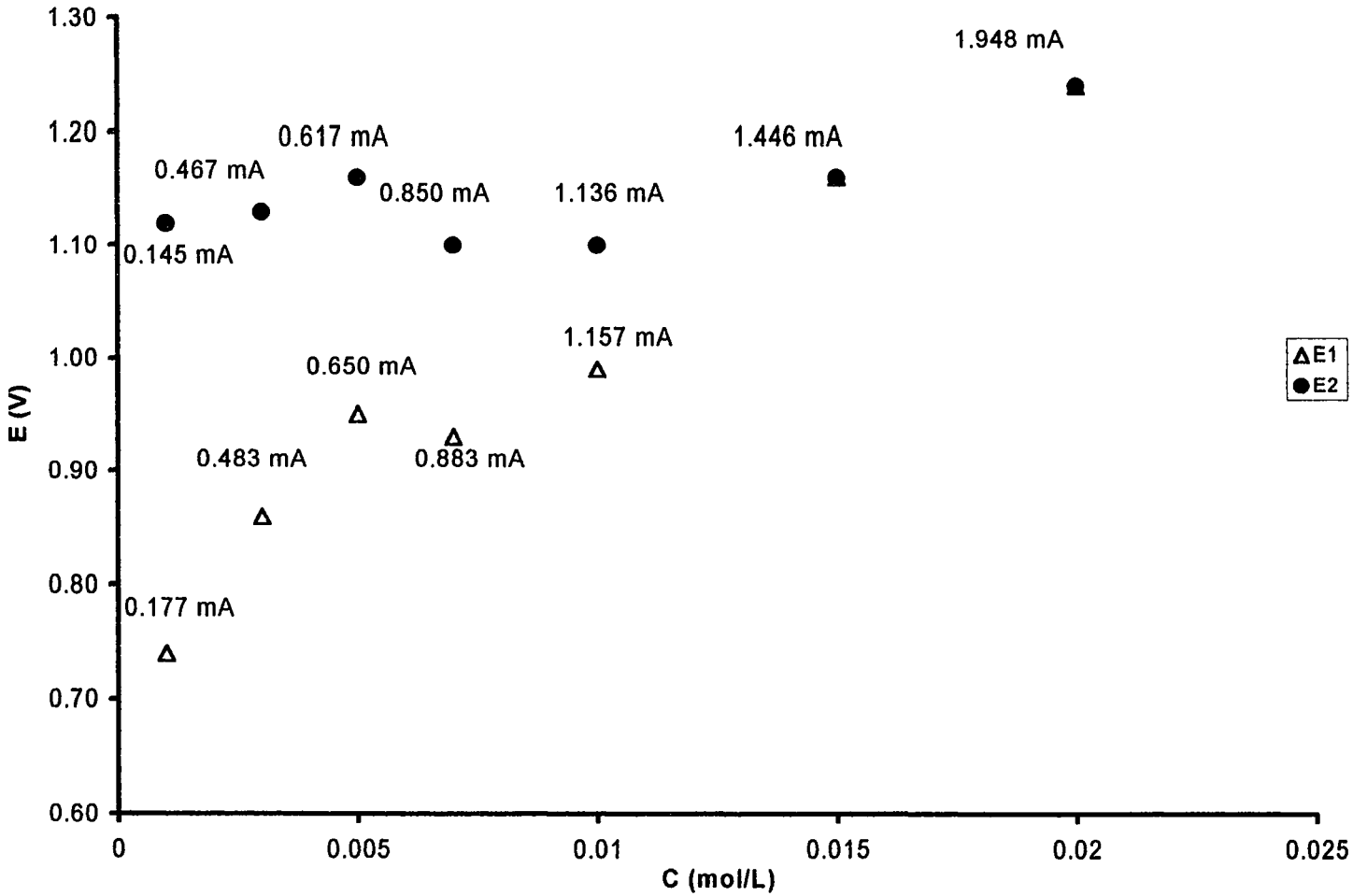

Figure 5.17: Potential dependence on the concentration for CC on the TiO_2 electrodes.

For CC, the presence of two adjacent hydroxyl groups provides the favorable structural configuration for strong adsorption on the TiO_2 surface[36, 37]. Since CC is very polar due to the presence of these hydroxyl groups in ortho position to one another, all the material deposited on the surface of the electrode would manifest itself as adsorbed species. On the other hand, 3,4-DHBA and 1,2,4-THB contain an additional functional group on the ring carbon number 4. The electronegativity of this functional group would significantly reduce the polarity of 3,4-DHBA and 1,2,4-THB compared to CC. Therefore, for the same amount of material placed on the electrode, less adsorption would take place, allowing the compound to diffuse into solution and reveal itself as an additional peak (diffusion-controlled). Thus, two peaks are seen for 3,4-DHBA and 1,2,4-THB. In the case of adsorbed 3,4-DHBA, the peak at about 0.5V-0.7V is absent (figure 5.18). Three oxidation peaks were observed for solubilized 3,4-DHBA (see figure 5.7). On the other hand, under imposed adsorption only two oxidation peaks were seen corresponding to the two oxidation peaks at most positive potentials (for solubilized 3,4-DHBA). No reference has been found, which would explain these observations. Therefore, the explanations given here are solely based on the author's understandings of the processes involved. 3,4-DHBA is slightly soluble in water, therefore there exists a possibility of weak adsorption on the TiO_2 surface[32 (c)]. On the other hand, its structural configuration (hydroxyl groups in ortho position to one another) favors strong adsorption[33, 36, 37]. Therefore, it is

possible that three processes are associated with the oxidation of 3,4-DHBA on the TiO_2 electrodes in an aqueous solution, namely, (i) weak adsorption, (ii) strong adsorption and (iii) diffusion. The absence of the oxidation peak at most negative potential (0.6 V-0.75 V) on the voltammograms obtained under imposed adsorption suggests that strong adsorption dominates under these conditions. Therefore, no adsorption peak due to weak adsorption of reactants would be detected under these conditions.

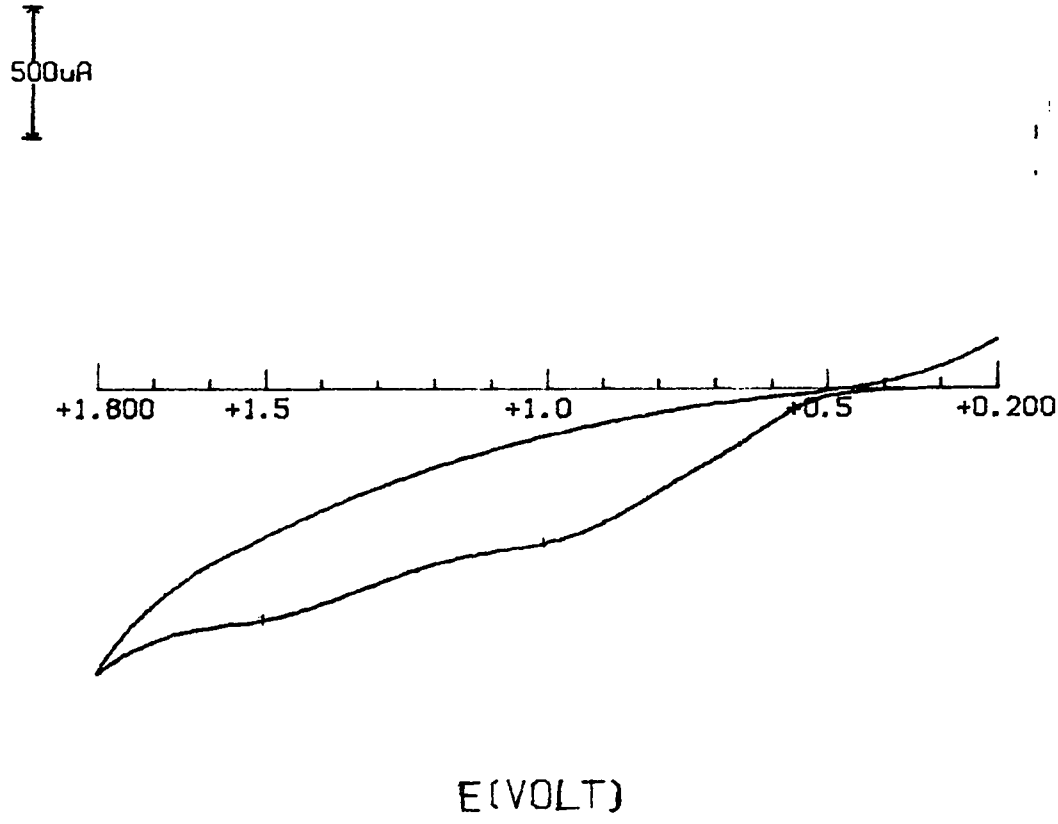

Figure 5.18: Voltammogram of adsorbed 3,4-DHBA on a TiO_2 electrode. Scan rate = 100 mV/S.

5.3 Effect of Illumination

The photoelectrochemical behaviors of these organic compounds have been examined on the TiO_2 electrodes and were compared to those obtained in the dark. Slight changes in peak currents were detected for these compounds under illumination; however, the changes are small and are comparable to the calculated experimental deviations. Therefore, the oxidation efficiency of these compounds has not improved under illumination. A shift in flat band potential was expected for TiO_2 under illumination, which would be detected by a shift in the oxidation potentials of these compounds on the illuminated TiO_2 electrodes. No such shift was detected with the exception of 1,2,4-THB, where a slight shift in the oxidation peak was observed. As noted earlier in chapter four, this may have been caused by the low intensity of the light source used in these experiments[42, 43, 49].

CC and 3,4-DHBA each showed a reduction potential in the dark. The reduction potential of CC vanished under illumination and the one for 3,4-DHBA was reduced to almost half of its value in the dark. The absence of the reduction peak for CC and reduced reduction current for 3,4-DHBA may be attributed to the fact that the band structure of TiO_2 does not favor the reduction processes under illumination (n-type semiconductor). Under illumination the surface of TiO_2 is positively charged due to migration of holes to the surface, therefore the reduction which requires the removal of an electron from the surface of the

electrode in not favored. A shift in baseline was observed for the illuminated TiO_2 electrode indicating the photoactivity of the electrode, however the magnitude of the photo-generated current seems to depend on the type of organic compound in solution and its polarity. The photocurrent was observed to decrease with decreasing polarity of the organic compounds. It was maximum for CC and decreased to zero for 1,2,4-THB. The polarity of these compounds was determined using PC MODELLING software, which showed that the polarity decreases in the following order: CC> 3,4-DHBA> 1,2,4-THB.

5.4 Effect of pH

A single compound was chosen to investigate the effect of pH on oxidation potentials of the strongly adsorbed substrates on TiO_2 electrodes. The compound of choice was CC for these experiments. Its redox behavior was first examined on a Pt electrode at pH 3 and pH 6, which were then compared to those obtained on the TiO_2 electrodes in the dark. No changes in the oxidation potentials of CC were seen at different pH values on the Pt electrode. However, the oxidation peak currents were higher at pH 3, while the reduction peak currents were lower at this pH compared to pH 6. These observations suggest that CC may have gone through a self-oxidation at higher pH[47]. Figure 5.19 depicts its redox behavior on a Pt electrode at pH 3 and pH6 respectively.

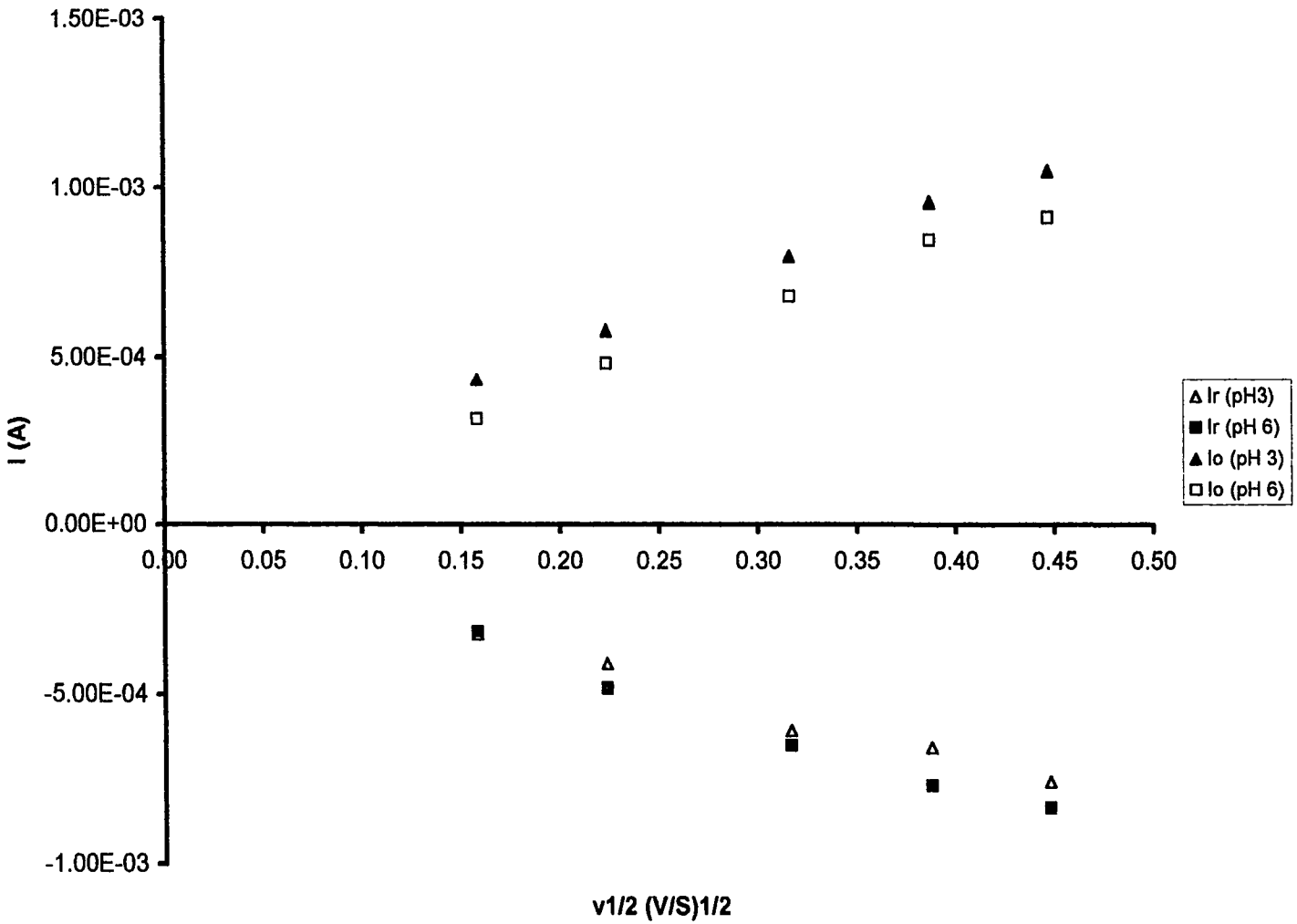

Figure 5.19: I_p vs. $v^{1/2}$ for CC on the Pt electrodes.

The oxidation potentials of adsorbed species remained the same regardless of the pH at which the experiments were performed (oxidation potentials at about 0.80 V to 1.00 V). However, the oxidations at most positive potentials (suspected to be due to diffusion-controlled processes) seem to vary with the change in pH (these oxidation potentials were lower at higher pH values). These observations indicate that only the oxidation potentials of diffusion-controlled processes are affected by the change in band positions associated with the pH change on the TiO_2 electrodes (band positions change by $-0.06 \times$ pH). Since the TiO_2 surface is positively charged at pH values lower than its point of zero charge[47], one would expect to see higher peak currents at lower pH values. However, larger peak currents were seen at pH 6 compared to pH 3. The larger peak currents may be attributed to higher concentration of reduced CC at pH 6, since this compound is known to go through self-oxidization at higher pH[47]

5.5 Summary

CC, 3,4-DHBA, 1,2,4,-THB were chosen to investigate the oxidation of strongly adsorbed organic compounds on the TiO_2 electrodes under various conditions. These compounds have shown a reversible redox behavior on Pt electrodes. Single oxidation peak was detected for CC and 3,4-DHBA on Pt electrode, but two oxidation peaks were seen for 1,2,4-THB, typical of quinones oxidation on a metal electrode. Multiple oxidation peaks were seen for these compounds on the TiO_2 electrodes, where the peak at most positive potentials was assigned to diffusion-controlled processes and those at lower potentials were accredited to adsorbed species. No shifts in either peak currents or peak potentials were detected under illumination. The unchanged peak potentials under illumination were attributed to the low intensity of the light source used in these experiments. The effect of pH on the oxidation potentials of CC was investigated at two different pH values (pH 3 and pH 6). Based on the obtained results, only the oxidation potentials of diffused CC is affected by the pH change while the one due to adsorption remains unchanged. Larger oxidation peak currents were seen at pH 6, which was attributed to larger amount of reduced CC present at this pH due to self-oxidation of CC at more basic pH.

5.6 Tables

Table 5.1: Oxidation potentials and peak currents for CC at pH 6. Working electrode = Pt

Scan Rate (V/S)	E_r (V)	$I_r \times 10^{-4}$ (A)	E_1 (V)	$I_1 \times 10^{-4}$ (A)
0.025	0.21	-3.17	0.60	3.17
0.050	0.16	-4.83	0.66	4.83
0.100	0.11	-6.50	0.70	6.83
0.150	0.10	-7.67	0.74	8.50
0.200	0.08	-8.33	0.74	9.17

Table 5.2: Oxidation potentials and peak currents for CC at pH 3. Working electrode = Pt.

Scan Rate (V/S)	E_r (V)	$I_r \times 10^{-4}$ (A)	E_1 (V)	$I_1 \times 10^{-4}$ (A)
0.025	0.21	-3.25	0.62	4.33
0.050	0.16	-4.11	0.67	5.79
0.100	0.12	-6.04	0.71	8.02
0.150	0.10	-6.56	0.74	9.58
0.200	0.08	-7.55	0.76	10.50

Table 5.3: Oxidation potentials and peak currents for CC at pH 6. Working electrode = TiO_2.

Scan Rate (V/S)	E_r (V)	E_1 (V)	E_2 (V)
0.025	-0.06±0.01	0.84±0.01	1.02±0.02
0.050	-0.13±0.01	0.86±0.02	1.01±0.01
0.100	-0.19±0.00	0.95±0.02	1.16±0.03
0.150	-0.19±0.01	0.95±0.01	1.19±0.01
0.200	-0.21±0.02	1.00±0.02	1.24±0.01
Scan Rate (V/S)	**$I_r \times 10^{-4}$(A)**	**$I_1 \times 10^{-4}$(A)**	**$I_2 \times 10^{-4}$(A)**
0.025	-1.78±0.07	3.42±0.22	3.44±0.13
0.050	-2.44±0.13	4.83±0.33	4.58±0.44
0.100	-3.29±0.46	6.50±0.00	6.17±0.17
0.150	-3.58±0.28	8.72±0.52	7.83±0.52
0.200	-4.28±0.30	8.83±0.28	8.17±0.44

Table 5.4: Oxidation potentials and peak currents for CC at pH 3. Working electrode = TiO_2.

Scan Rate (V/S)	E_r (V)	E_1 (V)	E_2 (V)
0.025	-0.07±0.00	0.82±0.02	1.07±0.01
0.050	-0.12±0.01	0.86±0.00	1.14±0.01
0.100	-0.19±0.01	0.91±0.01	1.22±0.02
0.150	-0.19±0.00	0.94±0.02	1.24±0.03
0.200	-0.20±0.00	0.97±0.02	1.32±0.04
Scan Rate (V/S)	**$I_r \times 10^{-4}$(A)**	**$I_1 \times 10^{-4}$(A)**	**$I_2 \times 10^{-4}$(A)**
0.025	-1.64±0.13	3.03±0.19	3.22±0.20
0.050	-2.35±0.21	4.11±0.15	4.33±0.11
0.100	-3.97±0.20	5.97±0.15	6.64±0.37
0.150	-4.01±0.55	6.75±0.39	7.03±0.56
0.200	-4.08±0.06	7.81±0.03	8.33±0.56

Table 5.5: Oxidation potentials and peak currents for CC under illumination at pH 6. Working electrode = TiO_2.

Scan Rate (V/S)	E_1 (V)	E_2 (V)
0.025	0.80±0.01	0.97±0.01
0.050	0.88±0.00	1.07±0.01
0.100	0.95±0.01	1.19±0.02
0.150	0.99±0.01	1.25±0.03
0.200	1.06±0.02	1.28±0.00
Scan Rate (V/S)	**$I_1 \times 10^{-4}$(A)**	**$I_2 \times 10^{-4}$(A)**
0.025	2.33±0.25	1.88±0.13
0.050	4.06±0.15	3.96±0.12
0.100	5.44±0.44	5.39±0.44
0.150	7.50±0.42	6.36±0.11
0.200	8.83±0.50	7.50±0.21

Table 5.6: Oxidation potentials and peak currents for CC under illumination at pH 3. Working electrode = TiO_2.

Scan Rate (V/S)	E_1 (V)	E_2 (V)
0.025	0.84±0.01	1.00±0.03
0.050	0.87±0.00	1.15±0.00
0.100	0.94±0.01	1.24±0.02
0.150	0.96±0.01	1.28±0.02
0.200	1.00±0.02	1.39±0.00
Scan Rate (V/S)	**$I_1 \times 10^{-4}$(A)**	**$I_2 \times 10^{-4}$(A)**
0.025	2.92±0.25	2.75±0.25
0.050	3.33±0.00	3.42±0.08
0.100	4.53±0.16	4.74±0.26
0.150	5.45±0.57	6.39±0.46
0.200	6.15±0.49	7.78±0.60

Table 5.7: Oxidation potentials and peak currents for adsorbed CC at pH 6. Working electrode = TiO_2.

Scan Rate (V/S)	E_o (V)	$I_o \times 10^{-4}$(A)
0.050	0.84±0.00	3.78±0.20
0.100	0.90±0.03	4.47±0.10
0.150	0.91±0.01	5.69±0.34
0.200	0.95±0.01	6.18±0.27

Table 5.8: Oxidation potentials and peak currents for adsorbed CC at pH 3. Working electrode = TiO_2.

Scan Rate (V/S)	E_o (V)	$I_o \times 10^{-4}$(A)
0.050	0.84±0.01	3.14±0.20
0.100	0.87±0.01	3.83±0.33
0.150	0.89±0.01	4.43±0.37
0.200	0.91±0.01	5.56±0.13

Table 5.9: Concentration profile for CC at pH 6.
Working electrode = TiO_2.

C [M]	E_r (V)	E_1 (V)	E_2 (V)
0.001	-0.14±0.01	0.74±0.01	1.12±0.00
0.003	-0.18±0.00	0.86±0.00	1.13±0.02
0.005	-0.19±0.00	0.95±0.02	1.16±0.03
0.007	-0.17±0.01	0.93±0.01	1.10±0.00
0.010	-0.15±0.00	0.99±0.01	1.10±0.00
0.015	-0.20±0.01	1.16±0.06	1.16±0.06
0.020	-0.20±0.01	1.24±0.01	1.24±0.01
C [M]	**$I_r \times 10^{-4}$(A)**	**$I_1 \times 10^{-4}$(A)**	**$I_2 \times 10^{-4}$(A)**
0.001	1.29±0.04	1.77±0.06	1.45±0.17
0.003	2.92±0.08	4.83±0.00	4.67±0.00
0.005	3.29±0.46	6.50±0.00	6.17±0.17
0.007	4.83±0.17	8.83±0.33	8.50±0.33
0.010	5.47±0.05	11.57±0.11	11.36±0.11
0.015	8.25±0.46	14.46±0.29	14.46±0.29
0.020	10.00±0.00	19.48±0.53	19.48±0.53

Table 5.10: Oxidation potentials and peak currents for 3,4-DHBA at pH 3.
Working electrode = Pt.

Scan Rate (V/S)	E_r (V)	$I_r \times 10^{-4}$ (A)	E_1 (V)	$I_1 \times 10^{-4}$ (A)
0.025	0.27	-1.67	0.72	3.75
0.050	0.24	-3.54	0.75	5.62
0.100	0.21	-4.58	0.79	7.50
0.150	0.19	-5.42	0.82	8.75
0.200	0.15	-5.83	0.85	9.79

Table 5.11: Oxidation potentials and peak currents for 3,4-DHBA at pH 3. Working electrode = TiO_2.

Scan Rate (V/S)	E_r (V)	E_1 (V)	E_2 (V)	E_3 (V)
0.025	0.11±0.00	0.68±0.00	0.92±0.00	1.42±0.02
0.050	0.09±0.00	0.69±0.01	0.92±0.00	1.44±0.01
0.100	0.04±0.02	0.71±0.01	0.97±0.02	1.48±0.02
0.150	0.00±0.00	0.71±0.01	0.98±0.02	1.50±0.02
0.200	0.011±0.01	0.74±0.01	0.99±0.01	1.52±0.01
Scan Rate (V/S)	**$I_r \times 10^{-4}$(A)**	**$I_1 \times 10^{-4}$(A)**	**$I_2 \times 10^{-4}$(A)**	**$I_3 \times 10^{-4}$(A)**
0.025	-0.86±0.09	2.67±0.08	3.66±0.17	2.64±0.26
0.050	-1.50±0.08	3.33±0.08	4.19±0.16	2.78±0.14
0.100	-2.79±0.29	4.39±2.20	6.00±0.37	3.29±0.24
0.150	-3.29±0.60	4.66±2.90	6.88±0.35	3.71±0.18
0.200	-3.86±0.10	5.32±0.10	7.60±0.50	3.64±0.31

Table 5.12: Oxidation potentials and peak currents for 3,4-DHBA under illumination at pH 3. Working electrode = TiO_2.

Scan Rate (V/S)	E_r (V)	E_1 (V)	E_2 (V)	E_3 (V)
0.025	----------	0.68±0.01	0.91±0.01	1.49±0.01
0.050	----------	0.69±0.01	0.95±0.00	1.49±0.01
0.100	0.09±0.01	0.72±0.02	0.97±0.02	1.51±0.02
0.150	0.01±0.01	0.71±0.01	1.01±0.00	1.52±0.01
0.200	0.00±0.01	0.72±0.01	1.04±0.00	1.57±0.01
Scan Rate (V/S)	**$I_r \times 10^{-4}$(A)**	**$I_1 \times 10^{-4}$(A)**	**$I_2 \times 10^{-4}$(A)**	**$I_3 \times 10^{-4}$(A)**
0.025	----------	2.57±0.17	3.77±0.27	2.33±0.20
0.050	----------	3.44±0.22	5.22±0.19	3.28±0.14
0.100	-1.25±0.21	4.17±0.47	5.72±0.38	3.54±0.11
0.150	-2.29±0.11	5.49±0.07	7.57±0.28	3.54±0.13
0.200	-2.87±0.19	6.17±0.18	8.61±0.41	3.82±0.21

Table 5.13: Oxidation potentials and peak currents for adsorbed 3,4-DHBA at pH 3. Working electrode = TiO_2.

Scan Rate (V/S)	E_1 (V)	$I \times 10^{-4}$(A)	E_2 (V)	$I \times 10^{-4}$(A)
0.050	0.96±0.01	3.65±0.09	1.46±0.03	2.49±0.49
0.100	1.02±0.01	4.79±0.73	1.53±0.15	3.05±0.49
0.150	1.08±0.00	6.46±0.50	1.57±0.07	3.44±0.07
0.200	1.06±0.02	6.25±0.55	1.55±0.04	3.54±0.14

able 5.14: Oxidation potentials and peak currents for 1,2,4-THB at pH 6. *Working electrode = Pt.*

Scan Rate (V/S)	E_r (V)	E_1 (V)	E_2 (V)
0.025	0.02	0.40	1.05
0.050	0.00	0.42	1.10
0.100	-0.03	0.46	1.15
0.150	-0.05	0.47	1.18
0.200	-0.08	0.50	1.22
Scan Rate (V/S)	**$I_r \times 10^{-4}$(A)**	**$I_1 \times 10^{-4}$(A)**	**$I_2 \times 10^{-4}$(A)**
0.025	-1.18	3.33	6.50
0.050	-1.25	5.84	10.84
0.100	-2.08	7.08	14.17
0.150	-2.50	8.75	16.25
0.200	-3.33	9.59	18.75

Table 5.15: Oxidation potentials and peak currents for 1,2,4-THB at pH 6. Working electrode = TiO_2.

Scan Rate (V/S)	E_1 (V)	$I \times 10^{-4}$(A)	E_2 (V)	$I \times 10^{-4}$(A)
0.025	0.34±0.01	3.34±0.34	0.62±0.01	3.84±0.08
0.050	0.40±0.00	5.75±0.42	0.69±0.01	6.09±0.28
0.100	0.42±0.02	6.35±0.35	0.78±0.01	8.02±0.10
0.150	0.45±0.01	5.52±0.31	0.80±0.00	8.71±0.36
0.200	0.47±0.00	6.25±0.05	0.87±0.03	10.40±0.41

Table 5.16: Oxidation potentials and peak currents for 1,2,4-THB under illumination at pH 6. Working electrode = TiO_2.

Scan Rate (V/S)	E_1 (V)	$I \times 10^{-4}$(A)	E_2 (V)	$I \times 10^{-4}$(A)
0.025	0.43±0.02	5.50±0.33	0.67±0.02	4.75±0.58
0.050	0.48±0.03	6.75±0.25	0.80±0.03	6.59±0.09
0.100	0.49±0.01	7.56±0.06	0.78±0.01	8.33±0.21
0.150	0.52±0.01	8.96±0.42	0.86±0.03	9.38±0.40
0.200	0.57±0.01	7.29±0.05	0.99±0.02	10.70±0.70

Table 5.17: Oxidation potentials and peak currents for adsorbed 1,2,4-THB at pH 6. Working electrode = TiO_2.

Scan Rate (V/S)	E_1 (V)	$I \times 10^{-4}$(A)	E_2 (V)	$I \times 10^{-4}$(A)
0.050	0.43±0.02	4.67±0.25	0.70±0.02	5.33±0.22
0.100	0.55±0.03	10.40±0.31	0.80±0.04	11.04±0.18
0.150	0.68±0.01	10.21±0.15	0.95±0.02	12.29±0.28
0.200	0.67±0.02	10.42±0.45	0.98±0.03	13.75±0.39

CONCLUSIONS

The redox reactions of selected aromatic compounds were examined on Pt and TiO_2 electrodes under various conditions. The results obtained indicate that their electrochemical behaviors are affected by the type and nature of the working electrode used, as well as the polarity of the organic compound under investigation. Similar redox behaviors were observed for weakly adsorbed organic compounds on both Pt and TiO_2 electrodes. Adsorption of these compounds on the TiO_2 electrodes was only noted under imposed adsorption conditions. Separate oxidation peaks were seen for adsorbed and free organics, with oxidation peak separation of 0.50 V to 0.70V. Under illumination, the observed peak current decreased in parallel with increasing number of chlorine atoms on the benzene ring.

The reversibility of the redox reaction of strongly adsorbed organics diminishes on TiO_2 due to the band structure and nature of these electrodes (reduction is not favored on an n-type semiconductor). Multiple oxidation peaks were detected on the TiO_2 electrodes for strongly adsorbed compounds; the peak at the most positive potentials was due to diffusion-controlled processes, while those at more negative potentials were assigned to adsorption. Based on these findings, it can be seen that associating the oxidation of these compounds to a single oxidation potential does not adequately describe the situation. An important distinction has to be made between free and adsorbed species,

depending on the type of working electrode being used. Figure 5.20 summarizes the determined oxidation potentials of both adsorbed and free model compounds on the TiO_2 electrode at pH 6. The position of the valence and the conduction band of TiO_2 at pH 6 is also shown.

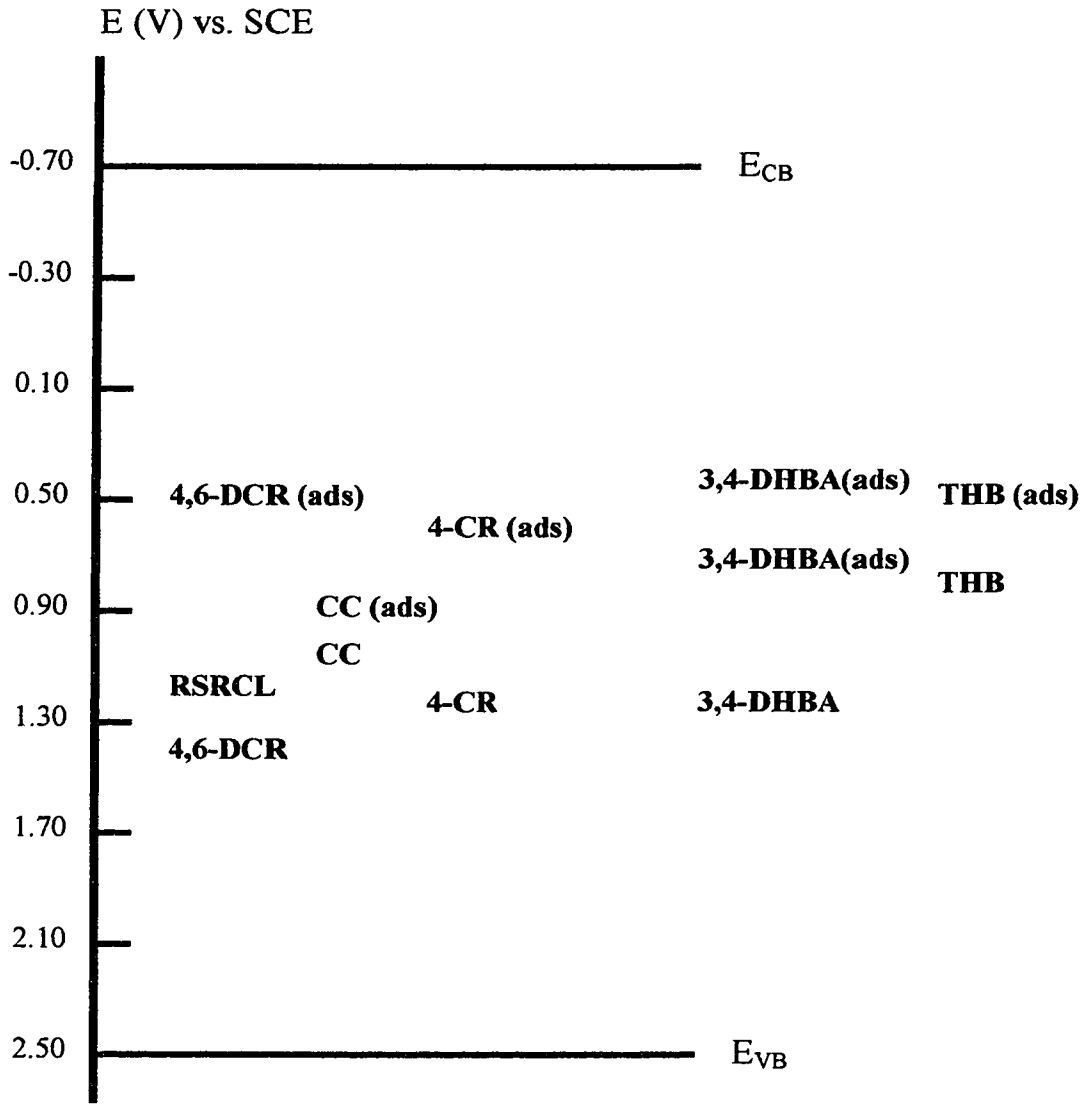

Figure 5.20: The oxidation potentials of model compounds on a TiO_2 electrode at pH 6.

References

1) Abelson, P. H.; *Science*, **1984**, *224*, 673.

2) Long, *J.; Chem. Eng. News*, **1984**, *62(5)*, 20.

3) Ollis, D. F.; in M. Schiavello (ed.), *Photocatalysis and the environment*, Kluwer, Dordrecht, **1989**, pp.663-677.

4) Turchi, C.S.; Ollis, D.F.*; J. Catal.*, **1990**, *122*, 178.

5) Linsebigler, A. L ; Lu, G ; Yates, J. T; *Chem. Rev.*, **1995**, *95*, 735-758.

6) Al-Ekabi, H ; Serpone, N ; *J. Phys. Chem.*, **1988**, *92*, 5726.

7) Vinodgopal, K ; Stafford, U ; Gray, K. A. ;Kamat, P. V. ; *J. Phys. Chem.*, **1994**, *98*, 6797.

8) Vinodgopal, K. ; Hotchandani, S. ; Kamat, P., V. ; *J. Phys. Chem.*, **1993**, *97*, 9040.

9) Gerischer, H.; Heller, A.; *J. Electrochem. Soc.*, **1992**, *139*, 113.

10) Stafford, U.; Gray, K.; Kamat, P.V.; Varma, A.*; Chem. Phys. Lett.*, **1993**, *55*, 205.

11) Mathews, R.W.; *J. Phys. Chem.*, **1987**, *91*, 3328.

12) Sabate, J.; Anderson, M.A.; Kikkawa, H.; Edwards, M.; Hill, C. G.; *J. Catal.*, **1991**, *127*, 167.

13) Peterson, M.W.; Turner, J.A.; Nozik, A.J.*; J. Phys. Chem.*, **1991**, *95*, 221.

14) Herrmann, J.M.; Pichat, P.; *J. Chem Soc. Faraday Trans. 1*, **1980**, *76*, 1138.

15) Mathews, R.W.; *J. Catal.*, **1988**, *111*, 264.

16) Barbeni, M.; Pramauro, E.; Pelizzetti, E.; Borgarello, E; Gratzel, M.; Serpone, N.*; Nouv. J. Chim.*, **1984**, *8*, 547.

17) Barbeni, M.; Pramauro, E.; Pelizzetti, E.; Vincenti, M.; Borgarello, E; Gratzel, M.; Serpone, N.; Jamieson, M.A.*; Chemosphere*, **1986**, *15*, 1913.

18) Terzian, R.; Serpone, N.; Minero, C.; Pelizzetti, E.; *J. Catal*, **1991**, *128*, 352.

19) Mills, A.; Morris, S.; Davies, R.; *J. Photochem. Photobiol. A: Chem.*, **1993**, *70*, 183.

20) Mills, A.; Morris, S.; *J. Photochem. Photobiol. A: Chem.*, **1993**, *71*, 285.

21) Sehili, T.; Boule, P.; Lemaire, J.; *J. Photochem. Photobiol. A: Chem.*, **1989**, *50*, 117.

22) Okamoto, K.; Yamamoto, Y.; Tanaka, H.; Tanaka, M.; Itaya, A.; *Bull. Chem. Soc. Jpn.*, **1985**, *58*, 2015.

23) Augugliaro, V.; Palmisano, L.; Sclafani, A.; Minero, C.; Pelizzetti, E.; *Toxicol. Environ. Chem.*, **1988**, *16*, 89.

24) Neguyen, T.; Ollis, D.F.; *J. Phys. Chem.*, **1984**, *88*, 3386.

25) Kaeuttler, B.; Brad, A.J.; *J. Am. Chem. Soc.*, **1978**, *100*, 2339.

26) Flinklea, H. O.; *J. Chem. Edu.*, **1983**, *60*, 325.

27) Mills, A. ; Morris, S. ; Davis, A. ; *J. Photochem. Photobiol. A: Chem.*, **1993**, *70*, 183.

28) Serpone, N.; and Pelizzetti, E.; " *Photocatalysis - Fundamentals and applications*", John Weily & Sons, New York, **1989**, p. 420.

29) Fox, M. A.; Dualy, M. T; *Chem. Rev.*, **1993**, 93, 341.

30) (a) Schmickler, W.; *"Interfacial Electrochemistry"*, Oxford University Press, **1996**, p. 82. (b) Ibid, p. 91. (c) Ibid. p. 21.

31) (a) Harris, D. C.; " *Quantitative Chemical Analysis* ", 2nd Edition, W. H. Freeman & Company, New York, **1987**, p. 458. (b) Ibid. p. 477.

32) (a) Kissinger, P. T.; Heineman, W. R.; " *Laboratory Techniques in Electroanalytical Chemistry* ", Marcel Dekker Inc., New York, **1984**, p. 321; b) p. 367; c) Ibid. p. 31.

33) Moser, J.; Punchihewa, S.; Infelta, P. P.; Gratzel, M.; *Langmuir*, **1991**, *7*, 3012.

34) Hubbard, A.T; Anson, F.C; *J. Anal. Chem.*, **1966**, *38*, 58.

35) Wopschall, R.H.; Shain, I; *J. Anal. Chem.*, **1967**, *39*, 1514.

36) Tunesi, S.; Anderson, M.; *J. Phys. Chem.*, **1991**, *95*, 3399.

37) Tunesi, S.; Anderson, M.; *Langmuir*, **1992**, *8*, 489.

38) McMurry, J.; " *Organic Chemistry* ", 2nd Edition, Brooks/Cole Publishing Company, Pacific Groove, California, **1988**, p. 39.

39) Terney, A. L.; " *Contemporary Organic Chemistry* ", W. B. Saunders Company, Toronto, Canada, **1976**, p. 681.

40) Koval, C. A.; Howard, J. N.; *Chem. Rev.*, **1992**, *92*, 411.

41) Sinn, C.; Meisser, D.; Memming, R.; *J. Electrochem. Soc.*, **1990**, *137*, 168.

42) Etman, M.; *J. Phys. Chem.*, **1986**, *90*, 1844.

43) Sawyer, D. T.; Sobkowiak, A.; Roberts, J. L.; " *Electrochemistry for Chemists* ", 2nd Edition, John Wiley & Sons Inc., New York, **1995**, p. 442.

44) Yan, S.G.; Hupp,ZJ.T.; *J. Phys. Chem.*, **1996**, *100*, 6867.

45) Redmond, G.; Fitzmaurice, D.; *J. Phys. Chem.*, **1993**, *97*, 1426.

46) Flinklea, H. O.; " *Semiconductor Electrodes* ", Elsevier Science Publishers B. V., New York, **1988**, p. 80.

47) Serpone, N.; Sauve, G.; Kosh, R.; Tahiri, H.; Pichat, P.; Piccinini, P.; Pelizzetti, E.; Hidaka, H.; *J. Photochem. Photobiol. A: Chem.*, **1996**, *94*, 191.

48) Gosser, Jr., D. K.; " *Cyclic Voltammetry Simulation and Analysis of Reaction Mechanisms* ", VCH Publisher Inc., **1993**, p. 71; **b)** p. 31.

49) Meissner, D.; Lauermann, I.; Memming, R.; Kastening, B.; *J. Phys. Chem.*, **1988**, *92*, 3484.

APPENDIX

SAMPLE VOLTAMMOGRAMS OF MODEL COMPOUNDS UNDER VARIOUS CONDITIONS

(All voltammograms were obtained at a scan rate of 50 mV/s)

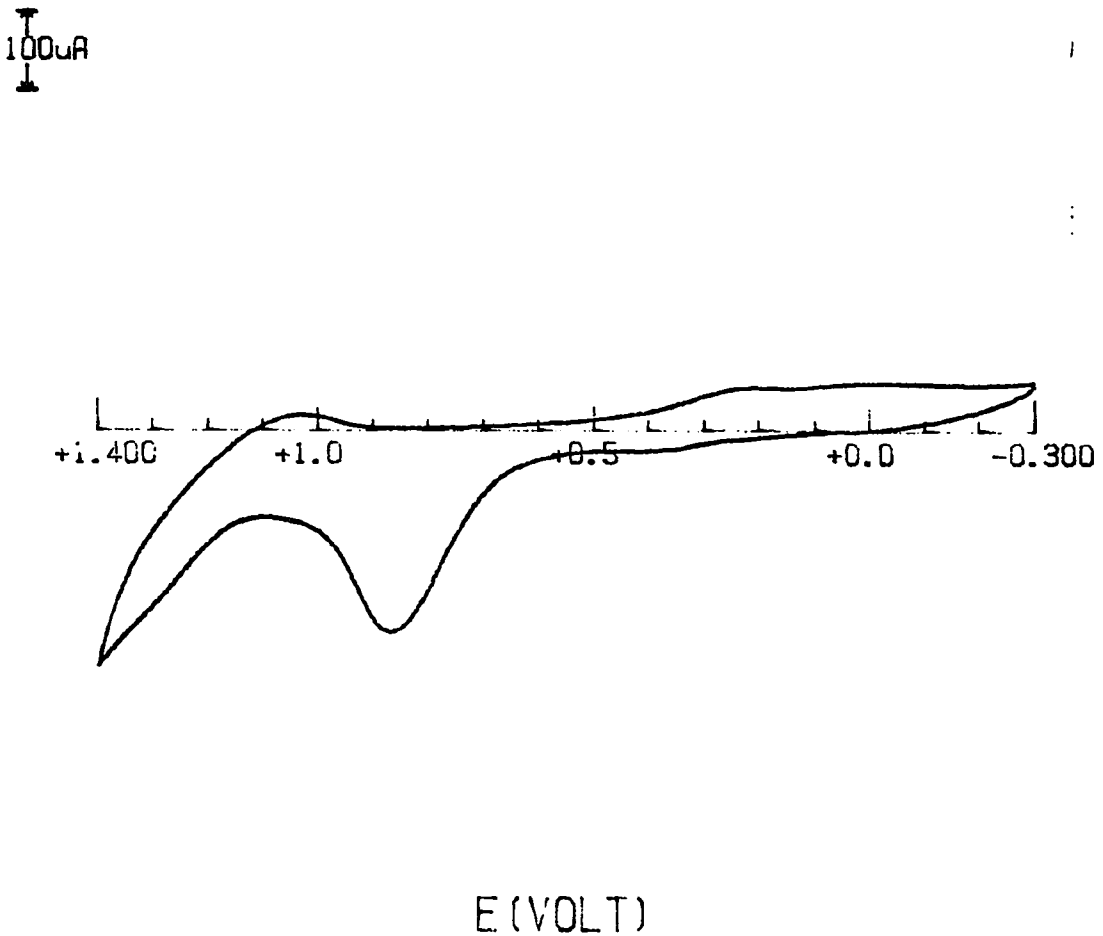

Figure A-1: Voltammogram of RSRCL on a Pt electrode.

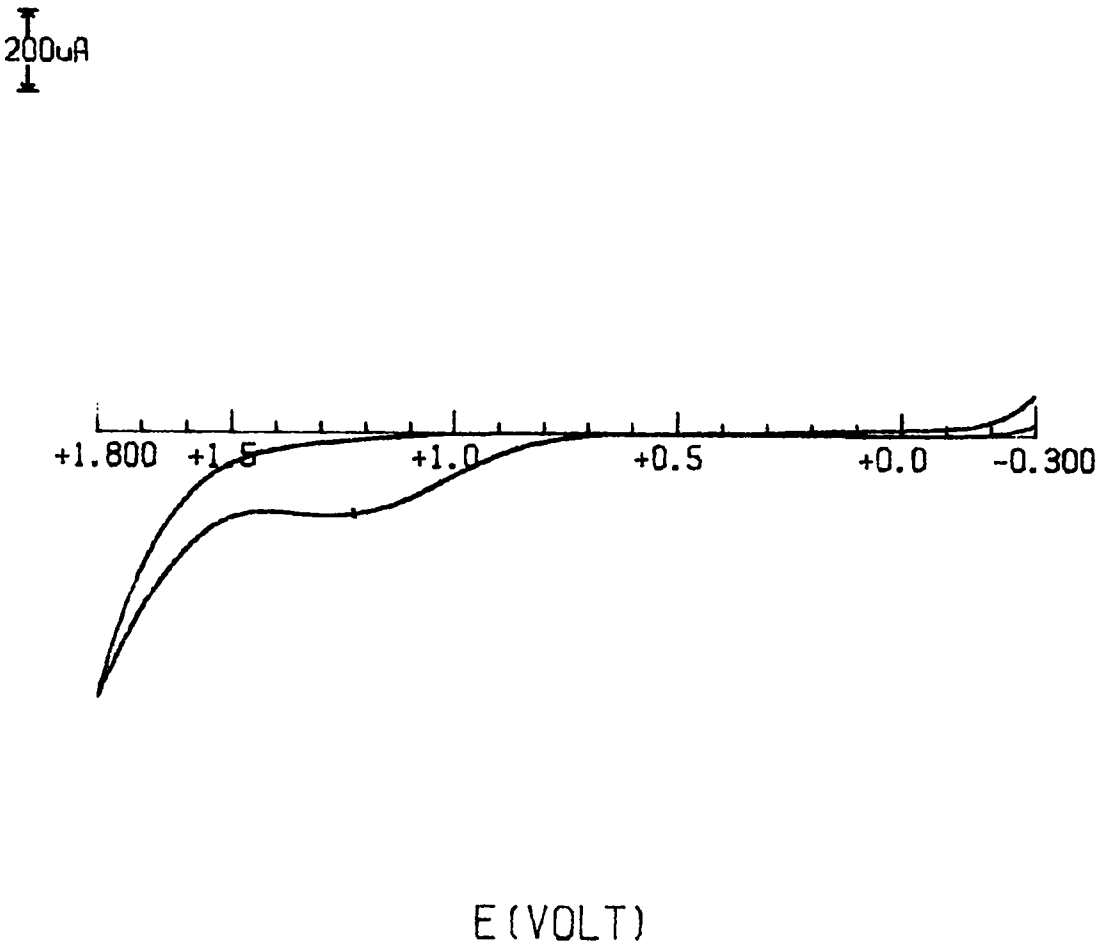

Figure A-2: Voltammogram of RSRCL on a TiO_2 electrode.

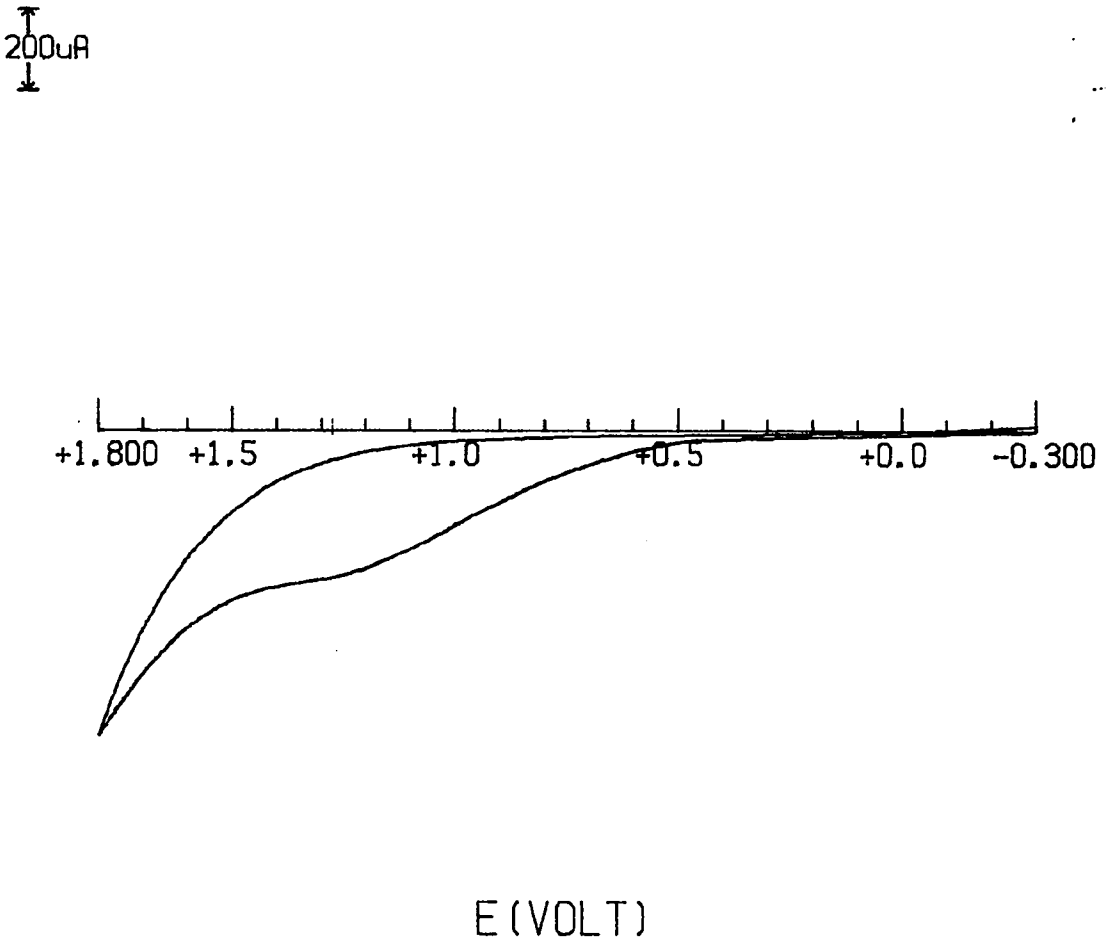

Figure A-3: Voltammogram of RSRCL on an illuminated TiO_2 electrode.

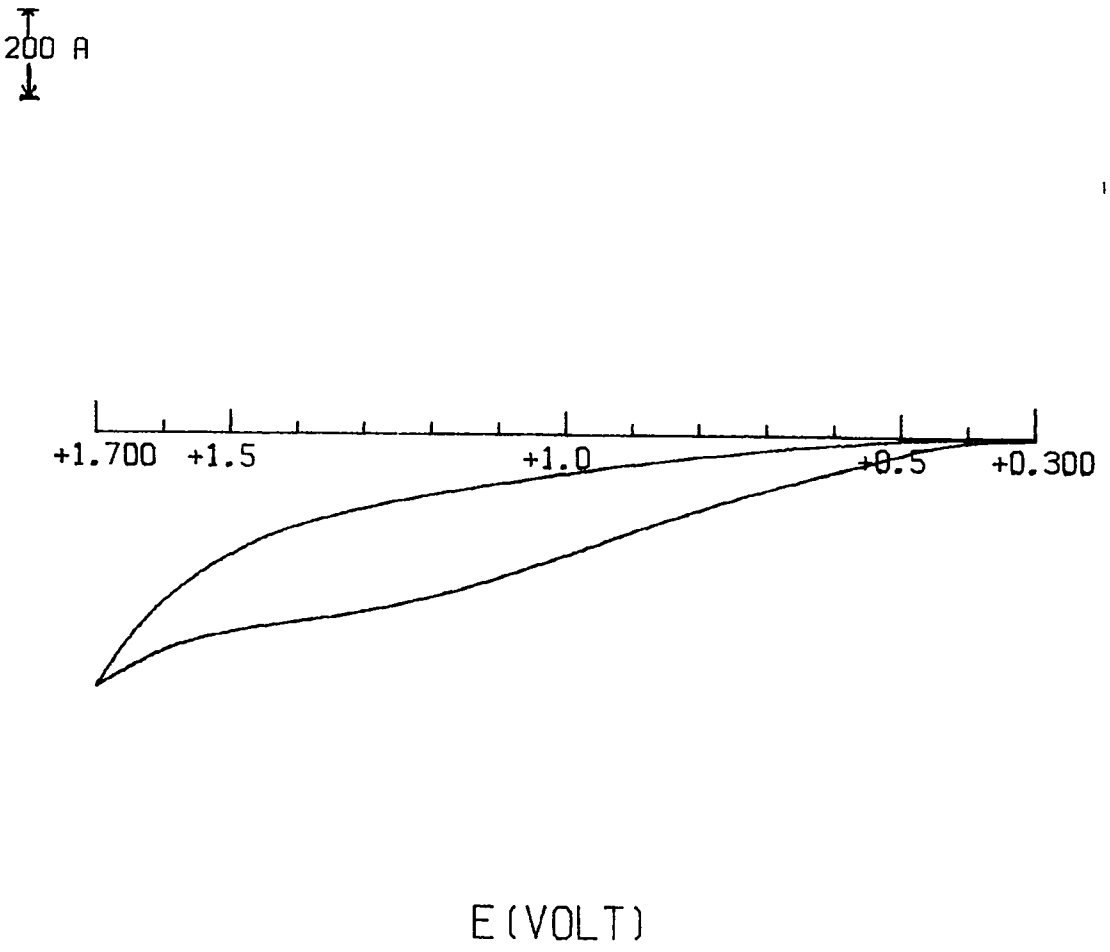

Figure A-4: Voltammogram of adsorbed RSRCL on a TiO_2 electrode.

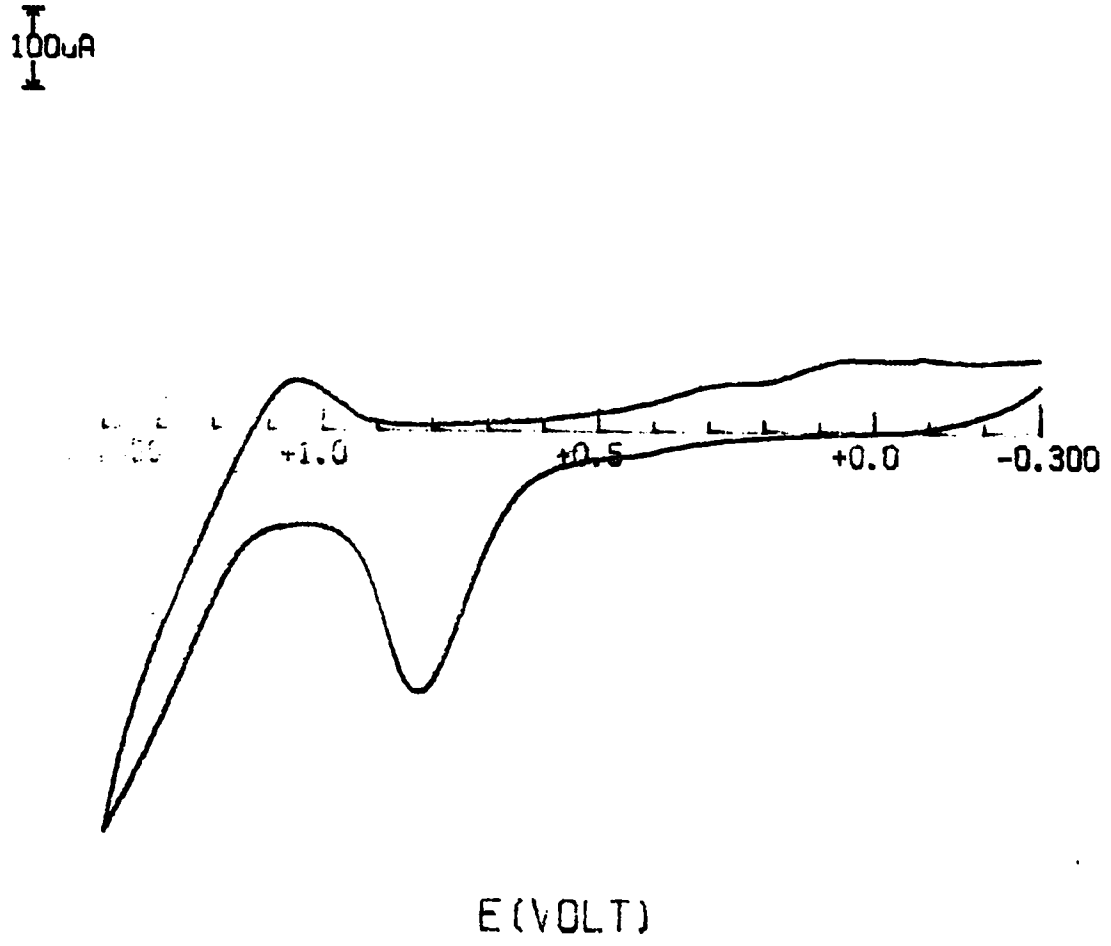

Figure A-5: Voltammogram of 4-CR on a Pt electrode.

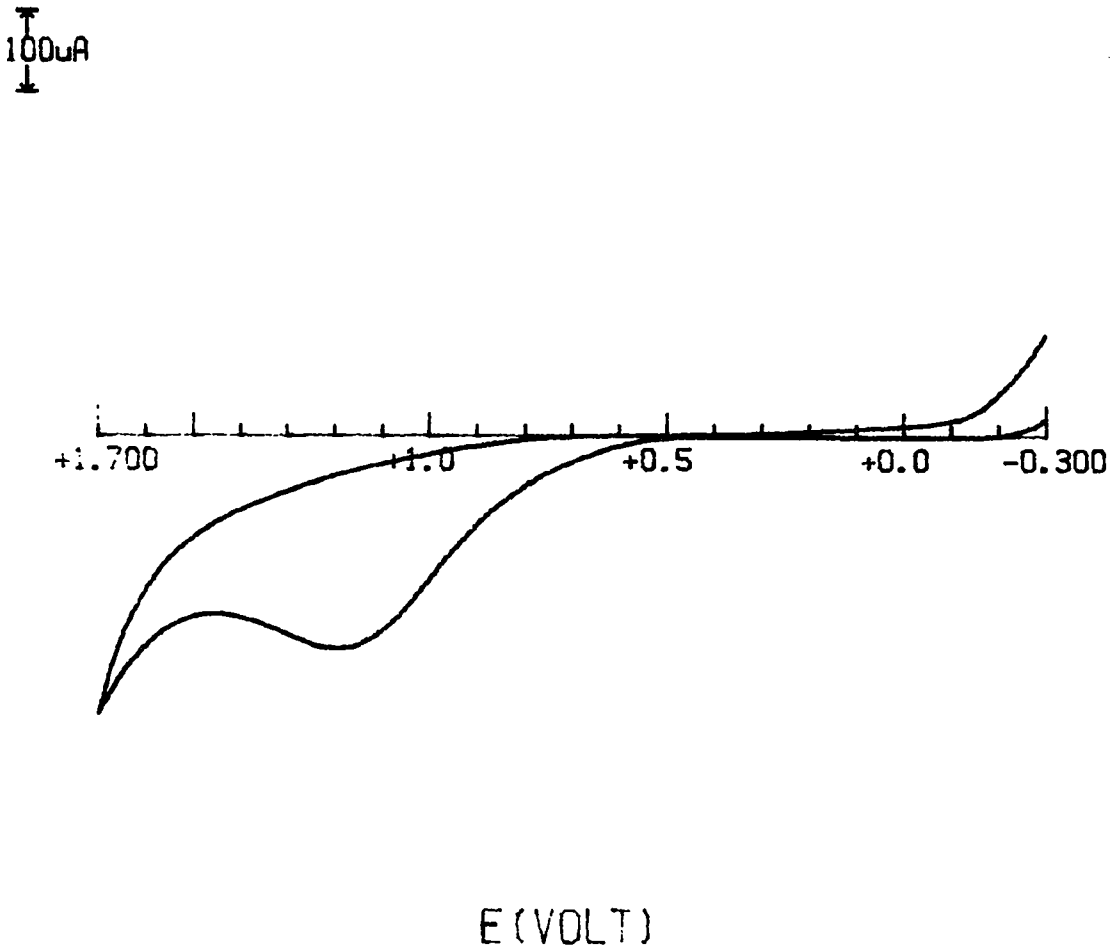

Figure A-6: Voltammogram of 4-CR on a TiO_2 electrode.

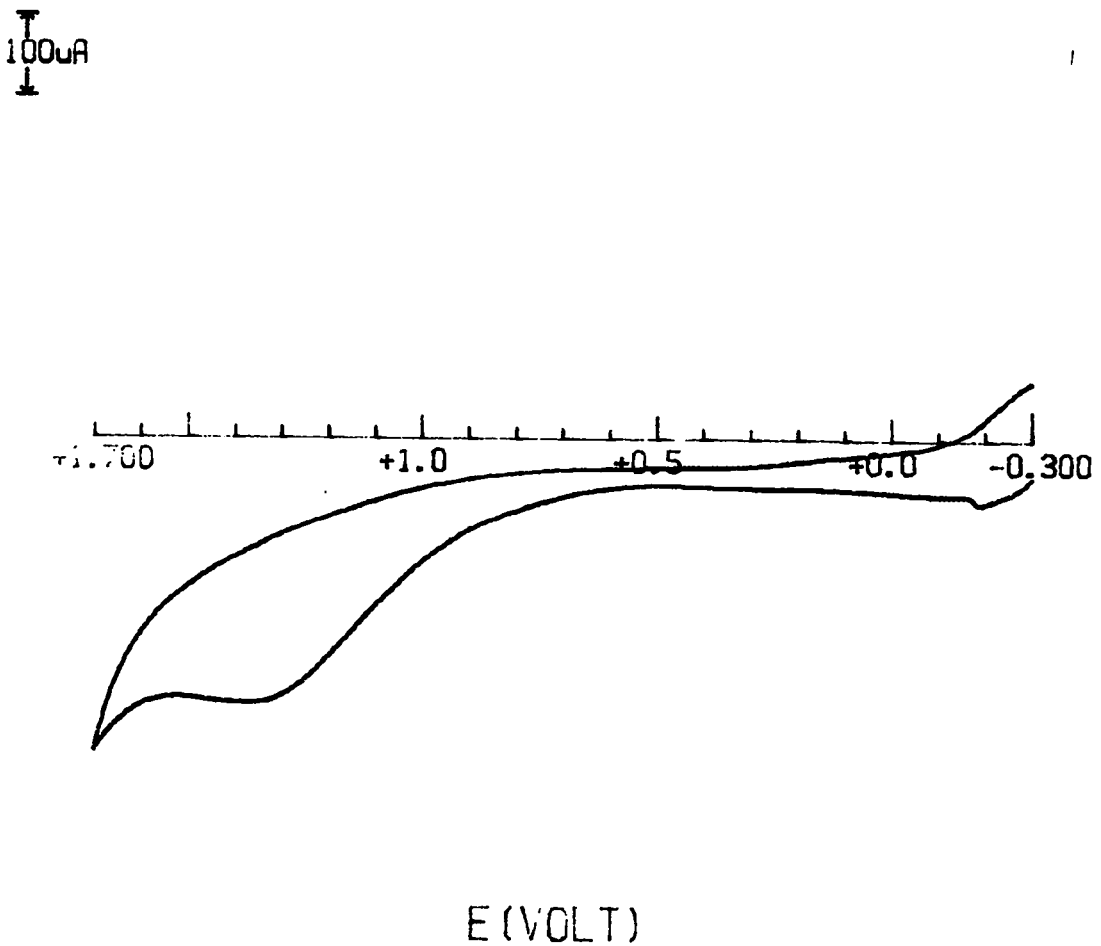

Figure A-7: Voltammogram of 4-CR on an illuminated TiO_2 electrode.

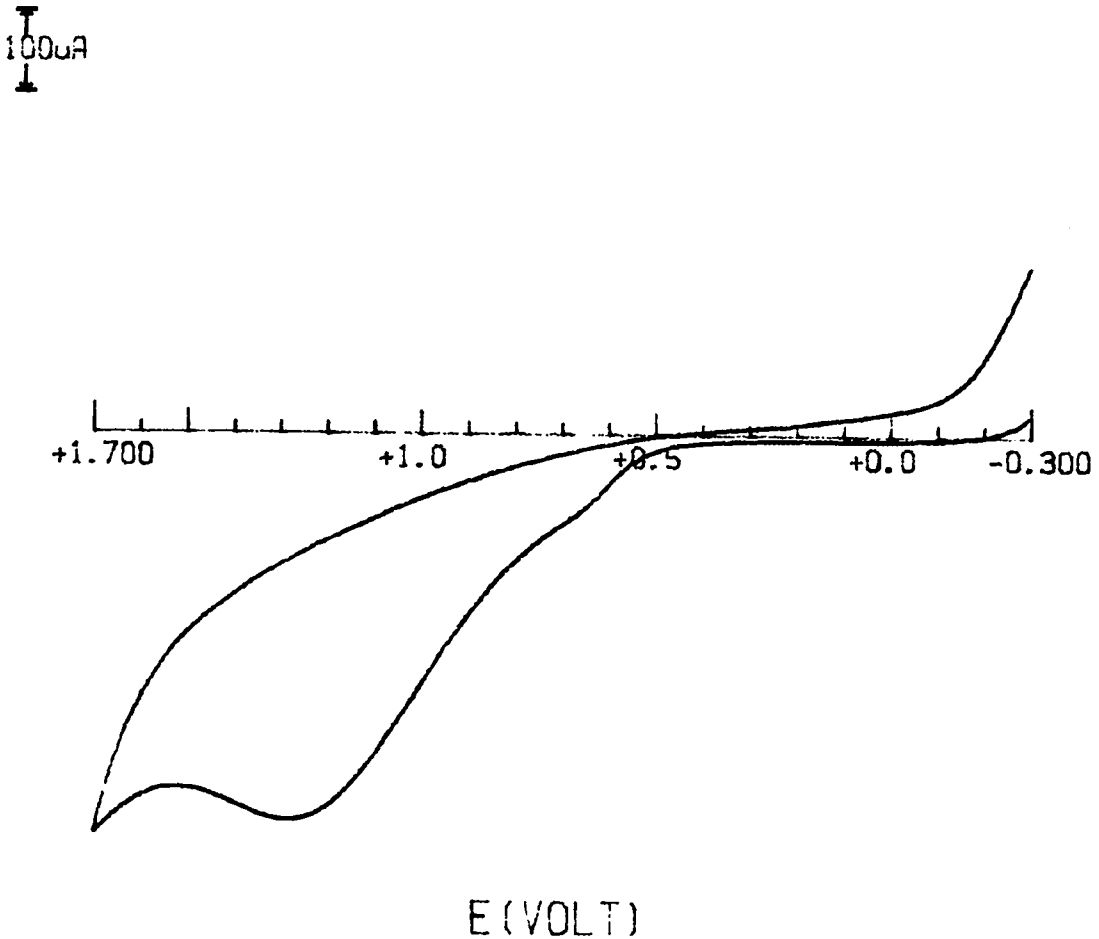

Figure A-8: Voltammogram of adsorbed 4-CR on a TiO_2 electrode.

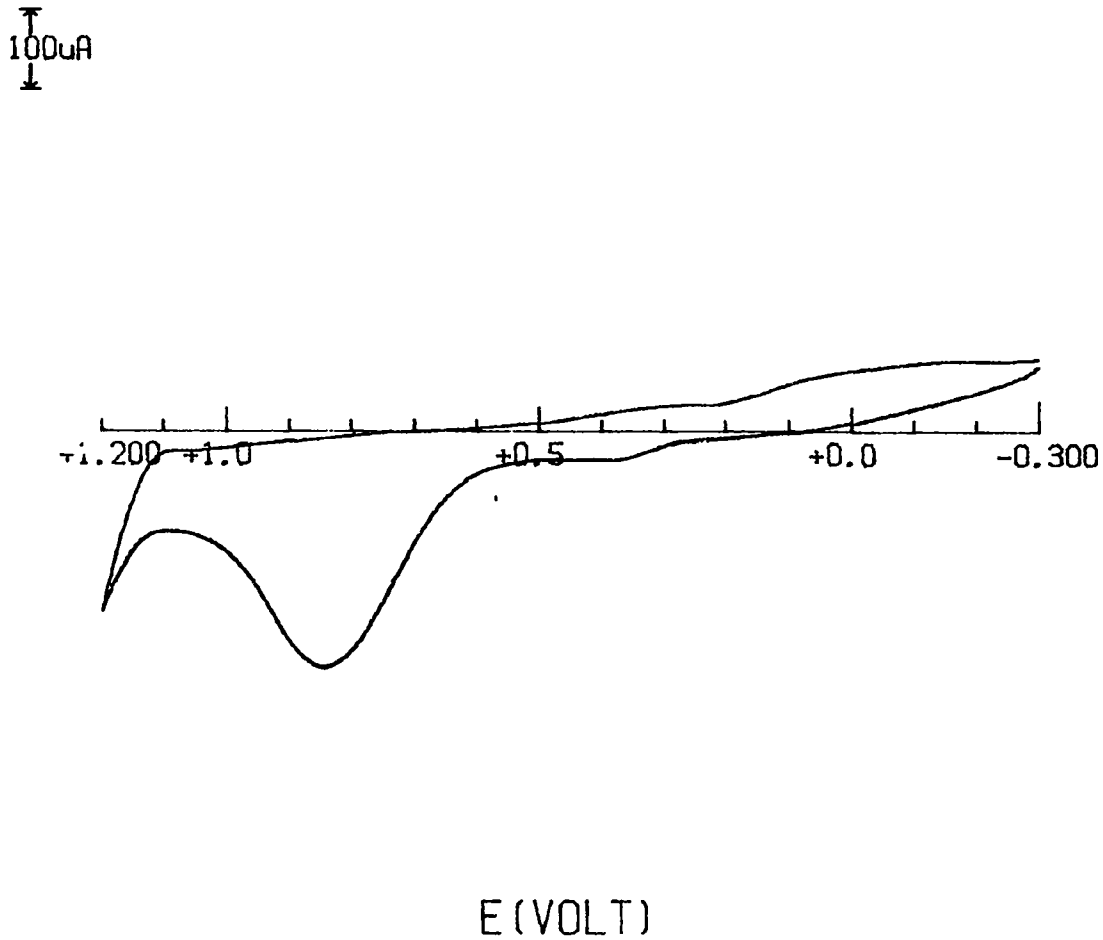

Figure A-9: Voltammogram of 4,6-DCR on a Pt electrode.

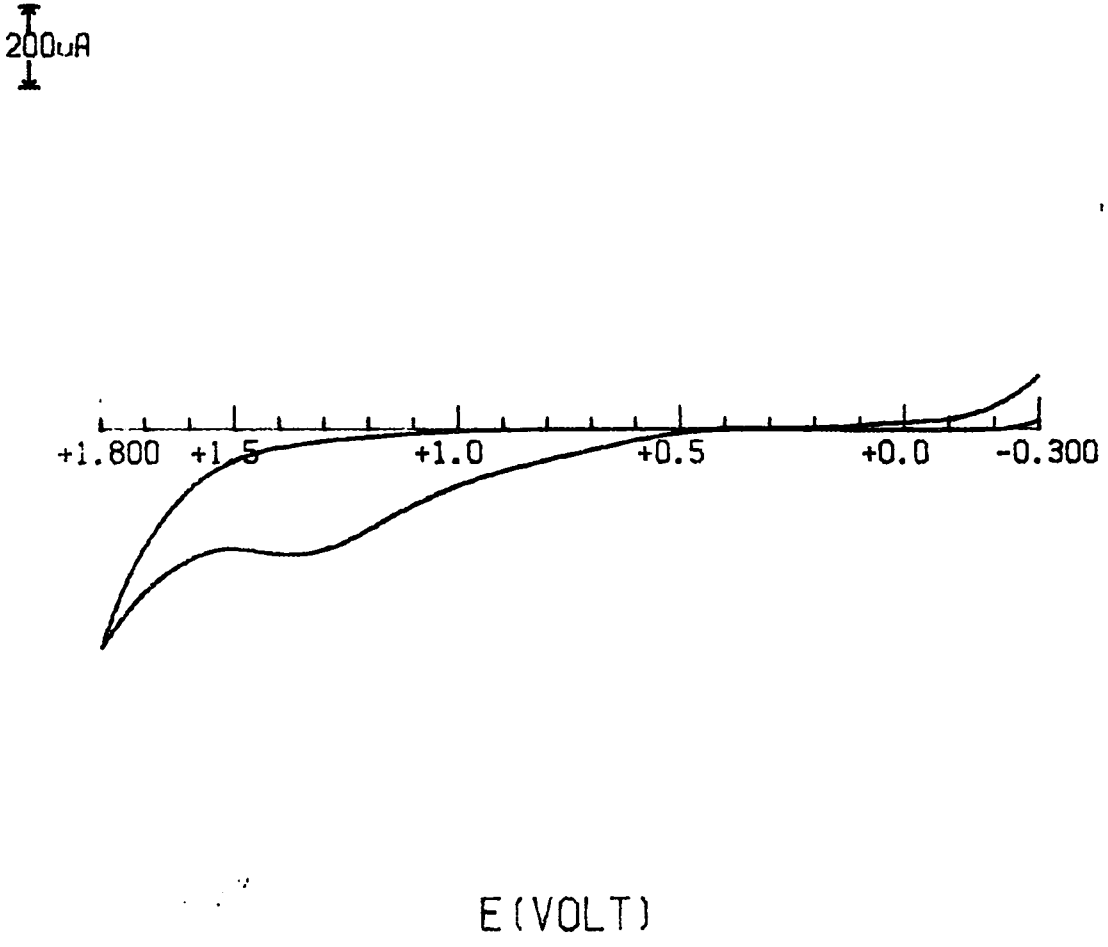

Figure A-10: Voltammogram of 4,6-DCR on a TiO_2 electrode.

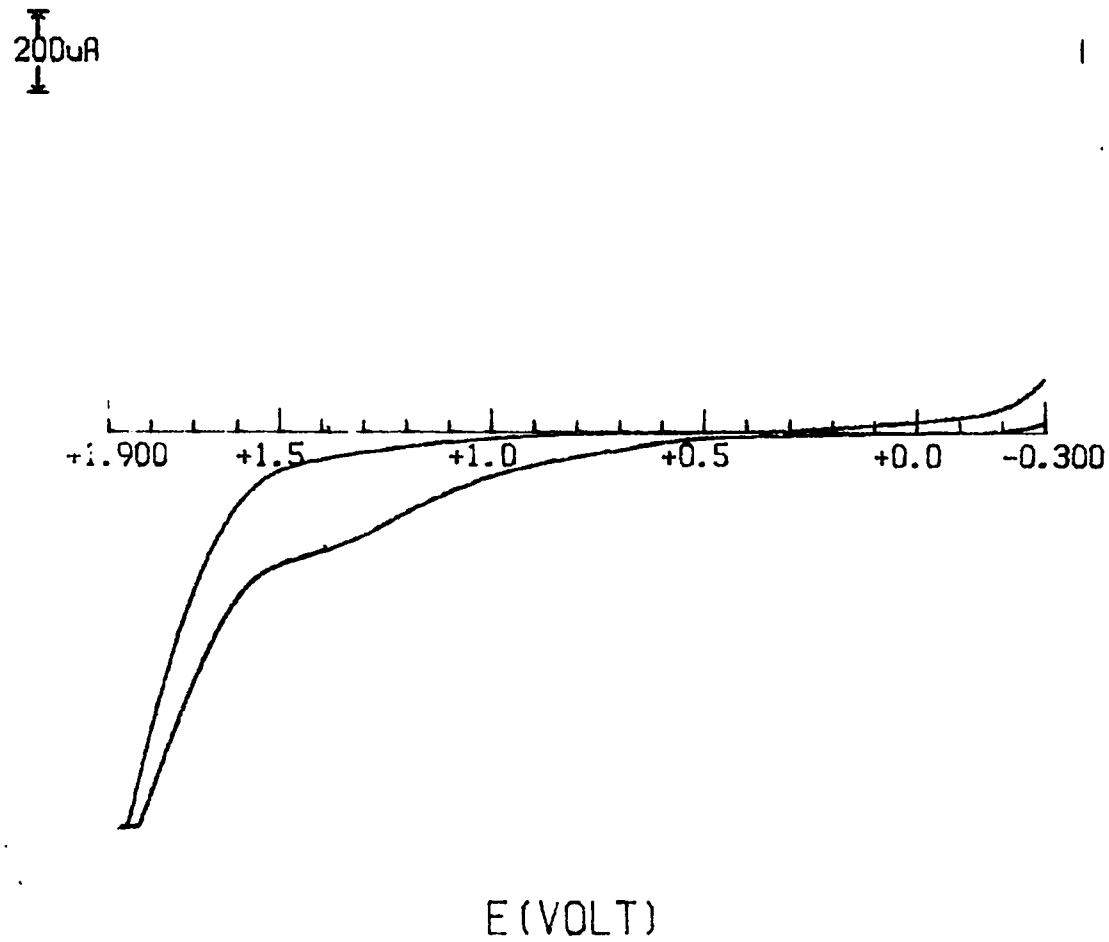

Figure A-11: Voltammogram of 4,6-DCR on an illuminated TiO_2 electrode.

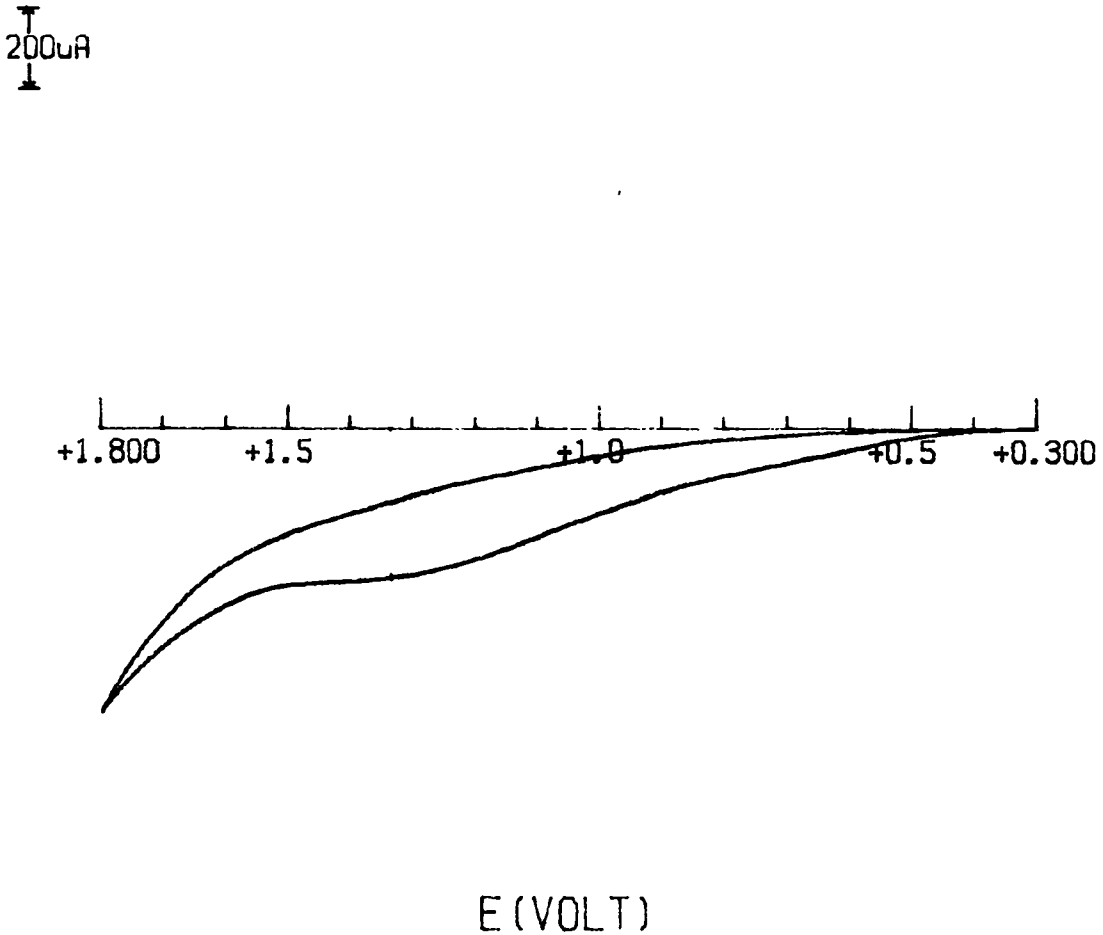

Figure A-12: Voltammogram of adsorbed 4,6-DCR on TiO_2 electrode.

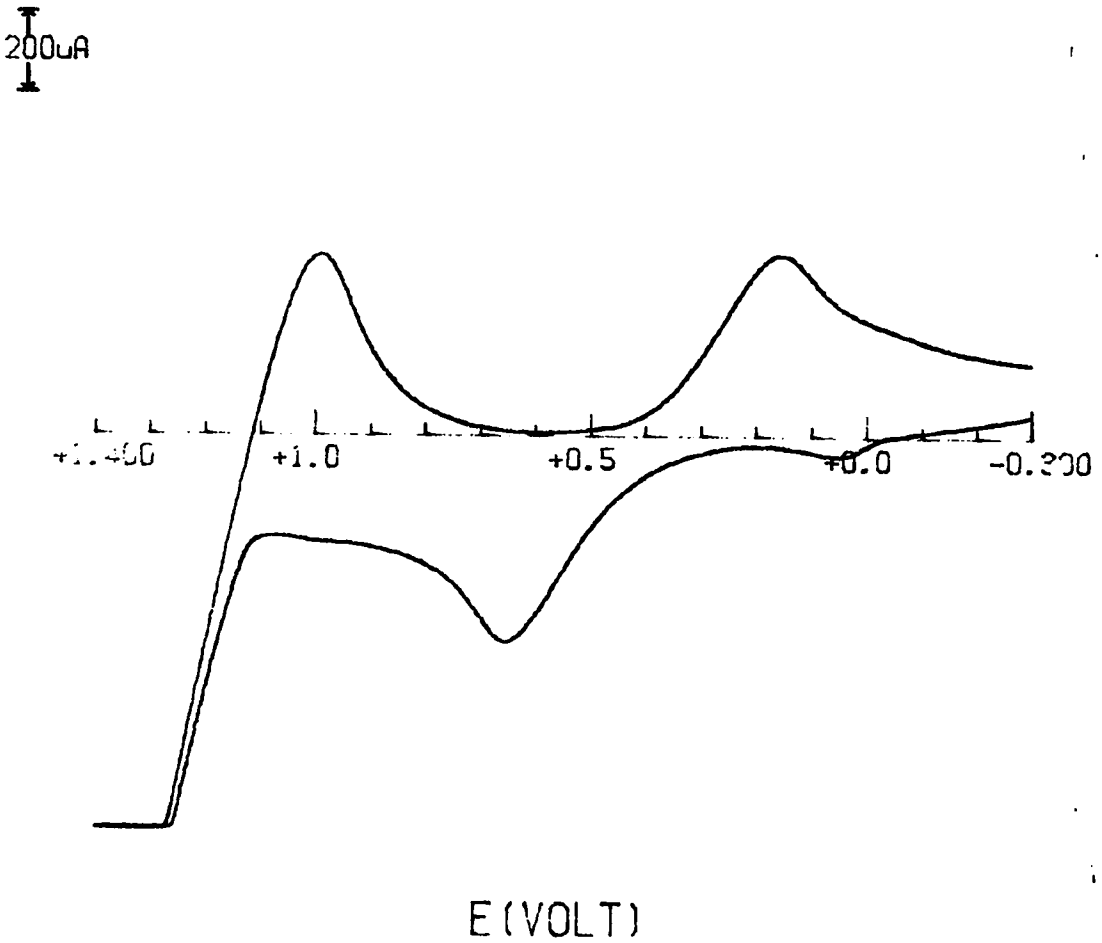

Figure A-13: Voltammogram of CC on a Pt electrode.

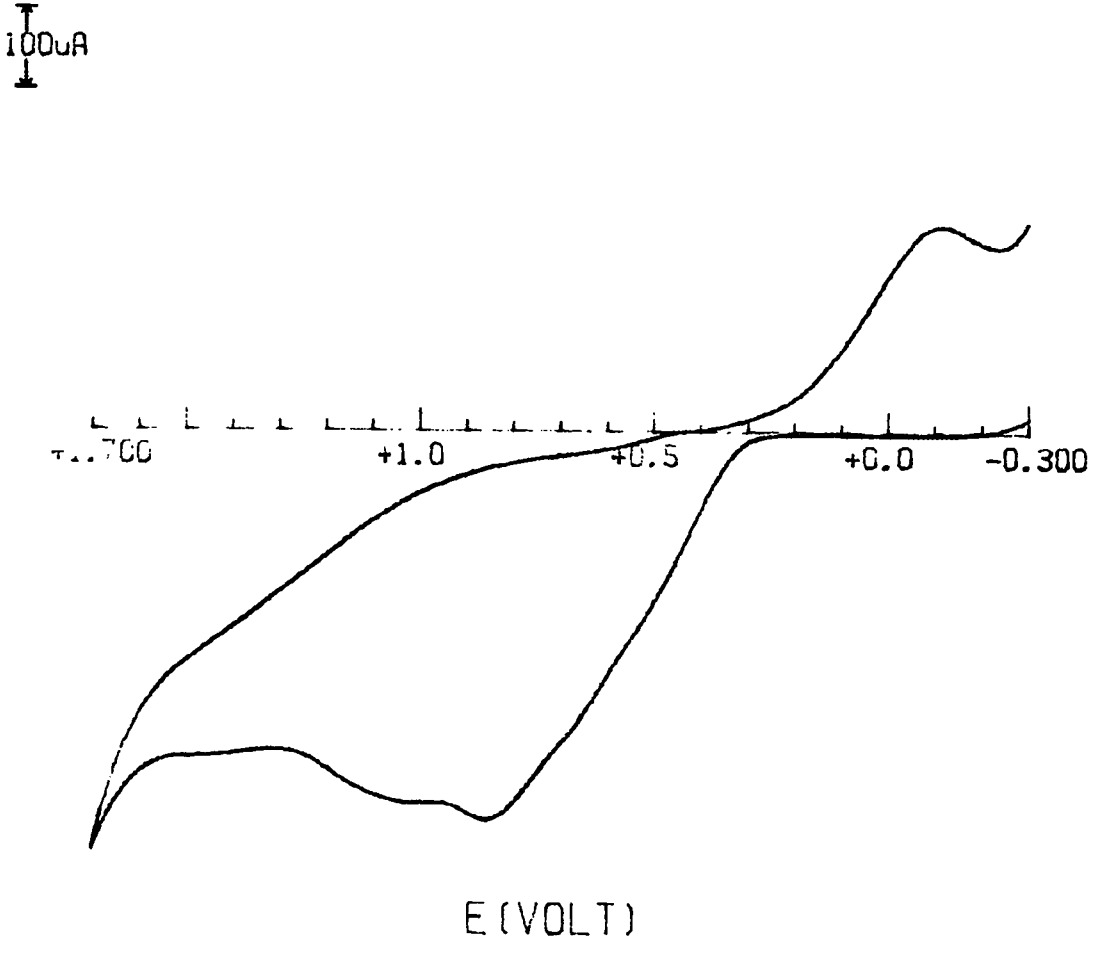

Figure A-14: Voltammogram of CC on a TiO_2 electrode.

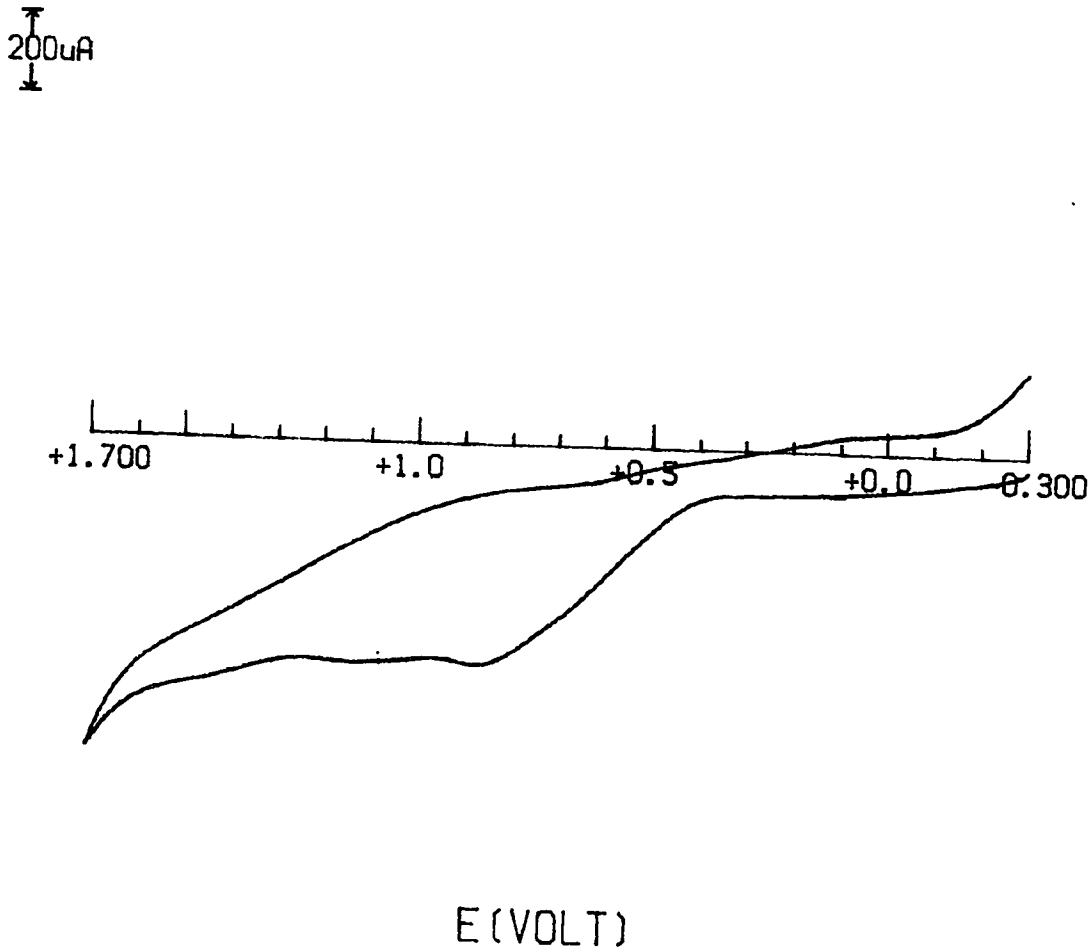

Figure A-15: Voltammogram of CC on an illuminated TiO_2 electrode.

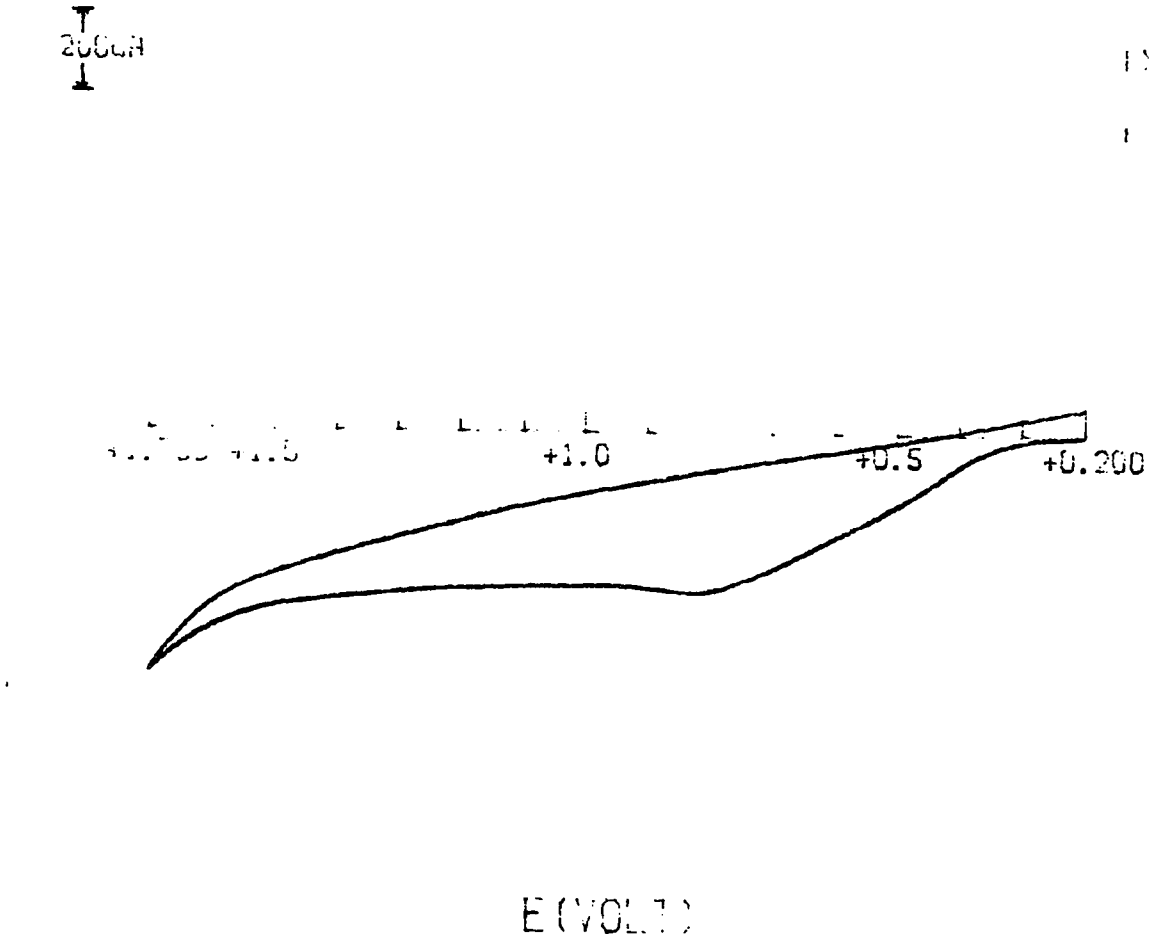

Figure A-16: Voltammogram of adsorbed CC on a TiO_2 electrode.

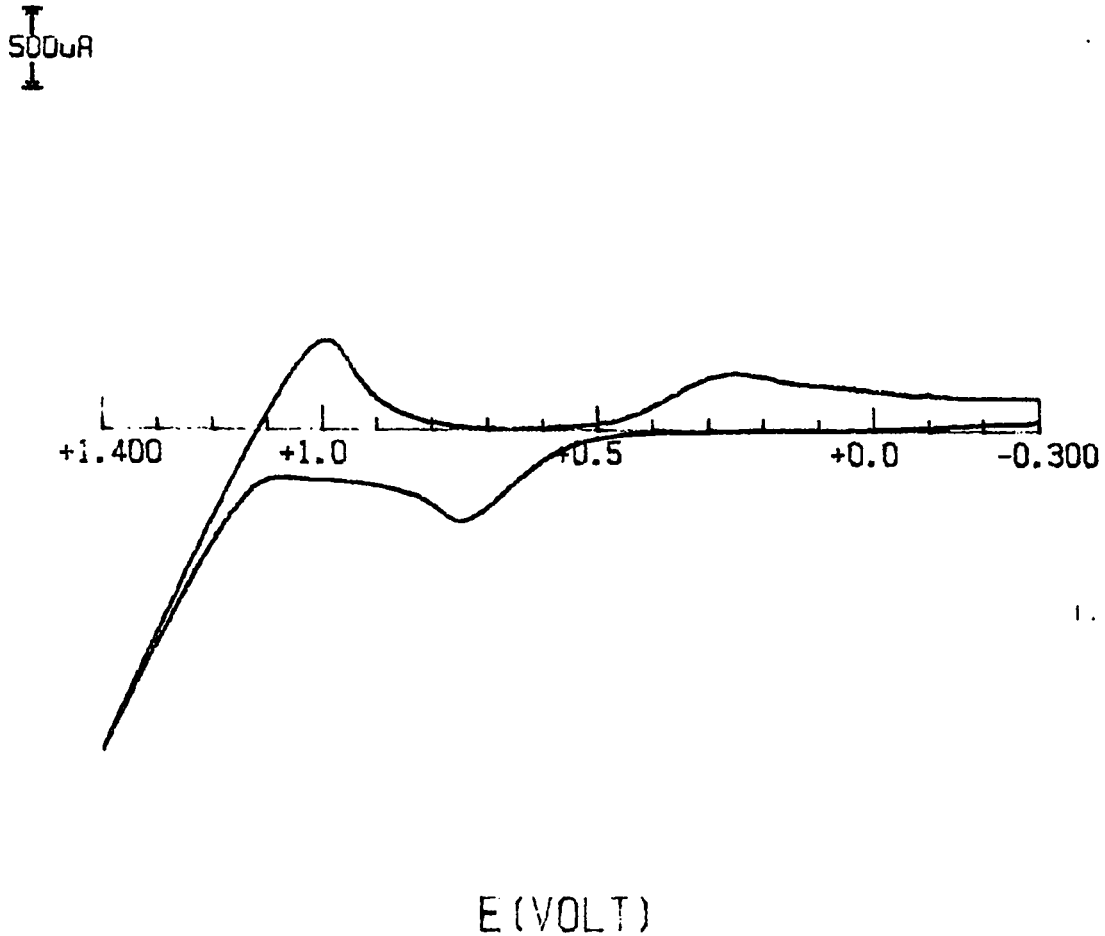

Figure A-17: Voltammogram of 3,4-DHBA on a Pt electrode.

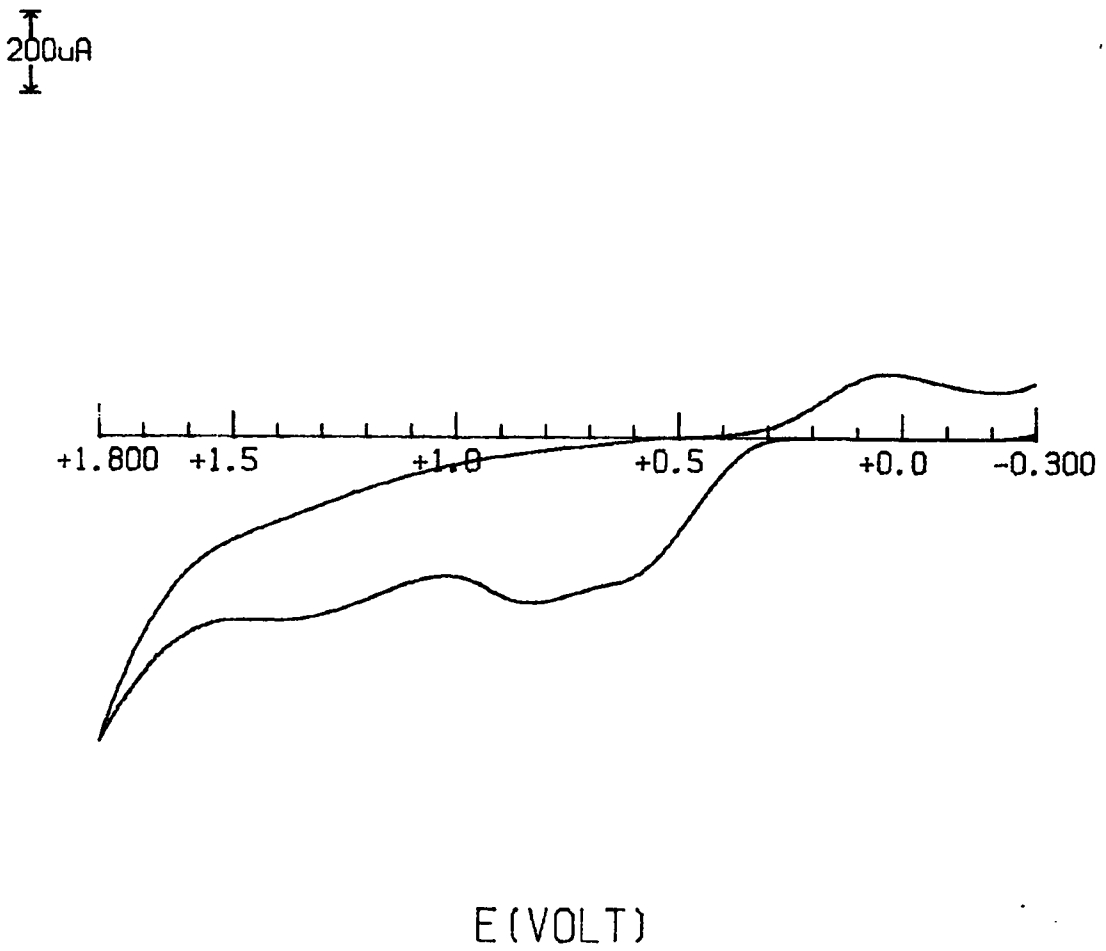

Figure A-18: Voltammogram of 3,4-DHBA on a TiO_2 electrode.

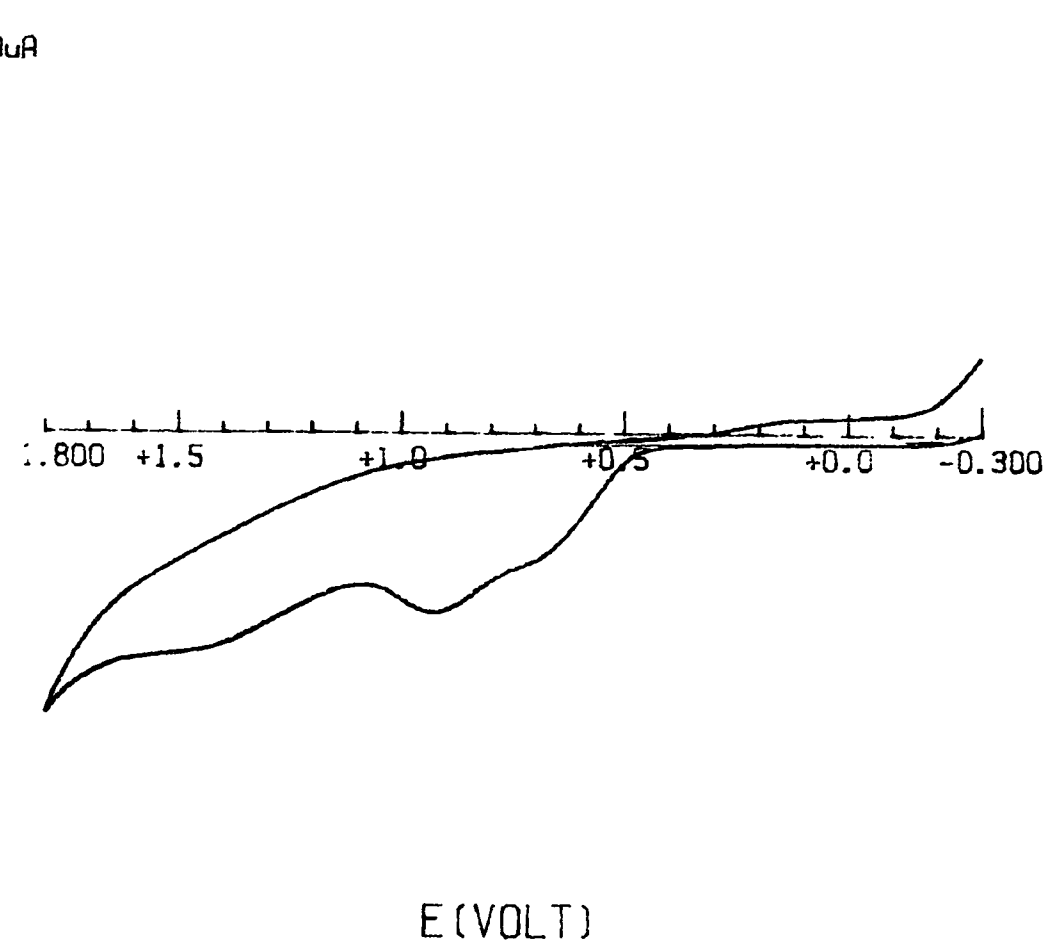

Figure A-19: Voltammogram of 3,4-DHBA on an illuminated TiO_2 electrode.

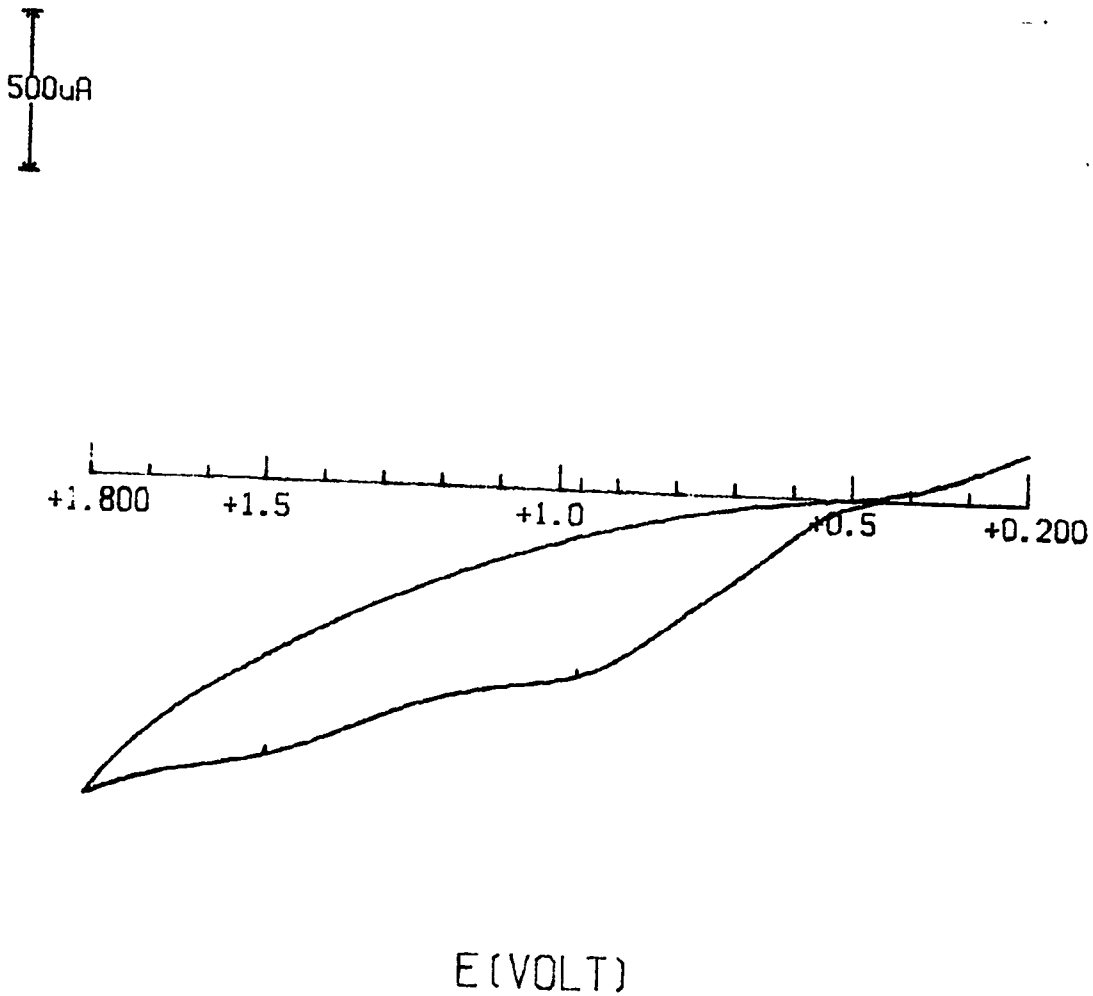

Figure A-20: Voltammogram of adsorbed 3,4-DHBA on a TiO_2 electrode.

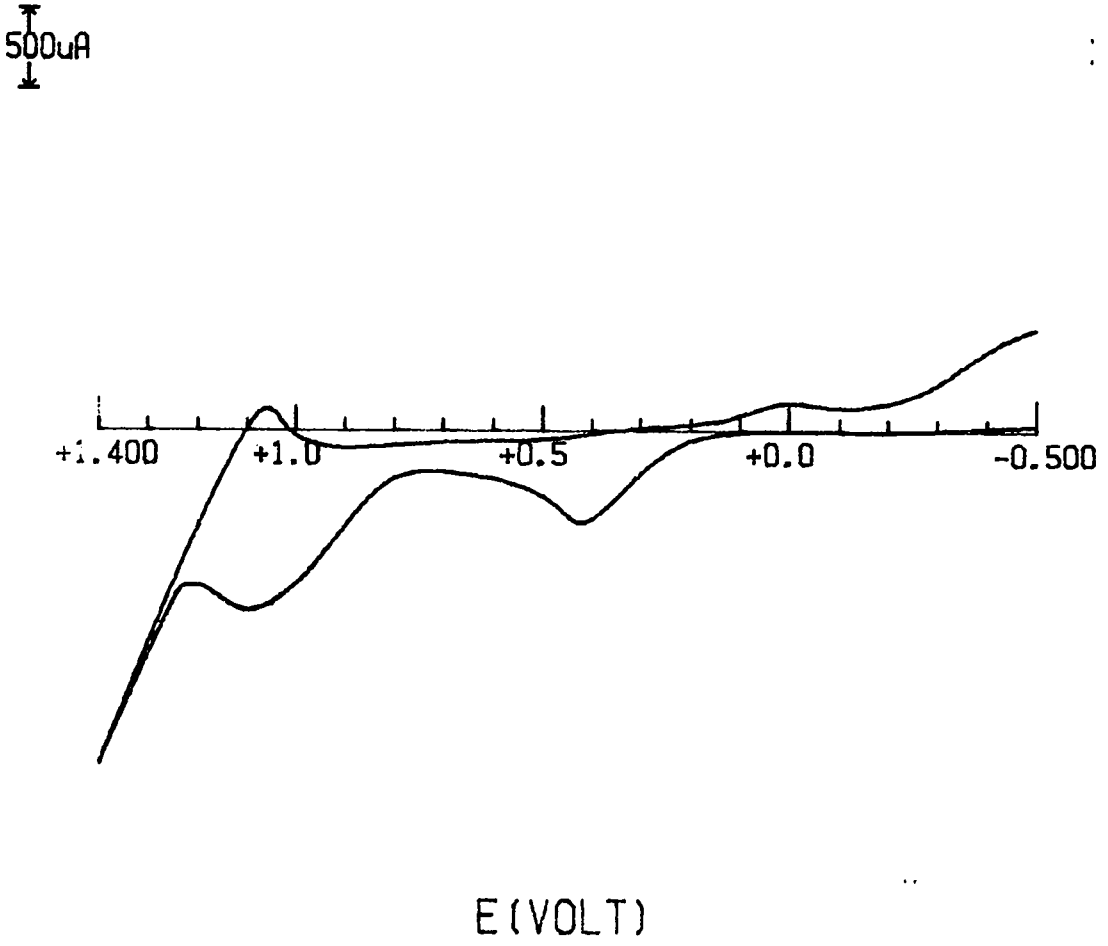

Figure A-21: Voltammogram of 1,2,4-THB on a Pt electrode.

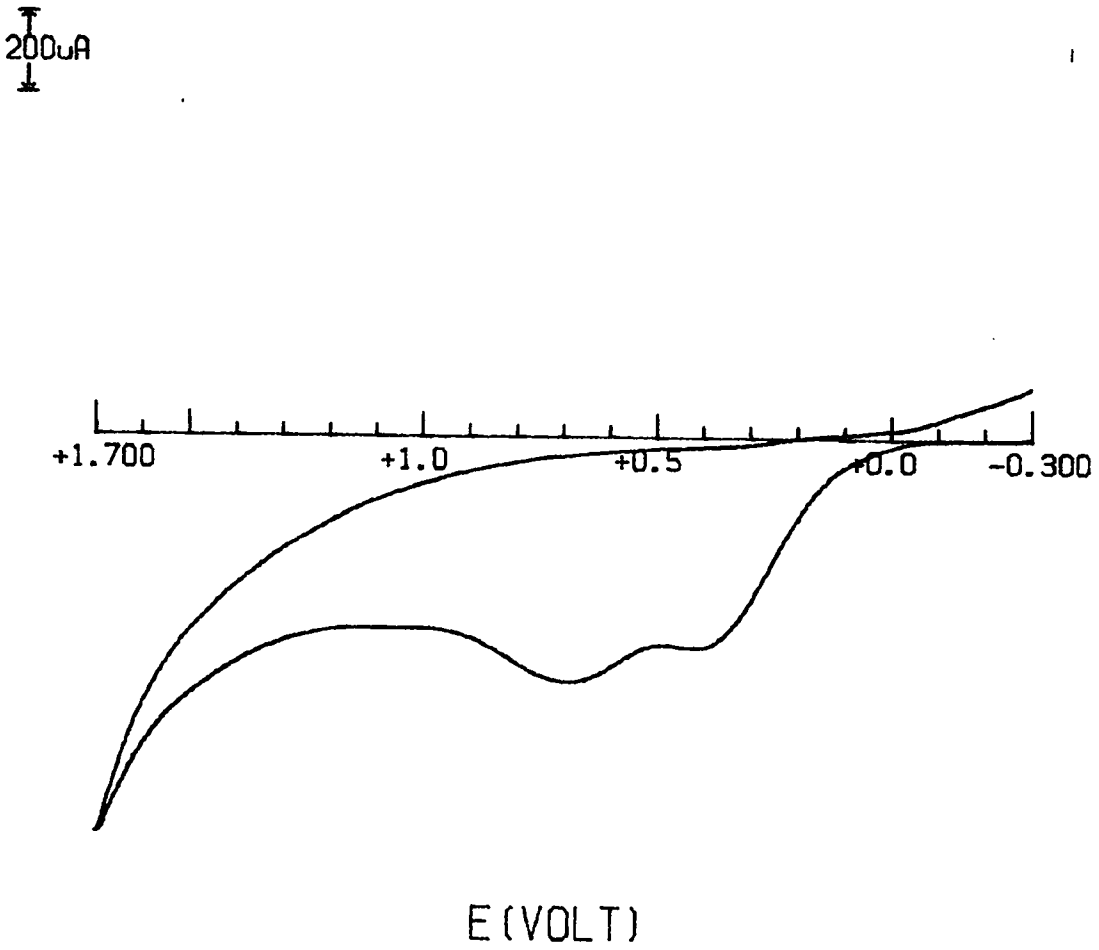

Figure A-22: Voltammogram of 1,2,4-THB on a TiO_2 electrode.

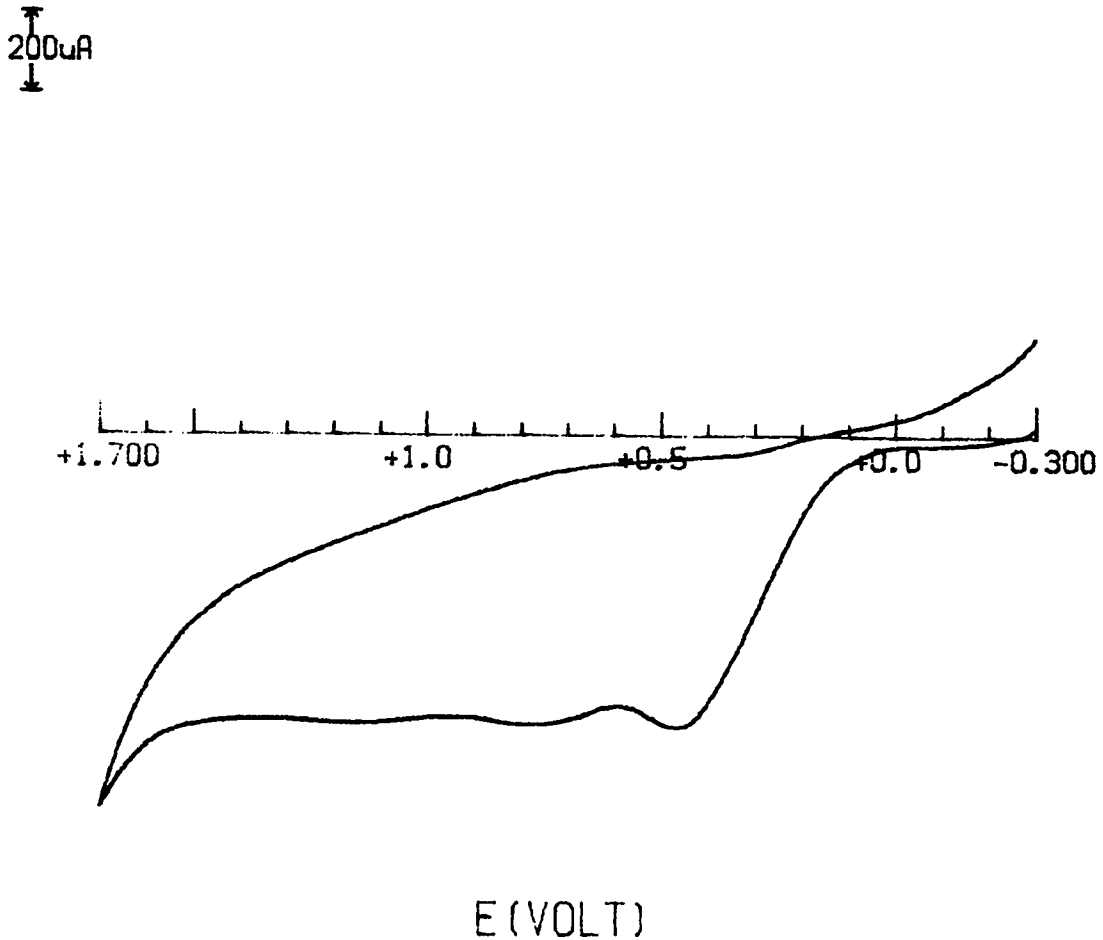

Figure A-23: Voltammogram of 1,2,4-THB on an illuminated TiO_2 electrode.

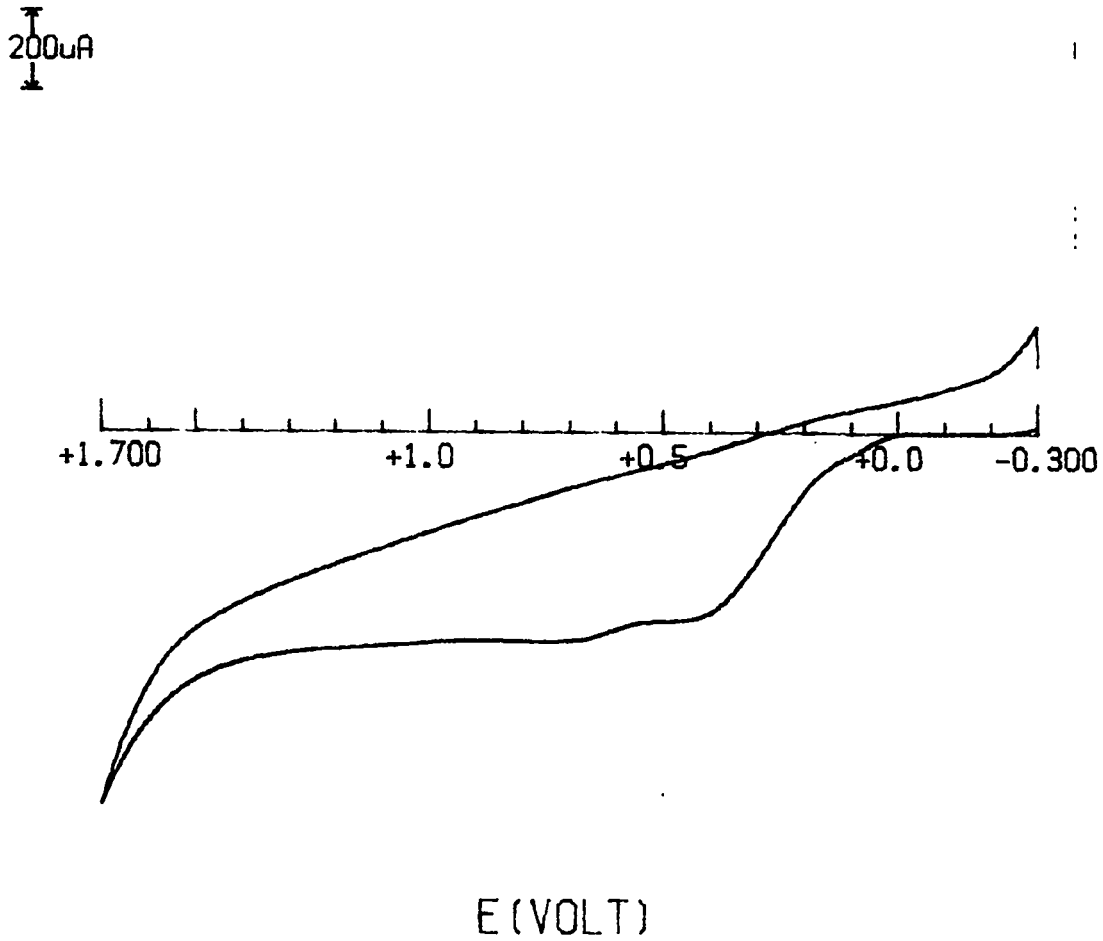

Figure A-24: Voltammogram of adsorbed 1,2,4-THB on a TiO_2 electrode.

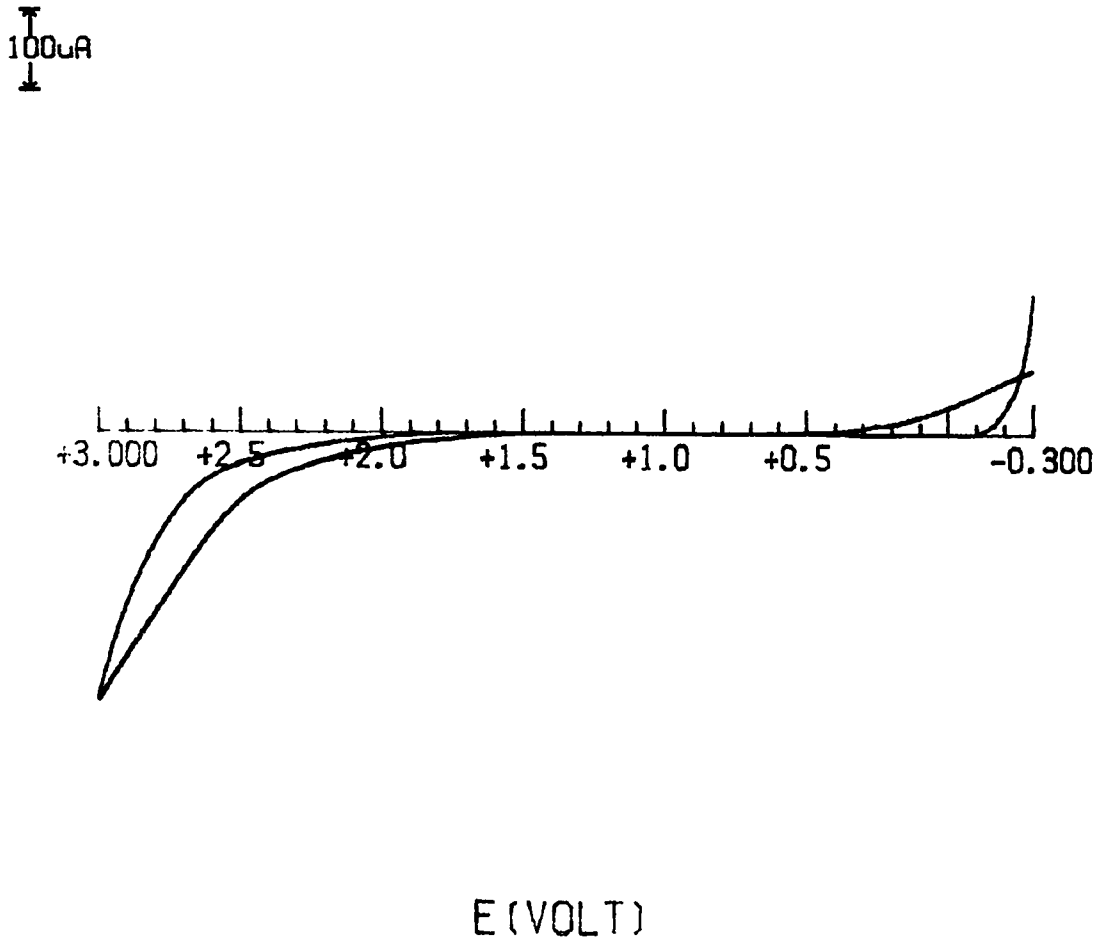

Figure A-25: Voltammogram of dry acetonitrile on a TiO_2 electrode.

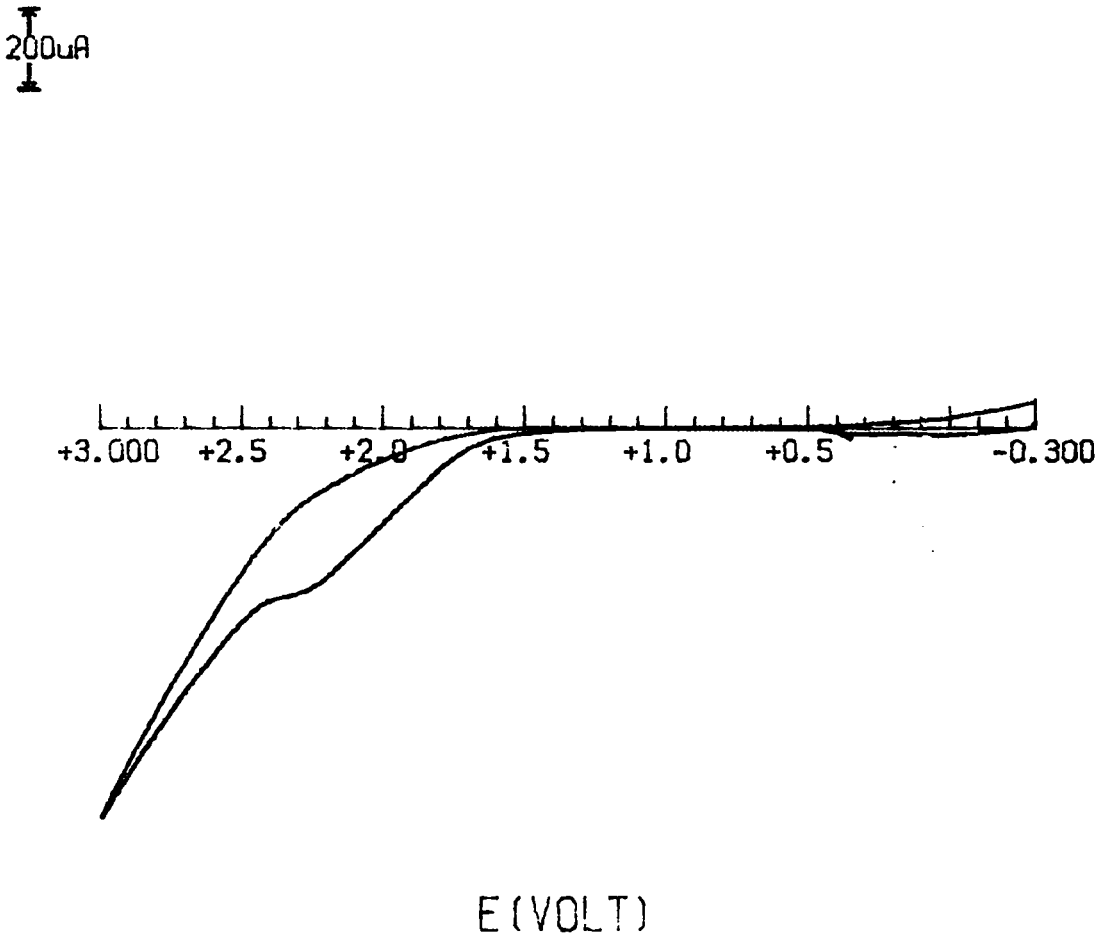

Figure A-26: Voltammogram of water in acetonitrile on a TiO_2 electrode.

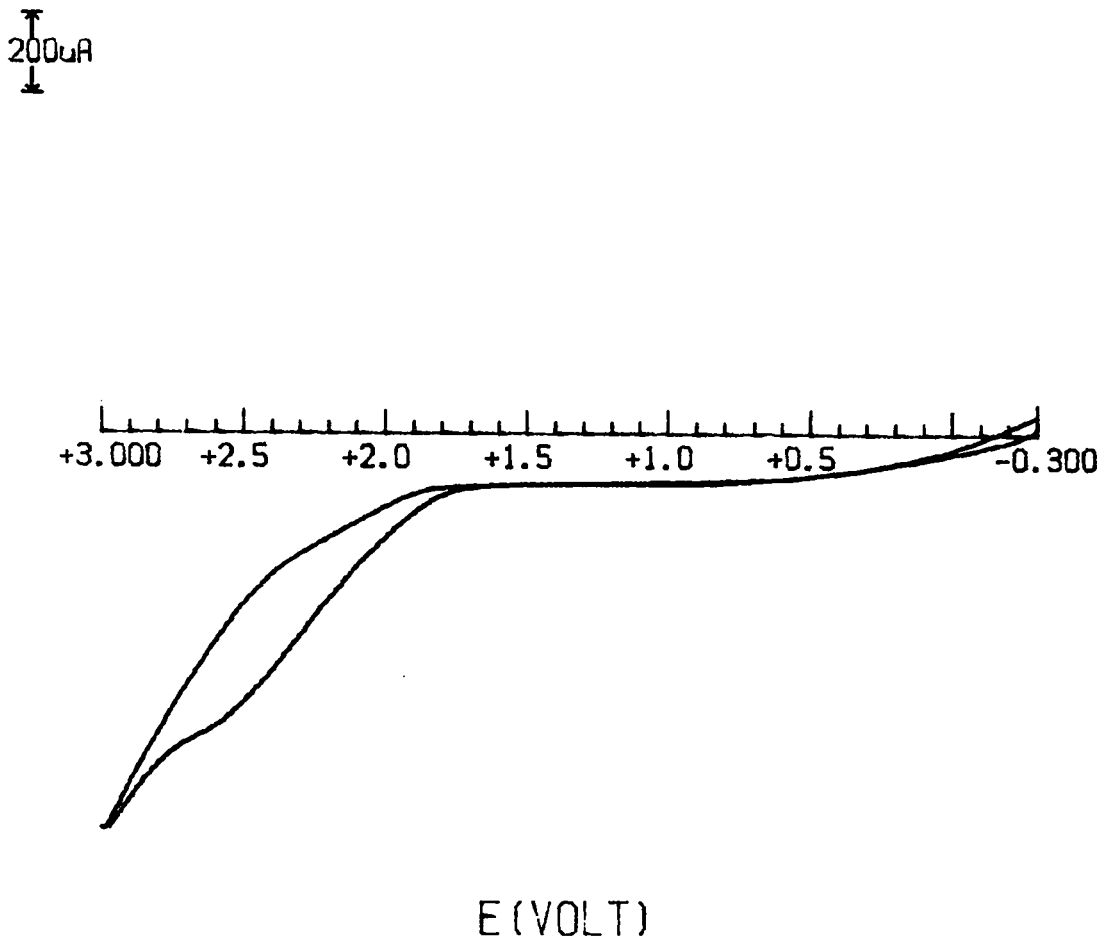

Figure A-27: Voltammogram of water in acetonitrile on an illuminated TiO_2 electrode.